DEVELOPMENT AND TESTING OF THE THREE DIMENSIONAL, TWO-FLUID CODE THERMIT FOR LWR CORE AND SUBCHANNEL APPLICATIONS

by

J.E. Kelly and M.S. Kazimi

MIT Energy Laboratory Electric Utility Program

Report No. MIT-EL 79-046

December 1979

Energy Laboratory
and
Department of Nuclear Engineering

Massachusetts Institute of Technology
Cambridge, Mass. 02139

DEVELOPMENT AND TESTING OF THE THREE DIMENSIONAL, TWO-FLUID CODE THERMIT FOR LWR CORE AND SUBCHANNEL APPLICATIONS

by

J.E. Kelly and M.S. Kazimi

Report of work performed from
October 1978 to September 1979

Date of Publication: December 1979

Sponsored by

Boston Edison Company
Consumers Power Company
Northeast Utilities Service Company
Public Service Electric and Gas Company
Yankee Atomic Electric Company

under

MIT Energy Laboratory Electric Utility Program

Report No. MIT-EL 79-046

EXECUTIVE SUMMARY

This report describes the effort involved in the development and assessment of the two-fluid computer code THERMIT for light water reactor core and subchannel analysis. The developmental effort required a reformulation of the coolant to fuel rod coupling, found in the original THERMIT code, as well as an improvement in the fuel rod modeling capability. With these modifications, THERMIT now contains consistent thermal-hydraulic models capable of traditional coolant-centered subchannel analysis. As such this code represents a very useful design and transient analysis tool for LWR's.

The advantages of THERMIT are that it contains the sophisticated two-fluid, two-phase flow model as well as an advanced numerical solution technique. Consequently, mechanical and thermal non-equilibrium between the liquid and the vapor can be explicitly accounted for and, furthermore, no restrictions are placed on the type of flow conditions. However, the formulation of the two-fluid model introduces interfacial exchange terms which have a controlling influence on the two-fluid equations. Therefore, the models which represent these exchange terms must be carefully defined and assessed.

In view of the importance of these interfacial exchange terms, a systematic evaluation of these models has been undertaken.

This effort has been aimed at validating THERMIT for both subchannel and core-wide applications. The approach followed has been to evaluate THERMIT for simple cases first and then work up to more complex flow conditions. Hence, the evaluation effort consists of performing comparison tests in the following order:

a) steady-state, one-dimensional cases,

b) steady-state, three-dimensional cases,

c) transient, one-dimensional cases, and

d) transient, three-dimensional cases.

For these comparison tests, experimental measurements have been used when available and, otherwise, comparisons have been made with COBRA-IV. While COBRA-IV is not as sophisticated as THERMIT, COBRA-IV is the only publicly available subchannel code capable of analyzing reverse flow conditions.

As a result of these comparisons, the following conclusions can be made. First, it is found that THERMIT can adequately predict the void fraction for a wide range of flow conditions. This result implies that both the subcooled vapor generation model and the interfacial momentum exchange model are appropriate.

A second conclusion is that, while the heat transfer model is generally appropriate, specific parts of this model may need to be improved. For example, the calculated critical heat flux is consistently too low. Hence, some improvement can be made in the prediction of the CHF location. However, the pre-CHF wall temperatures are satisfactorily predicted and do not require improvement. The post-CHF temperatures are also adequately predicted even though there are some differences between the measured and predicted values. These

differences are not uncommon for the post-CHF regime since the data base for the heat transfer correlations is limited. Nevertheless, some of these differences may be due to the method in which the heat transfer model is coupled to the fluid dynamic solution. Consequently, this coupling needs to be evaluated to insure that it is appropriate.

A third conclusion is that in order to accurately predict the flow and enthalpy distribution in subchannel geometry, a turbulent mixing model must be added to THERMIT. Both single-phase and two-phase measurements illustrate this point. Without such a model, the mass flux and quality predictions are poorly predicted.

In addition to the above mentioned validation efforts, the core-wide and transient capabilities have also been assessed. From these comparisons it can be concluded that, on a core-wide basis, THERMIT can accurately predict the core exit temperature distribution. This conclusion is based on comparisons with both measurements and COBRA-IV predictions.

It has also been found that THERMIT can accurately predict one-dimensional blowdown transients. For transients of this type, the wall friction and vapor generation rate have the greatest effect on the code predictions.

Finally, for multidimensional transients it can be concluded that the predictions of THERMIT appear to be qualitatively correct and, additionally, THERMIT is at least as computationally efficient as COBRA-IV (explicit). Differences between the predictions of the two codes may be anticipated in light of their respective two-phase flow models.

TABLE OF CONTENTS

LIST OF FIGURES

LIST OF TABLES

NOMENCLATURE

A	Area
C_p	Specific heat
D_h	Hydraulic Diameter
e	Internal Energy
f	Friction Factor
F_g	Gravitational Force
F_i	Vapor-Liquid Interfacial Momentum Exchange Rate
F_w	Wall Frictional Force
g	Gravitational Constant
G	Mass Flux
h	Enthalpy
H	Heat Transfer Coefficient
J_v	Superficial Vapor Velocity
k	Thermal Conductivity
K_i	Interfacial Momentum Exchange Coefficient
L	Length
N	Bubble Number Density
P	Pressure
Q_i	Interfacial Heat Transfer Rate
Q_w	Wall Heat Transfer Rate
$\dot{q}$	Power
q''	Heat Flux

Re	Reynolds Number
S_{ij}	Gap Spacing Between Coolant Channels
t	Time
T	Temperature
T_d	Bubble Departure Temperature
T_s	Saturation Temperature
V	Velocity
V_R	Relative Velocity
w'_{ij}	Turbulent Mixing Rate
X	Quality
α	Void Fraction
β	Mixing Parameter
Γ	Vapor Generation Rate
ρ	Density
μ	Viscosity

SUBSCRIPTS

i,j,k	Nodal Locations
ℓ	Liquid
s	Saturation
v	Vapor
x,y,z	Spatial Directions

1. INTRODUCTION

In the last few years, the need for improved assessment of nuclear reactor safety has lead to the rapid development of methods for multidimensional two-phase thermal-hydraulic analysis. These methods have become progressively more complex in order to account for the many physical phenomena encountered in two-phase flow. These phenomena include non-equilibrium conditions between the vapor and the liquid such as subcooled liquid boiling, vapor condensation and relative motion of the two phases. Furthermore, elaborate solution methods have been used so that the complex flow patterns encountered in postulated transients may be analyzed. For example, in a loss of coolant accident (LOCA) or a severe anticipated transient without scram (ATWS), flow reversal may occur and the numerical method must be capable of handling such a condition. Hence, these new multidimensional thermal-hydraulic computer codes combine complex physical modeling with advanced numerical solution techniques.

The MIT developed computer code, THERMIT (1), is an example of these advanced codes. THERMIT solves the three-dimensional, two-fluid equations describing the two-phase flow and heat transfer dynamics of light water reactor cores in rectangular coordinates. The two-fluid equations describe the two-phase flow as two separate fluids, i.e., liquid and vapor.

A complete set of conservation equations is written for each phase, accounting for the interactions between the phases. These equations are very general and are only limited by the choice of the interaction terms. Hence, both BWR and PWR cores can be modeled and analyzed under steady-state as well as transient conditions.

The two-fluid equations are solved in first-order finite difference form with a semi-implicit solution technique. This technique is a modified version of the ICE method (2,3) and has a stability restriction in the form of a maximum allowable time step:

$$\Delta t < \Delta X/V \qquad (1.1)$$

where ΔX is the mesh size and V is the larger of the vapor and liquid velocities. At each time step, the equations are solved with a Newton iteration method which reduces the system of equations to simplified boundary value problem for pressures only. A unique feature of this method is that convergence can always be obtained if small enough time steps are chosen. Consequently, this solution is ideally suited for severe transient analysis.

Although originally developed as a tool for core-wide analysis, THERMIT is flexible enough to be adapted to analyze other types of two-phase flow conditions. One useful extension would be to modify the code so that it is capable of subchannel

analysis. Such a tool would have several advantages over widely used codes such as COBRA IIIC/MIT (4) or COBRA IV (5). For analyses of two-phase conditions, compared to COBRA IIIC/MIT THERMIT has the advantages listed in Table 1.1. It is seen that both the improved physical model and the numerical method lead to significant improvements. Similarily, a subchannel version of THERMIT would also have advantages over COBRA IV as summarized in Table 1.2. Again the improved physical model and numerical method lead to improvements although not as many as in the COBRA IIIC/MIT case.

In view of these advantages, the development of a subchannel version of THERMIT has been undertaken. The purpose of this effort is to provide the utilities with an advanced tool capable of both core-wide and subchannel thermal-hydraulic analysis. With such a tool, it is now possible to analyze problems which could not have been analyzed using less advanced methods. Furthermore, it is also possible to assess the applicability of these less sophisticated methods. Hence, the development of a subchannel version of THERMIT represents a significant advancement in core thermal-hydraulic analysis.

The strategy for developing the subchannel version of THERMIT has been to

a) modify the code structure and numerical method as necessary,

b) verify and assess existing models for physical phenomena and

c) implement improved models as necessary.

Table 1.1 THERMIT Advantages over COBRA-IIIC/MIT

A. Permanent Advantages of the Physical Model and Numerical Method

1. True 3-D flow equations, i.e., no approximation in transverse momentum equation

2. The two-phase flow model allows:
   a) Unequal temperatures for each phase
   b) Superheated vapor
   c) Compressibility effects
   d) Countercurrent or cocurrent flow of the two phases

3. The numerical method allows:
   a) Flow reversals
   b) Pressure boundary conditions
   c) Guaranteed convergence

B. Current Advantages*

1. Improved heat transfer model which includes:
   a) Complete boiling curve heat transfer calculations
   b) Advanced gap conductance model
   c) Temperature dependent fuel properties
   d) Fully-implicit clad-coolant coupling

*(COBRA-IIIC/MIT is being upgraded to compensate for these advantages)

Table 1.2 THERMIT Advantages over COBRA-IV

1. True 3-D flow equations, i.e., no approximation in transverse momentum equation
2. The two-phase flow model allows:
   a) Unequal velocities for each phase (explicit version only)
   b) Unequal temperatures for each phase
   c) Subcooled liquid boiling (explicit version only)
   d) Compressibility effects
   e) Countercurrent or cocurrent flow of the two phases
3. Improved heat transfer modeling which includes:
   a) Advanced gap conductance model
   b) Temperature dependent fuel properties
4. More advanced numerical method which allows:
   a) Guaranteed convergence
   b) Flow reversals (implicit version only)
   c) Pressure boundary conditions (implicit version only)

Modifications, such as providing the capability to analyze coolant centered subchannels, are discussed in Chapter 2. Improvements which have been implemented in THERMIT are also discussed in Chapter 2. The verification and assessment of the models in THERMIT are discussed in Chapter 3.

2. THERMIT DEVELOPMENT

2.1 Introduction

In this section the effort to develop the capability for subchannel representation and the modification of the models provided in THERMIT are described. The original THERMIT code structure and models are detailed in Reference 1. It is assumed here that only the changes from that structure need be discussed in detail. A brief account of the original THERMIT formulation will be given also.

2.2 The Two-Fluid Model and Solution

2.2.1 Two-Fluid Model

The two-fluid model in THERMIT treats each phase (either liquid or vapor) as a separate fluid which results in the following conservation equations:

Conservation of Vapor Mass: (2.1)

$$\frac{\partial}{\partial t}(\alpha\rho_v) + \nabla\cdot(\alpha\rho_v\vec{V}_v) = \Gamma$$

Conservation of Liquid Mass: (2.2)

$$\frac{\partial}{\partial t}[(1-\alpha)\rho_\ell] + \nabla\cdot[(1-\alpha)\rho_\ell\vec{V}_\ell] = -\Gamma$$

Conservation of Vapor Energy: (2.3)

$$\frac{\partial}{\partial t}(\alpha\rho_v e_v) + \nabla\cdot(\alpha\rho_v e_v\vec{V}_v) + P\,\nabla\cdot(\alpha\vec{V}_v) + P\,\frac{\partial\alpha}{\partial t} = Q_{wv} + Q_i$$

Conservation of Liquid Energy:

$$\frac{\partial}{\partial t}[(1-\alpha)\rho_\ell e_\ell] + \nabla\cdot[(1-\alpha)\rho_\ell e_\ell \vec{V}_\ell] + P\nabla\cdot((1-\alpha)\vec{V}_\ell) - P\frac{\partial \alpha}{\partial t} = Q_{w\ell} - Q_i \tag{2.4}$$

Conservation of Vapor Momentum:

$$\alpha\rho_v \frac{\partial \vec{V}_v}{\partial t} + \alpha\rho_v(\vec{V}_v\cdot\nabla)\vec{V}_v + \alpha\nabla P = -\vec{F}_{wv} - \vec{F}_i - \alpha\rho\vec{g} \tag{2.5}$$

Conservation of Liquid Momentum:

$$(1-\alpha)\rho_\ell \frac{\partial \vec{V}_\ell}{\partial t} + (1-\alpha)\rho_\ell(\vec{V}_\ell\cdot\nabla)\vec{V}_\ell + (1-\alpha)\nabla P = -\vec{F}_{w\ell} + \vec{F}_i - (1-\alpha)\rho_\ell \vec{g} \tag{2.6}$$

(See Nomenclature Table on page 9 .)

In addition to these conservation equations there are four equations of state, i.e.

$$\rho_v = \rho_v(P, T_v) \tag{2.7}$$

$$\rho_\ell = \rho_\ell(P, T_\ell) \tag{2.8}$$

$$e_v = e_v(P, T_v) \tag{2.9}$$

$$e_\ell = e_\ell(P, T_\ell) \tag{2.10}$$

In total then there are ten conservation equations (2 mass, 2 energy, 6 momentum) and four equations of state or fourteen total equations. The fourteen corresponding unknowns are the void fraction, α, the pressure, P, the densities, ρ_v and ρ_ℓ, the internal energies, e_v and e_ℓ, the temperatures, T_v

and T_ℓ, and finally the three components of the velocity vectors, $\vec{V}_v$ and $\vec{V}_\ell$. It is clear therefore that the liquid and vapor pressures within any control volume are assumed equal.

This two-fluid formulation of the conservation equations introduces terms that represent interactions within any given control volume. These interactions can be classified as being either vapor — liquid or fluid-wall interactions. The vapor-liquid interaction terms are the vapor production rate (or the mass exchange rate), Γ, the interfacial momentum exchange rate, F_i, and the interfacial heat transfer rate, Q_i. Each of these processes represents a transfer mechanism across the phase boundary. The fluid-wall interaction terms are the wall heat transfer, Q_w, and the wall friction loss, F_w. Each of these processes represent a transfer mechansim between either the liquid or vapor and the structural material (e.g. fuel rods, grids). Models for each of these interaction terms, usually referred to as the constitutive equations, are required to close the system of equations. These models are empirically or semi-empirically based. Due to the precise physical interpretation of these terms, the models should be valid over a wide range of conditions.

Hence, it is seen that the two-fluid model is rather complex. Nevertheless, the model is not restricted by assumptions such as the homogeneous equilibrium assumption ($\vec{V}_\ell = \vec{V}_v$, $T_\ell = T_v = T_{sat}$). Therefore, the two-fluid model is well-suited for severe transient analysis, where non-equilibrium

effects may be significant.

2.2.2 Solution Procedure

The above set of equations is solved with a semi-implicit numerical method as discussed in Reference 1. This method can be outlined as follows. The conservation equations are first approximated by a linearized set of finite difference equations. The density and internal energy in these equations are then eliminated in favor of the pressure and temperatures by using the equations of state. The momentum equations are then used to derive a relationship between velocity and pressure which can be used to eliminate the velocity in the mass and energy equations. The resulting system of equations for each node can be represented as follows:

$$\begin{bmatrix} x & x & x & x \\ x & x & x & x \\ x & x & x & x \\ x & x & x & x \end{bmatrix} \begin{bmatrix} P_i \\ \alpha \\ T_v \\ T_\ell \end{bmatrix} + \begin{bmatrix} x & x & x & x & x & x \\ x & x & x & x & x & x \\ x & x & x & x & x & x \\ x & x & x & x & x & x \end{bmatrix} \begin{bmatrix} P_{i+1} \\ P_{i-1} \\ P_{j+1} \\ P_{j-1} \\ P_{k+1} \\ P_{k-1} \end{bmatrix} = \begin{bmatrix} x \\ x \\ x \\ x \end{bmatrix} \qquad (2.11)$$

where each x represents a known coefficient. One notes that these equations couple together the pressure in the node, the void fraction, the liquid and vapor temperatures and the pressures in the six adjacent cells. By multiplying through by the inverse of the 4 x 4 matrix, the only unknowns in the first equation that remain are the pressures. This equation is solved iteratively for every node with each sweep through the core referred to as an inner iteration. Once the pressure

distribution is found, the other unknowns (α, T_v, T_ℓ) can be found by back substitution. The inversion of the 4 x 4 matrix and subsequent back substitution is referred to as a Newton or outer iteration.

This method converges on the pressure distribution with the user controlling the convergence criteria and the number of iterations (both inner and Newton). If convergence is not attained in the specified number of iterations, the code has the capability of reducing the time step size. The advantage of this feature is that if the time step size is small enough, the method will always converge. Hence, this solution method is extremely reliable for any type of flow conditions.

2.2.3 Capabilities of Initial Version of THERMIT

The numerical method in THERMIT was originally developed for core-wide analysis. In other words, transients which could be analyzed using a coarse mesh (i.e., assembly-sized control volumes) would be well-suited for THERMIT. Consequently, the initial developmental effort at M.I.T., which was sponsored by EPRI, focused on the idea of using assembly-sized control volumes in THERMIT. The thrust of our current effort is to demonstrate that analyses with subchannel sizes can also be handled by the basic scheme.

With large control volumes, certain practical simplifications can be made. For example, since only the average fluid conditions are calculated in each assembly, only one average fuel rod per assembly needs to be modeled. This greatly

simplifies the coupling between the coolant and fuel rod. Additionally, the effects of turbulent mixing should be small and the above effects may be neglected. Hence, it is seen that the use of assembly-sized control volumes can lead to some modeling simplifications.

In view of this type of application for THERMIT, the various constitutive models were tuned for use with large control volumes. For example, the interfacial friction model was developed using BWR bundle average void fraction data. Modeling of the transverse wall friction was also based on assembly-size volumes, since the friction correlation was developed for flow normal to an infinite rod array.

2.3 Subchannel Version

For a large number of applications, details of the two-phase within an assembly are of interest. Although a coarse mesh core modeling had originally been envisioned when using THERMIT, there is no intrinsic reason to limit the code applicability to small mesh sizes. From a numerical point of view, the solution method would not explicitly restrict the size of the mesh. However, due to stability considerations, a mesh size smaller than 2×10^{-4}m may lead to problems (6). This limit is at least 30 times smaller than subchannel size. The primary limitation on the applicability of THERMIT regarding subchannel applications was that the constitutive models may not have been applicable for these applications. In particular, the lack of a turbulent mixing model and the infinite-array

transverse friction model were significantly inappropriate. Another shortcoming was that only one fuel rod per channel could be modeled. Consequently, the traditional coolant centered subchannel, in which four fuel rods (actually quarters of fuel rods) and the gaps between them make up the boundaries of the subchannel, could not be modeled.

In order to overcome these restrictions, a code development effort has been undertaken. This effort has been directed at improving THERMIT by developing a subchannel version and evaluating the code's predictive capabilities. The specific modifications to THERMIT are discussed below.

2.3.1 Coolant Centered Channels

The first step in this development was to modifiy the code so that coolant centered subchannels could be modeled. This process involved changing all the coupling between the clad and coolant temperatures. This coupling occurs in the energy equations as outlined in Reference 1. These equations were changed so that each coolant channel could be coupled to a maximum of four fuel rods. Hence, the source term in the energy equations would become a sum of up to four terms, one from each adjacent rod.

Changes were also required in the wall friction selection logic. As originally programmed in THERMIT, the partitioning of the wall friction would be as follows:

$$\left.\begin{aligned} F_{wv} &= 0 \\ F_{w\ell} &= F_{wT} \end{aligned}\right\} \text{ if } T_w < T_{CHF} \qquad (2.12)$$

$$\left.\begin{aligned} F_{w\ell} &= 0 \\ F_{wv} &= F_{wT} \end{aligned}\right\} \text{ if } T_w > T_{msfb} \tag{2.13}$$

$$\left.\begin{aligned} F_{wv} &= \frac{q''_v}{q''_\ell + q''_v} F_{wT} \\ F_{w\ell} &= \frac{q''_\ell}{q''_\ell + q''_v} F_{wT} \end{aligned}\right\} \text{ if } T_{CHF} < T_w < T_{msfb} \tag{2.14}$$

This logic is dependent on the clad temperature or more appropriately the wetting characteristics of the clad. With the potential of four heated surfaces in a channel, it became necessary to define which clad temperature should be used in this logic. A search routine was added to determine the maximum clad temperature in each coolant node and this value would be used in the wall friction selection logic.

2.3.2 Fuel Rod Modeling

Along with applications involving coolant centered subchannels came the need to have detailed fuel rod modeling. In practical terms this meant having the ability to calculate four clad temperatures per fuel rod. With this capability, the fuel rod modeling would be consistent with the clad-coolant coupling.

This was accomplished by allowing each quarter of a fuel rod to be modeled separately. Hence, it would be possible to have four clad temperatures per fuel rod. In fact, a complete heat transfer calculation is performed for each rod section (whether it be a quarter, half or full rod) so that the temperatures throughout the section are calculated.

Consequently, for any given rod modeled as four sections, there will be four centerline temperatures calculated which are not necessarily equal. This may not always be accurate due to azimuthal heat conduction effects which are neglected here. For cases of practical importance which have been run, negligible differences in the centerline temperatures were calculated. Another minor disadvantage of this method is that the computational time will be increased, but this increase should not be excessive. Therefore, on the whole, the fuel pin modeling together with the coolant-centered subchannel capabilities provide THERMIT with the geometrical flexibility required for subchannel analysis.

2.4 Other Code Improvements

A number of other improvements in the overall THERMIT model have been implemented. Some of these improvements modify the original constitutive models which are described in Reference 1. The models affected are the vapor generation model, Γ, the interfacial momentum exchange model, F_i, and the critical heat flux model. Other improvements have been added to reduce the computational effort required to obtain a steady-state solution. Each of these improvements is discussed below.

2.4.1 Vapor Generation Model

In the original version of THERMIT, only one vapor generation model had been available; namely the Nigmatulin model. Since its initial release, a second option has been

added to THERMIT. This model has been termed the subcooled boiling model because it allows vapor generation even for subcooled fluid conditions. Consequently, subcooled boiling can now be predicted, which was not the case in the original version.

The formulation of this model is based on the work of Ahmad [7]. In this model it is assumed that the heat flux to the coolant can be divided into two parts. One part raises the liquid temperature and the other part generates vapor. A prescription is then given for the fraction of the heat flux used to generate vapor. Then using a simple heat balance and a condensation model based on non-equilibrium effects the vapor generation model is obtained. The details of this model are given in Appendix A.

To illustrate the advantages of this new model a comparison between this model and the Nigmatulin model has been performed. In this test case, a BWR bundle has been modeled as a single channel and a void fraction versus axial length comparison has been made. As seen in Figure 2.1, over the last 60% of the channel the two models are in good agreement which simply indicates that both predict the same vapor generation rate in saturated boiling conditions. However, in the subcooled boiling regime (first 40% of the channel) there is a substantial difference in the vapor generation rate and, consequently, the void fractions differ. With the subcooled boiling model, boiling is predicted to occur earlier in the channel. The void fraction differences are significant for

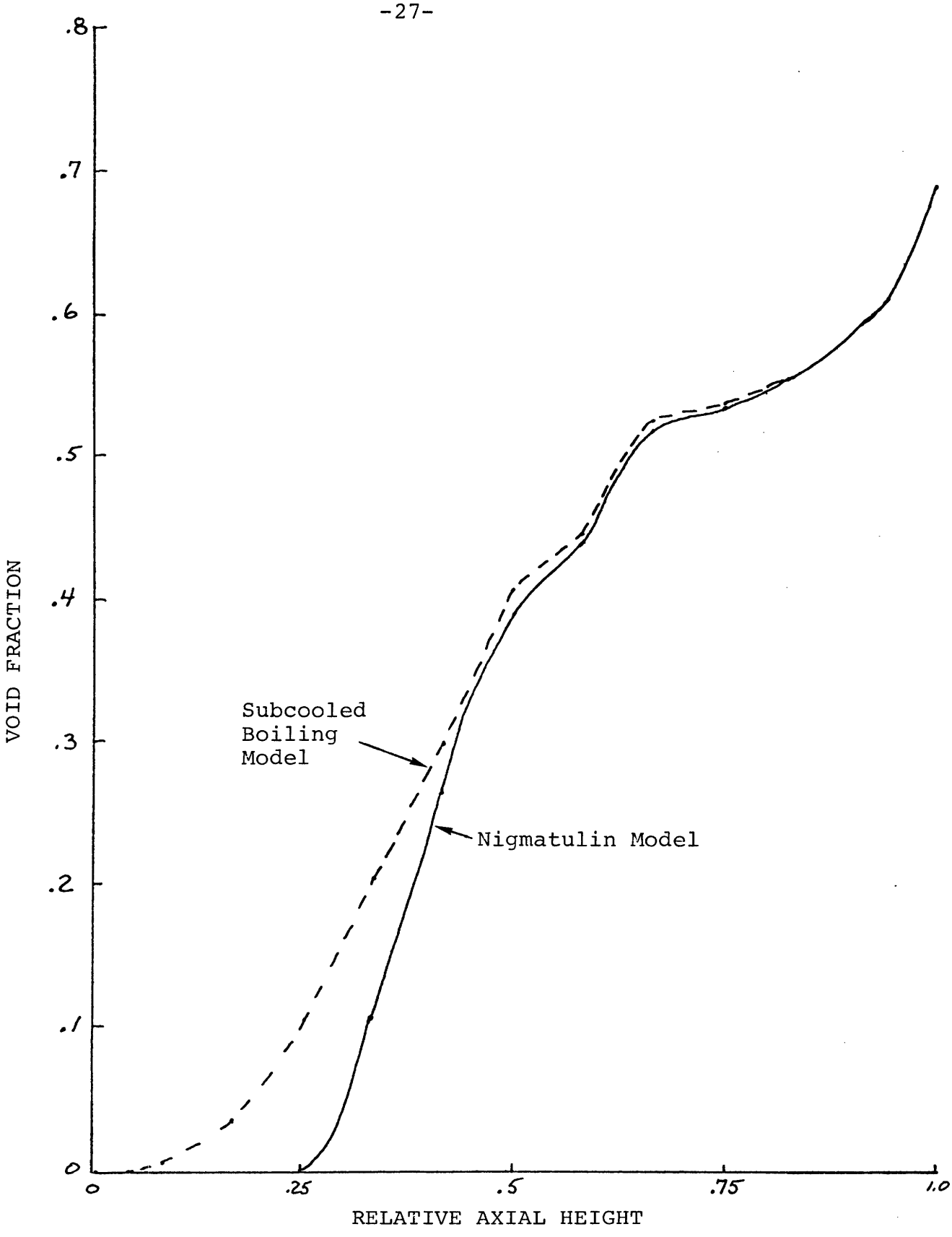

Figure 2.1 Comparison of Void Fraction Profiles.

reactivity considerations and, hence, the subcooled boiling model would yield the more realistic results for BWR and PWR cases.

2.4.2 Interfacial Momentum Exchange Model

The interfacial momentum exchange model provided in the original THERMIT did not prove to be very accurate and has been replaced. In fact, two models were added which give more realistic results. The first model was developed by Stewart [8] at M.I.T. and the second one is used in the two-fluid models at LASL [9]. Each of these models has been used in void fraction comparisons which are discussed in Section 3.2.1. The details of each model are given in Appendix B.

2.4.3 CHF Correlation

The original version of THERMIT contained only one CHF correlation. This correlation, namely the Biasi correlation, is part of the BEEST heat transfer package [10] which has been developed for blowdown heat transfer analysis. The selection of the Biasi correlation for blowdown applications is based primarily on its data base, which covers a wide range of pressures and includes both upflow and downflow conditions. Essentially, this correlation is a "dry-out" type CHF correlation which is consistent with the expected CHF type during blowdown. However, for DNB type CHF or for non-uniform axial power distributions, the Biasi correlation would not be applicable. Therefore, in view of these shortcomings, additional CHF correlations have been added to THERMIT.

The two correlations selected to complement the Biasi correlation are the W-3 correlation and the CISE correlation. Each of these correlations can be found in the open literature and are reproduced in Appendix C. The W-3 correlation can be used for steady-state and transient PWR conditions while the CISE correlation can be used for similar problems in BWR systems. Together with the Biasi correlation, these correlations should cover the range of practical interest.

2.4.4 Steady-State Options

Although the semi-implicit solution method in THERMIT is well-suited for transient analysis, there is no convenient way to obtain steady-state solutions with this method. The reason for this is that some of the temporal finite difference equations are written explicitly and, hence, the maximum permissible time step size is limited by the Courant velocity condition (i.e. $\Delta t < \Delta x/v$). Consequently, an infinite value for Δt cannot be used as one would like to use for steady-state problems (i.e. $1/\Delta t = 0$). Instead, steady-state solutions are found by starting from an initial guess and then running an unperturbed transient until an equilibrium solution is achieved. This equilibrium solution is the steady-state solution from which a true transient may be initiated.

This method of finding steady-state solutions by solving an initial value problem cannot be changed except by going to a fully implicit method. Therefore, techniques for improving the computational efficiency of this method have been investigated and implemented into THERMIT. These techniques

take advantage of the presumed nature of the steady-state solution. For example, the fuel rod heat flux in steady-state must equal the linear power rate divided by the heated perimeter. Therefore, there is no need to solve for the heat transfer coefficients and clad temperatures until the fluid dynamics have converged. In other words, the heat transfer calculations are initially eliminated. Basically, this technique decouples the heat source from the coolant which can lead to substantial CPU savings (See Table 2.1).

Another technique which has been developed to increase the computational efficiency of finding steady-state solutions is called the isolated channel method. It takes advantage of two features of the steady-state solution procedure and one physically based assumption. The first feature of the solution procedure is that one-dimensional problems converge much quicker than do three-dimensional problems. For example, four isolated channel require less CPU time to reach steady-state than do four connected channels. A second feature is that the closer the initial conditions are to the steady-state, the quicker the method will converge. This means that if one can improve the selection of the initial conditions, then a steady-state solution may be obtained with less computational effort. The physical assumption is that in most cases the transverse flow between channels is small. This assumption means that the pressure and flow distributions can be approximately determined by treating the channels as though they were isolated. Hence, a good initial guess can be

TABLE 2.1

SUMMARY OF REMEDIES USED TO REDUCE

CPU REQUIREMENTS FOR STEADY-STATE SOLUTIONS

Remedy	Reduction of CPU
Isolated Channel Method [+]	25 - 90%
Elimination of Heat Transfer Calculation	10 - 25%
Double Precision*	7%

[+] The isolated channel case essentially provides a good guess of the flow and pressure fields. This remedy will work as long as the transverse flow is small so that the radial pressure distribution is not significantly altered when the gaps between channels are assumed open.

* This remedy was tested and showed limited improvement, but due to the increase in core storage it has not been implemented.

obtained using the calculational results of the isolated channel problem which require very little computational effort. Then, once this solution is obtained, the interconnecting gaps can be opened to allow the appropriate flow redistribution to occur. The unperturbed transient is then continued until a true steady-state is reached. As seen in Table 2.1, this method leads to a substantial reduction of the CPU time. It should be noted that this technique may not be as beneficial in cases where large inter-channel crossflows are expected in steady-state, since the isolated channel case would no longer represent a good initial guess.

Both the option to eliminate the heat transfer calculations (i.e., use a constant heat flux boundary condition) and the option to use the isolated channel method have been implemented into THERMIT. The use of either option is controlled by an input flag. The input flag *iqss* controls the type of heat transfer boundary condition:

$$iqss \begin{cases} = 0 & \text{constant heat flux} \\ = 1 & \text{normal} \end{cases}$$

The input flag *itam* controls the use of the isolated channel method:

$$itam \begin{cases} = 0 & \text{isolated channel method} \\ = 1 & \text{normal} \end{cases}$$

Both of these input flags must be specified by the user and can be changed with the restart option. Hence, a steady-state

would be obtained by initially running an unperturbed transient with *iqss* = 0 and *itam* = 0 for a specified length of time (typically 2.0 seconds). The problem would then be restarted with *iqss* = 1 and *itam* = 1 and the unperturbed transient would be continued until steady-state is reached (typically an additional 2-3 seconds). Using this technique the computational efficiency of finding steady-state solutions is greatly increased.

3. VALIDATION AND ASSESSMENT OF THERMIT

3.1 Introduction

In conjunction with the developmental effort discussed in Chapter 2 a program for validating and assessing the models in THERMIT has been undertaken. The goals of this program are: (1) To validate the predictive capabilities of THERMIT and (2) To define the needed models and assist in developing them. The emphasis in this effort has been directed toward evaluating the code for subchannel applications. In particular, the following models and capabilities have been investigated:

a) Γ, the vapor generation rate model,

b) F_i, the interfacial momentum exchange rate model,

c) Q_w, the wall heat transfer rate model, and

d) The three dimensional flow modeling.

In addition to developing and verifying a subchannel version of THERMIT, the original version of THERMIT has also been assessed.

In order to meet the goals of this program, an orderly progression of tests and comparisons has been performed. These include comparisons with both one-dimensional and three-dimensional experimental data and multidimension comparisons with other computer codes (e.g., COBRA IV). The order in which these comparisons have been made is structured so that individual models can be validated and assessed in a logical manner. This procedure entails first selecting a set of

experimental data which can be used to validate a specific model independent of the other models in the code. Once a model has been validated, it can be used with some confidence in the effort to validate the other models. For cases in which experimental data are not available, comparisons can be made with other computer codes. In this way, the data base for the code is built-up in a systematic manner.

Experimental measurements suitable for model evaluation need to be simple so that individual models can be validated without introducing extraneous effects. Consequently, steady-state, one dimensional measurements serve as a logical starting point for the validation program. Measurements of this type do not contain any temporal or multi-dimensional effects and the conservation equations can be greatly simplified. The next step in complexity would be isothermal, steady-state, three dimensional tests. In measurements of this type, there is no heat transfer so that the energy equation can be eliminated. Next, steady-state, heated, three-dimensional experiments can be used. Measurements of this type have additional complexities and, hence, it is imperative that the simpler cases are evaluated first. Finally, after completing these steady-state evaluations, both one-dimensional and multi-dimensional transient conditions would be investigated.

In this systematic procedure, the initial evaluation has been performed using steady-state, one-dimensional void fraction data. Measurements of this type can be used to evaluate

both the vapor production rate, Γ, and the interfacial momentum exchange rate, F_i. A large number of data sets have been compared with THERMIT and these comparisons are discussed in section 3.2.1.

The second type of data used in this effort is steady-state, one-dimensional heat transfer data. This data is in the form of clad temperature distributions and is useful for evaluating the heat transfer model. Comparisons between the data and THERMIT predictions have been performed and are discussed in section 3.2.2.

Steady-state, three-dimensional measurements have also been used. Measurements for both isothermal and heated subchannel experiments have been compared with THERMIT. A discussion of these comparisons can be found in sections 3.3.1. and 3.3.2. Measurements of the core exit temperature distributions have also been compared with THERMIT. These comparisons require using the core-wide modeling approach and are discussed in section 3.3.3.

The first transient case which has been compared to THERMIT is a one-dimensional blowdown application. Experimental measurements for this case have been used to assess the ability of THERMIT to analyze a very severe transient. The results of this comparison are discussed in section 3.4.

The final case, which has been used in this evaluation program, is a two-dimensional simulation of a rod ejection accident (REA). For this case, THERMIT has been compared to

COBRA-IV in order to assess the transient capabilities of THERMIT. Two different REA's are considered in this analysis. The first REA is initiated from a hot zero power condition while the other REA is initiated from a low flow, low power condition. The comparisons for these cases are discussed in section 3.5.

This evaluation program is summarized in Table 3.1. These tests do not cover all possible conditions of interest and futher testing is required. However, this evaluation program establishes a reasonable format for future investigations.

3.2 Steady-State, One Dimensional Comparisons

3.2.1 Void Fraction Comparisons

The ability to accurately predict the void fraction distribution is of major importance for both reactor safety and design purposes. Hence, it is essential that THERMIT be able to predict the void fraction distribution. However, in THERMIT there is no correlation for the void fraction as is found in other codes (e.g., COBRA IV). Instead, the void fraction is a variable in the solution method and is controlled by a combination of the vapor generation rate and the interfacial momentum exchange rate. Hence, the void fraction will depend on the selection of these two models.

The way in which these models affect the void fraction can be explained by considering each model separately. The vapor generation rate model must account for two types of

TABLE 3.1

SUMMARY OF EVALUATION PROCEDURE

1. Steady-State One Dimensional
    A. Void Fraction
    B. Clad Temperatures

2. Steady-State Three Dimensional
    A. Unheated Subchannel Data
    B. Heated Subchannel Data
    C. Core Wide Temperature Distribution

3. Transient One-Dimensional
    A. Blowdown Transient Data

4. Transient Multi-Dimensional
    A. Simulated Rod Ejection Accident
        1) Hot Zero Power Initial Condition
        2) Low Power, Low Flow Initial Condition

boiling conditions; namely subcooled boiling and saturated boiling. In the subcooled boiling regime, this model must predict the location where boiling begins as well as the amount of vapor being generated. In the present model, the Ahmad correlation is used to determine the bubble departure location and non-equilibrium effects are accounted for in the subcooled vapor generation rate (11). In the saturated boiling regime, the model reduces to an equilibrium model in which all the heat added to the channel results in vapor production, i.e.,

$$\Gamma = \dot{q}/h_{fg} \tag{3.1}$$

This model is continuous over the entire boiling length so that numerical difficulties are avoided. Hence, this model predicts the vapor generation rate for all types of boiling conditions.

Intuitively, the vapor generation rate must be related to the void fraction. One way to view this relationship is to examine the steady-state, one-dimensional vapor continuity equation, i.e.,

$$\frac{\partial}{\partial z} (\alpha \rho_v V_v) = \Gamma \tag{3.2}$$

By using the definition of the flow quality,

$$X \equiv \alpha \rho_v V_v / G \ , \tag{3.3}$$

this equation may be rewritten as

$$\frac{\partial}{\partial z} (XG) = \Gamma \tag{3.4}$$

Since the mass flux, G, is constant, one finds that the vapor generation rate is directly related to the quality. Furthermore, the quality and void fraction are related by

$$\alpha = \frac{1}{1 + \frac{(1-X)}{X} \frac{\rho_v V_v}{\rho_\ell V_\ell}} \tag{3.5}$$

Hence, the void fraction is seen to depend not only on the quality but also on the slip ratio, V_v / V_ℓ.

It is in the determination of the relative velocities of the two phases that the interfacial momentum exchange model becomes important. This model has a functional form which can be written as

$$F_i = (K_1 + K_2 \ |V_v - V_\ell|) \ (V_v - V_\ell) \tag{3.6}$$

$$= (K_1 + K_2 \ |V_R|) \cdot V_R \tag{3.7}$$

The interfacial force is nearly proportional to V_R^2. This strong coupling means that the relative velocity can be controlled by adjusting K_1 and K_2 and, in turn, the void fraction is changed. If two cases are computed, which are identical except for the values of K_1 and K_2, the case which has the higher values of K_1 and K_2 will have the larger void fraction predictions. It is also clear that if K_1 and K_2 approach infinity, V_R approaches zero. Thus for a given vapor generation rate, the homogeneous flow has the highest void fraction.

With this background, it is now possible to see how void fraction data can be used to assess the vapor production model and the interfacial momentum exchange model. For a typical void fraction plot (Figure 3.1), three distinguishing features can be identified. The first is the point where boiling begins, point A. This point can be used to validate the boiling inception point of the vapor generation model. The second feature is region B in which the slip ratio is nearly equal to 1.0 so that the void fraction is independent of F_i. Consequently, the subcooled vapor generation rate can be verified in this region. The third feature is region C in which the vapor generation rate is independent of the flow conditions, so that the void fraction will be determined by the interfacial momentum exchange model. Therefore in this region, F_i can be assessed using the data. Thus, with a

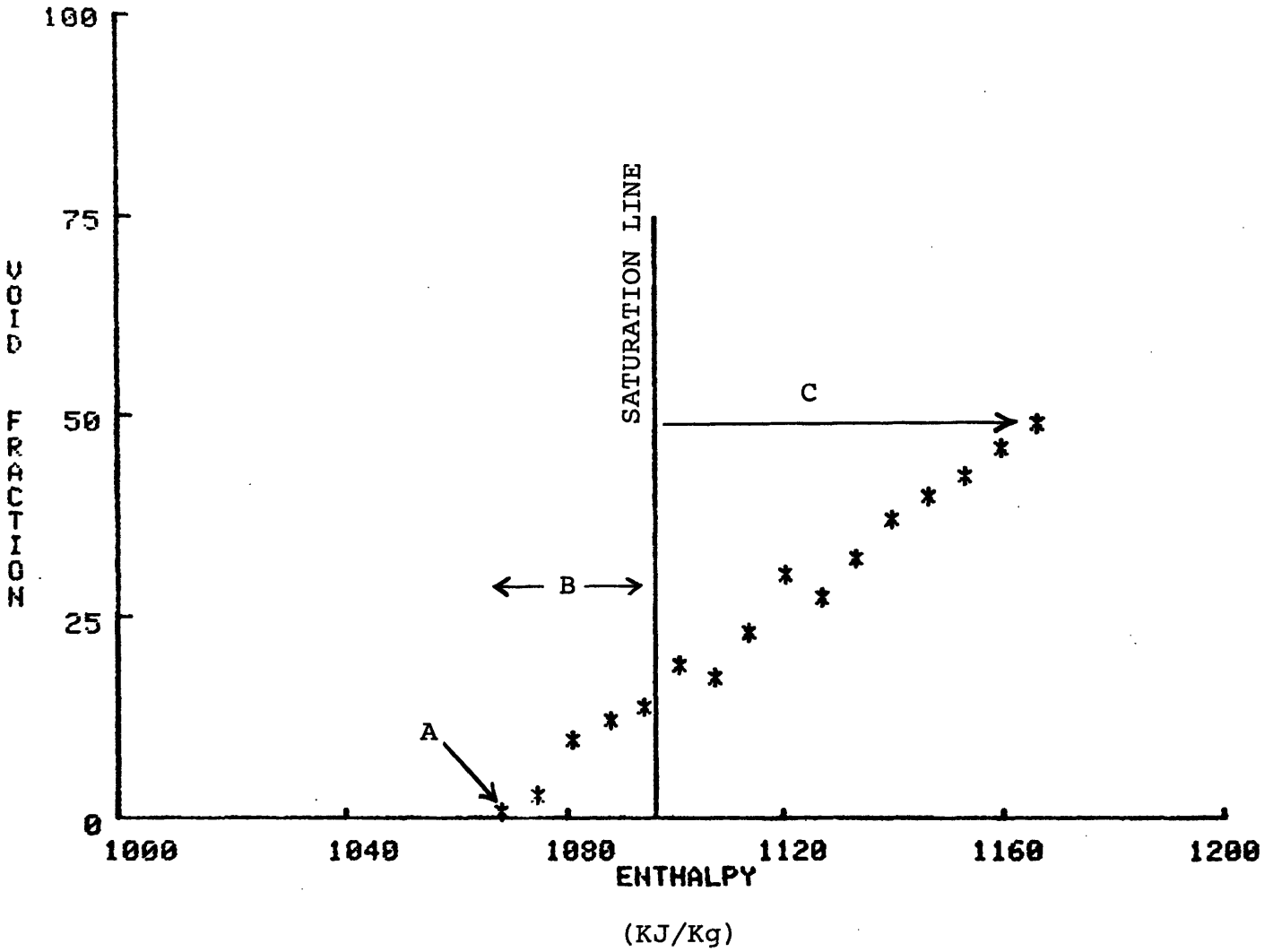

Figure 3.1 Typical Void Fraction versus Enthalpy Data

proper interpretation of the physical situation, the vapor generation rate and the interfacial momentum exchange rate can be evaluated using steady-state, one-dimensional void fraction data.

In the actual testing of THERMIT a large number of experimental cases have been used. In all cases, the subcooled boiling model described in Appendix A and the M.I.T. interfacial momentum exchange model described in Appendix B have been used. For many cases, the LASL interfacial momentum exchange model has also been employed in order to investigate the sensitivity of the results to this model. All of the comparison cases are presented in Appendix D and only a few examples are discussed here. Table 3.2 summarizes all the experiments used in this investigation.

The first experimental comparisons have been performed using the data of Maurer (12). These data have been taken for high pressure water (1200-2000 psia) with a variety of mass fluxes (0.4-4.0 Mlb/hr ft^2), and heat fluxes (0.1-1.2 MBtu/hr ft^2) in a 27 inch long rectangular test section (D_h = 0.18 inches). These data have been compared to THERMIT predictions and, overall, the agreement between the two is very good. As seen in Figure 3.2, the code predictions for this case are in good agreement over the entire boiling length. The start of boiling is predicted correctly as is the void fraction at high qualities. These trends are also observed for the other Maurer

TABLE 3.2

TEST CONDITIONS FOR ONE-DIMENSION STEADY-STATE DATA

Test	Pressure Range (psia)	Hydraulic Diameter (in)	Mass Flux Range (Mlb/hr ft^2)	Heat Flux Range (MBtu/hr ft^2)	Inlet Subcooling Range (Btu/lb)
Maurer	1200-1600	0.16	0.4 - 0.9	0.09 - 0.6	63 - 150
Christen-sen	400-1000	0.7	0.47-0.7	0.06 - 0.16	4 - 30
Marcha-terre	260-615	0.444	0.44 - 1.1	0.015-0.08	4 - 27
Bennett	1000	0.497	0.49-3.82	0.18-0.56	31 - 63

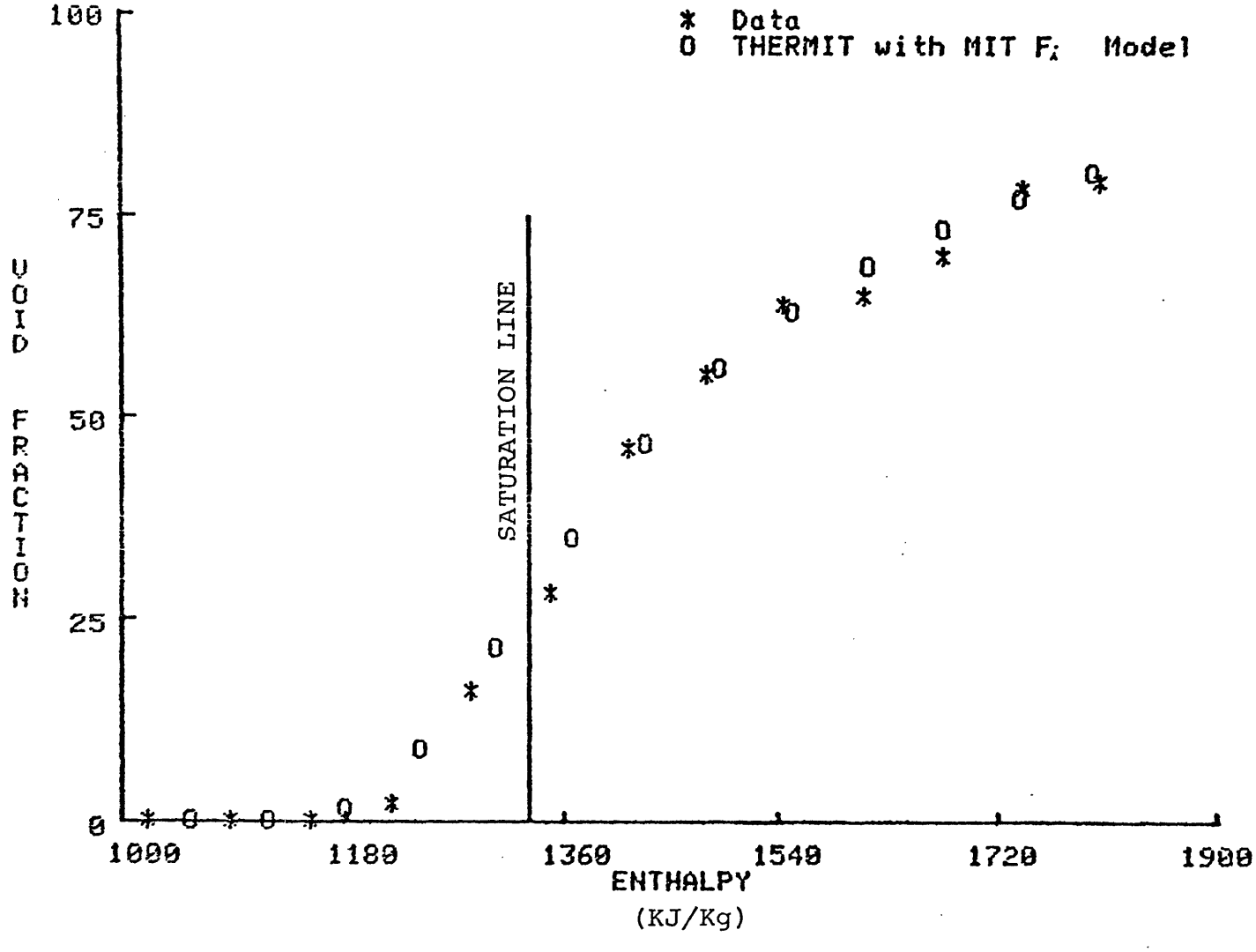

Figure 3.2 Void Fraction Versus Enthalpy - Maurer Case 214-3-5

cases which have been studied. Hence, the comparisons with this data would indicate that both the vapor generation model and the M.I.T. interfacial momentum exchange model are indeed correct.

However, the good agreement found in the above comparisons is not necessarily seen in all the cases which have been analyzed. For example, the comparisons between THERMIT and the data of Christensen (13) show some minor discrepencies. This data has been taken in a 50 inch rectangular test section (D_h = 0.7 inch) for a range pressures (400 - 1000 psia), mass fluxes (0.4 - 0.7 Mlb/hr ft^2) and heat fluxes (0.07 - 0.16 MBtu/ hr ft^2). A typical comparison curve is seen in Figure 3.3. In this case, the code predictions are in fairly good agreement with the data, although there are some differences. A second comparison case is shown in Figure 3.4. The only difference in test conditions between this case and the previous one is the amount of inlet subcooling. Yet, in this case the measurements are not well predicted by THERMIT over the entire boiling length. The start of boiling and the amount subcooled vapor production coincide with the data, but the void fraction at high qualities is underpredicted by THERMIT. However, a composite curve of both cases (Figure 3.5) shows that at high qualities the void fraction measurements show considerable scatter. This result indicates some type of dependency on the inlet subcooling. On the other hand, the THERMIT

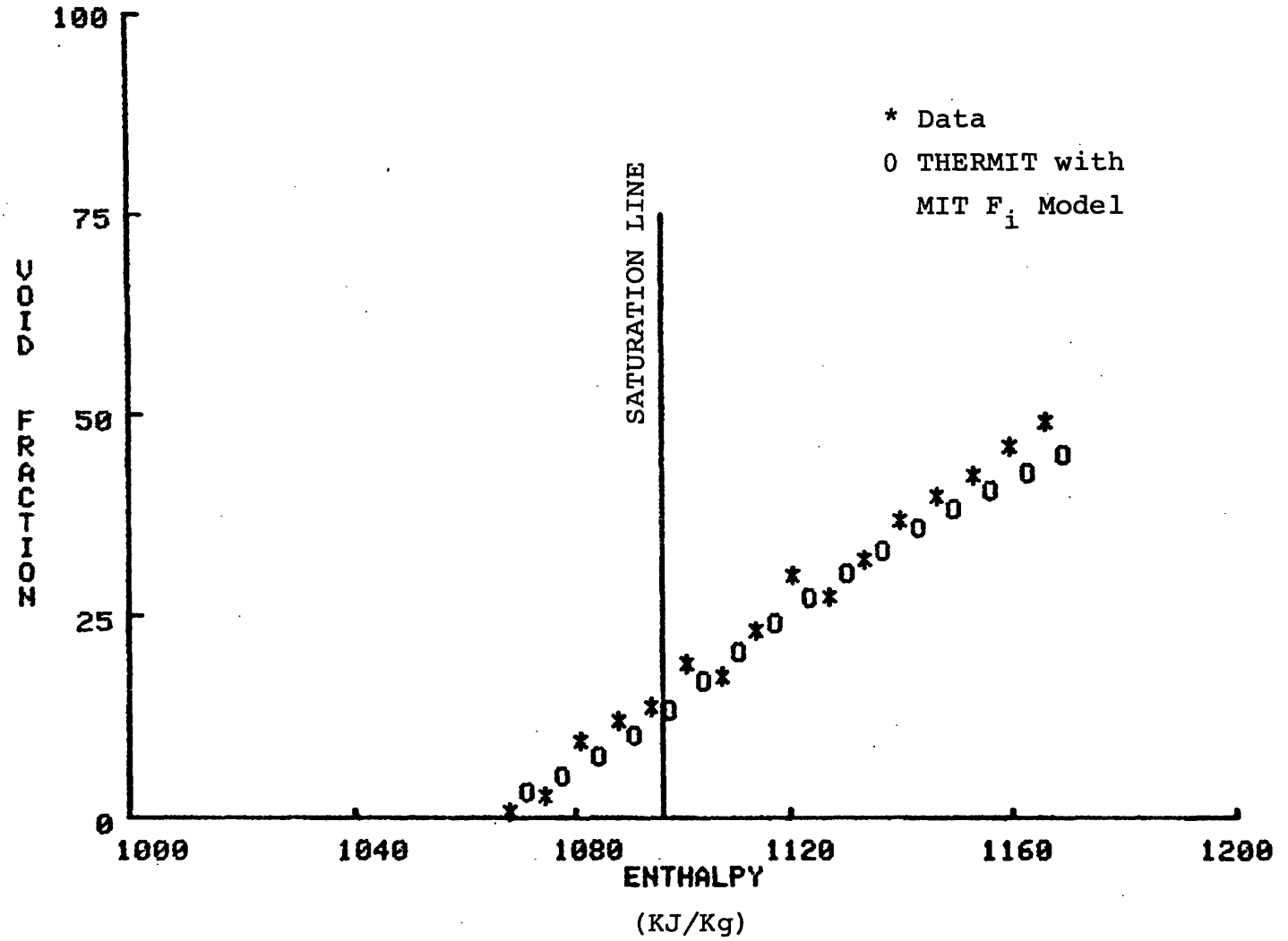

Figure 3.3 Void Fraction versus Enthalpy
Christensen Case 12

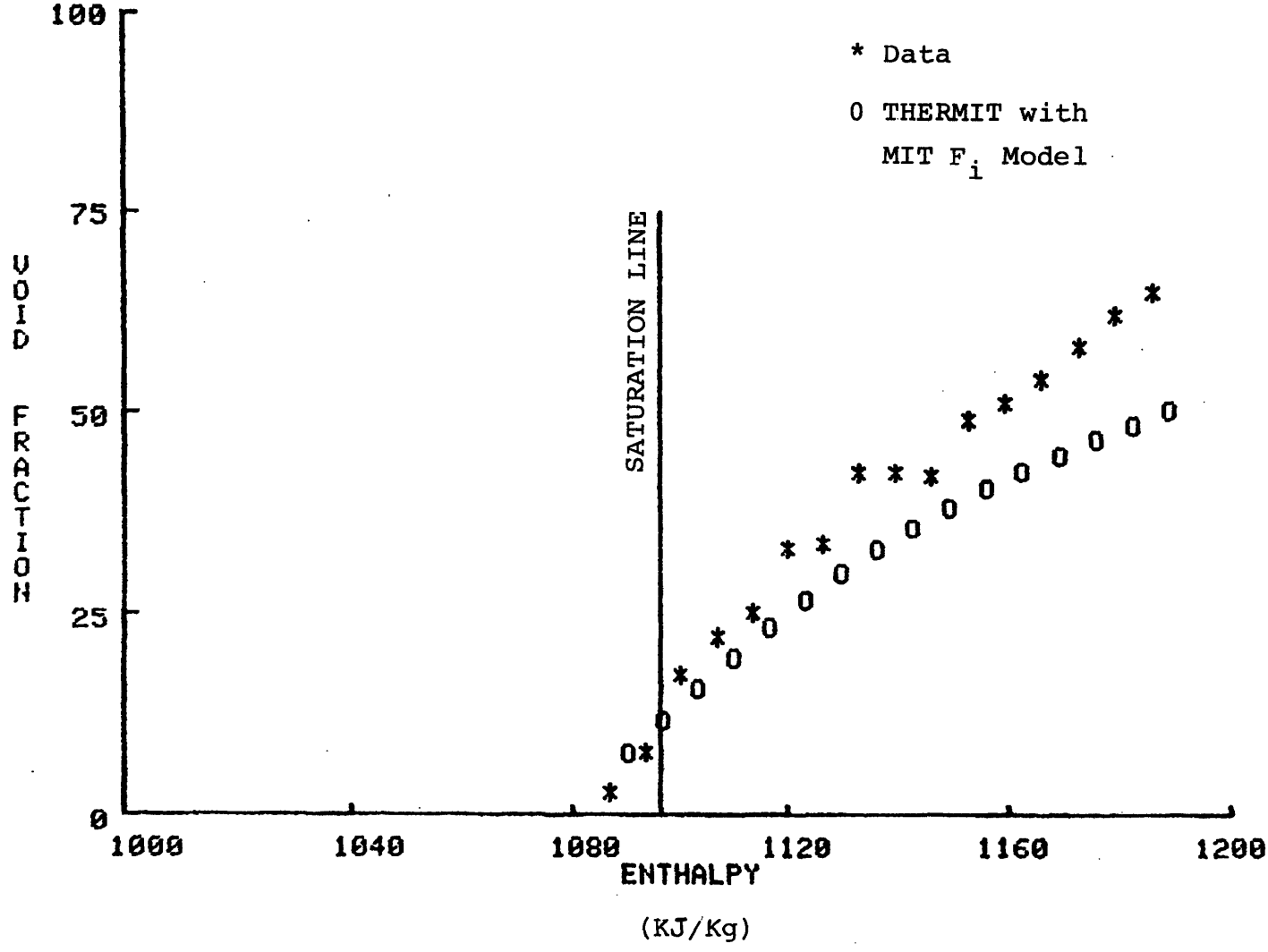

Figure 3.4 Void Fraction versus Enthalpy
Christensen Case 13

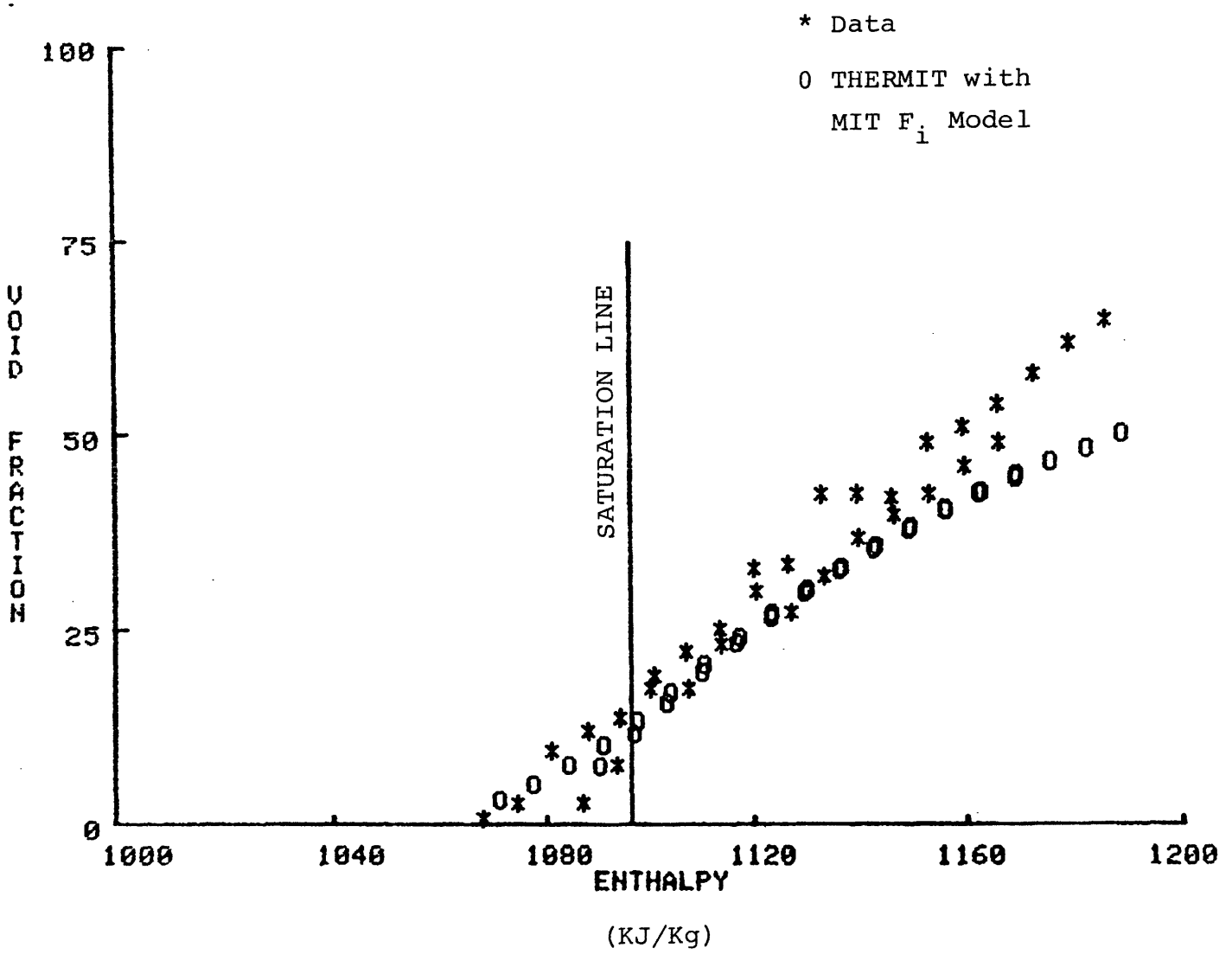

Figure 3.5 Void Fraction versus Enthalpy Composite of Chrsitensen Cases 12 and 13

predictions show no dependence on the inlet subcooling which is what one might expect. Hence, it is difficult to assess the correct high quality behavior based on this data alone.

A third set of measurements, those of Marchaterre (14), have also been compared with THERMIT. These measurements are for a 60 inch rectangular test section (D_h = 0.44 in.) with a range of pressures (160 - 600 psia), mass fluxes (0.6 - 1.1 Mlb/hr ft^2) and heat fluxes (0.04 - .25 MBtu/hr ft^2). The comparison of these data show results similar to those seen above. For example, as seen in Figure 3.6 the code predictions for this case are in good agreement with the data. However, for another case, seen in Figure 3.7, the predictions fall below the data. The agreement in this case is not as good at high qualities, but is still good at low qualities. Hence, the boiling inception point and the amount of subcooled boiling are predicted correctly, but the void fraction at high qualities tends to be underpredicted.

As discussed above, the void fraction at high qualities is a function of the interfacial momentum exchange rate. The above comparisons indicate that at high qualities the void fraction is too low or, in other words, the slip ratio, is too high. In order to lower the slip ratio, the interfacial momentum exchange rate needs to be increased. A simple comparison of the LASL model and the MIT model indicates that the LASL model predicts a transfer rate which is about a factor

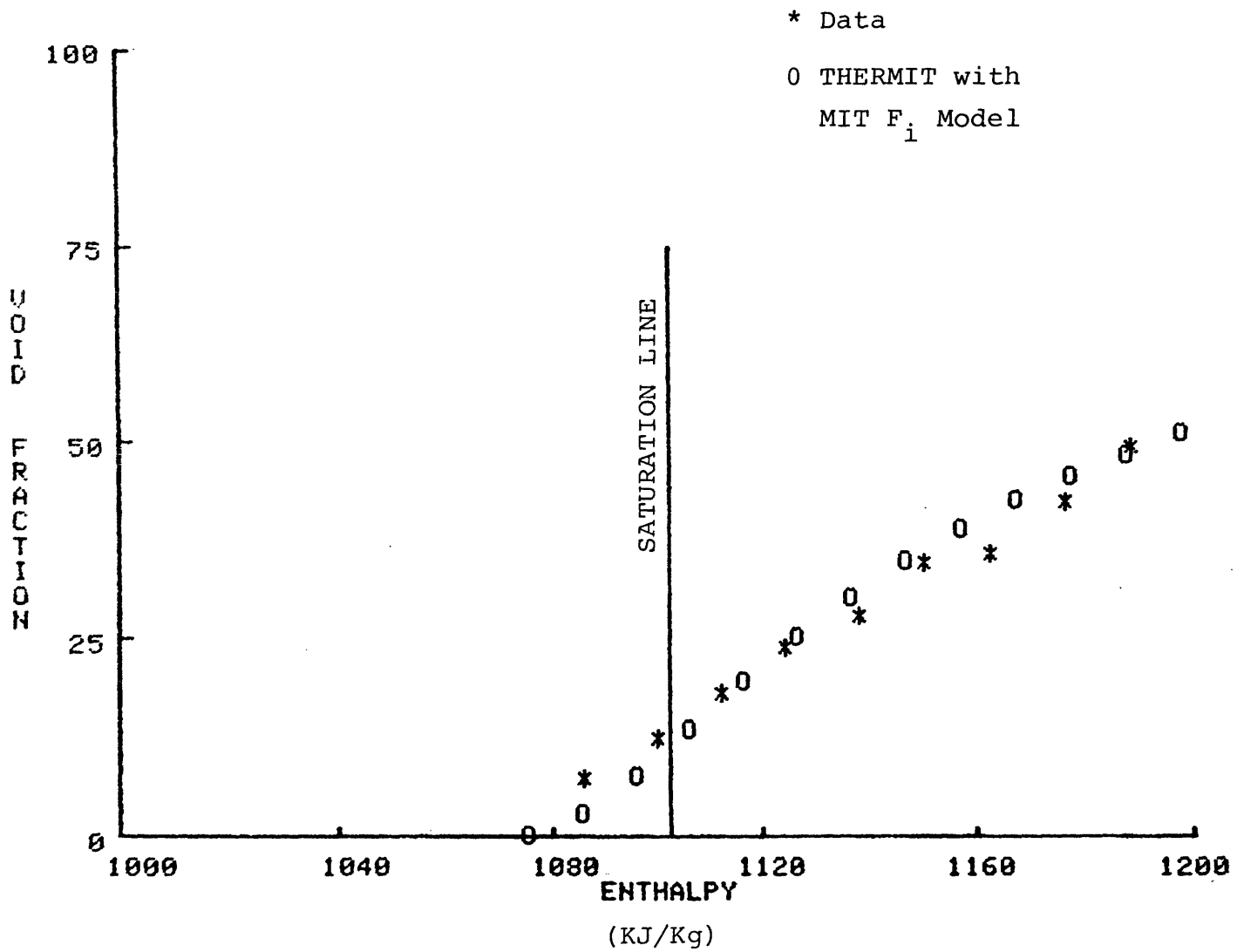

Figure 3.6 Void Fraction versus Enthalpy
Marchaterre Case 168

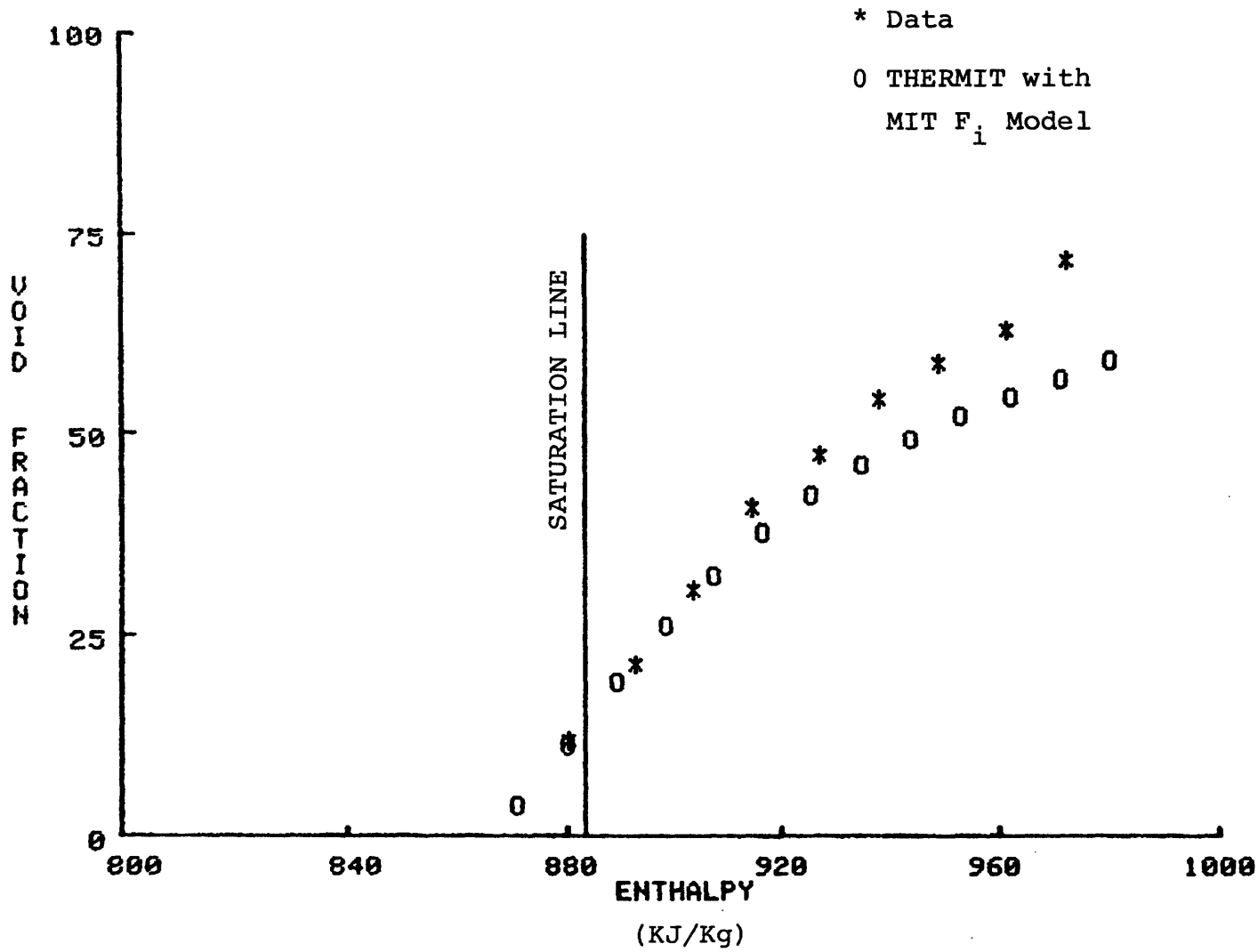

Figure 3.7 Void Fraction versus Enthalpy
Marchaterre Case 184

of 10 higher. Consequently, the Christensen and Marchaterre cases have also been analyzed using the LASL model in order to investigate the sensitivity of the void fraction predictions to this model (see Appendix D).

In general, the void fraction predictions with the LASL model are higher than the data at high qualities. This result, illustrated in Figure 3.8, shows that the data lies between the predictions using the LASL model and those using the M.I.T. model. At low qualities the void fraction predictions are nearly independent of the F_i model. Consequently, as expected, the interfacial momentum exchange rate only affects the void fraction at high qualities.

In order to assess the interfacial momentum exchange model, it is necessary to consolidate all of the data and then make a comparison with the code predictions. This process can be accomplished by plotting the superficial vapor velocity, J_v, versus the void fraction. A plot of this type is useful for comparing the data of a particular test section in which the pressure, flow rate and power have been varied. For example, all of Christensen's data are plotted in Figure 3.9. The data show a definite trend with a certain amount of scatter. The code predictions are included in Figure 3.10 and it is seen that the two interfacial momentum exchange models bracket the data. The M.I.T. model slightly underpredicts the void fraction while the LASL model overpredicts the void fraction.

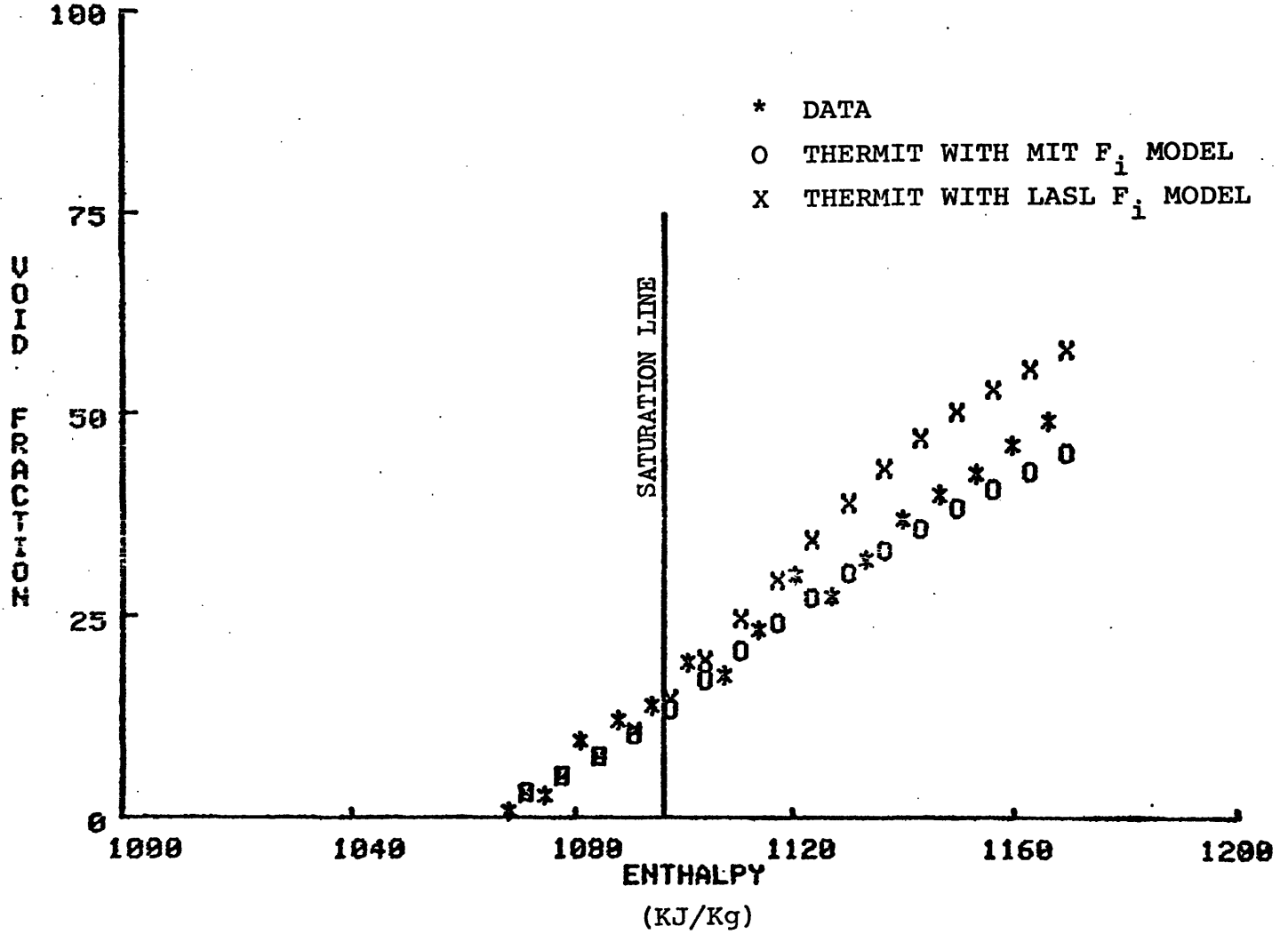

Figure 3.8 Void Fraction Versus Enthalpy - Christensen Case 12

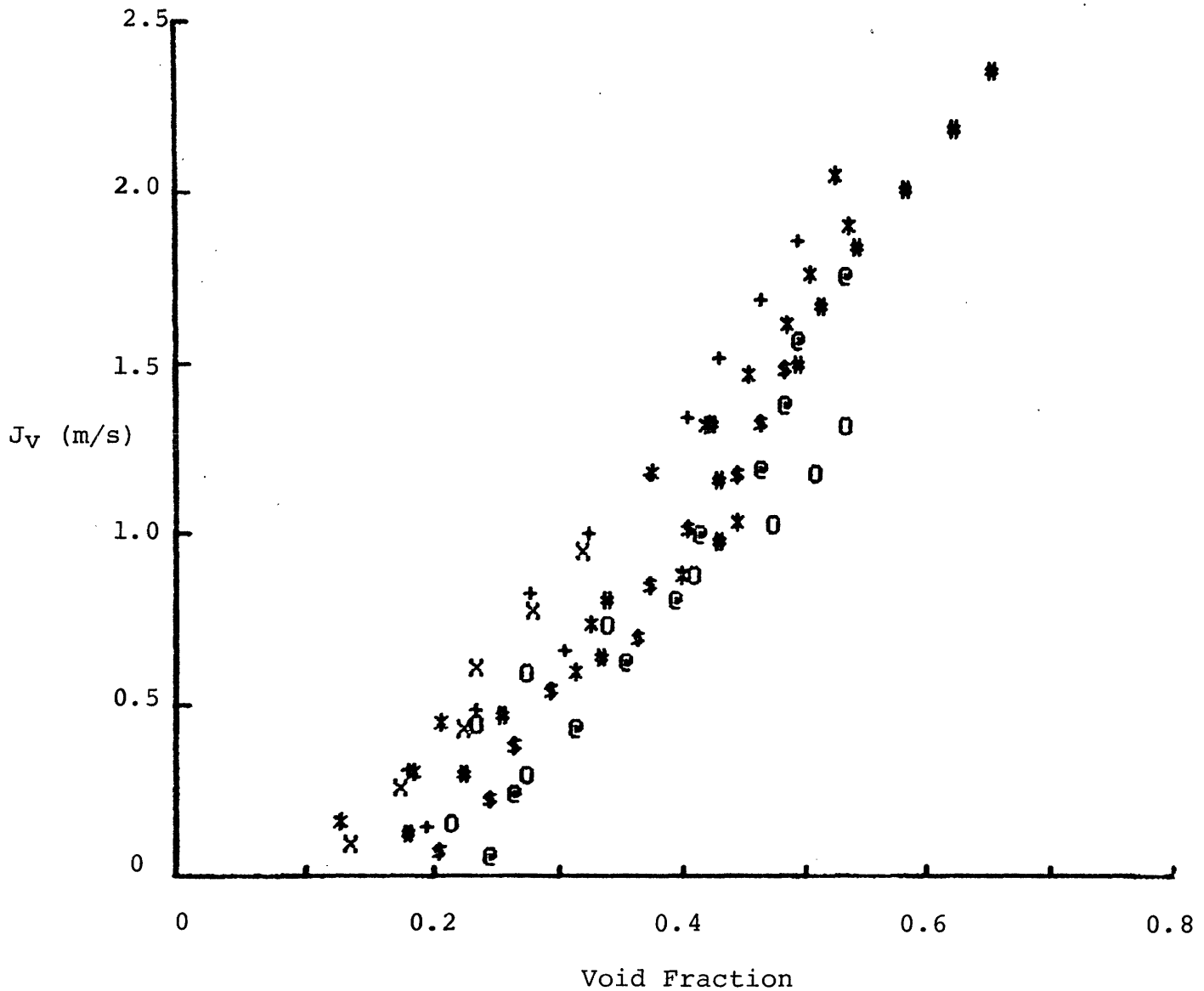

Figure 3.9 Vapor Superficial Velocity versus Void Fraction for Christensen Data.

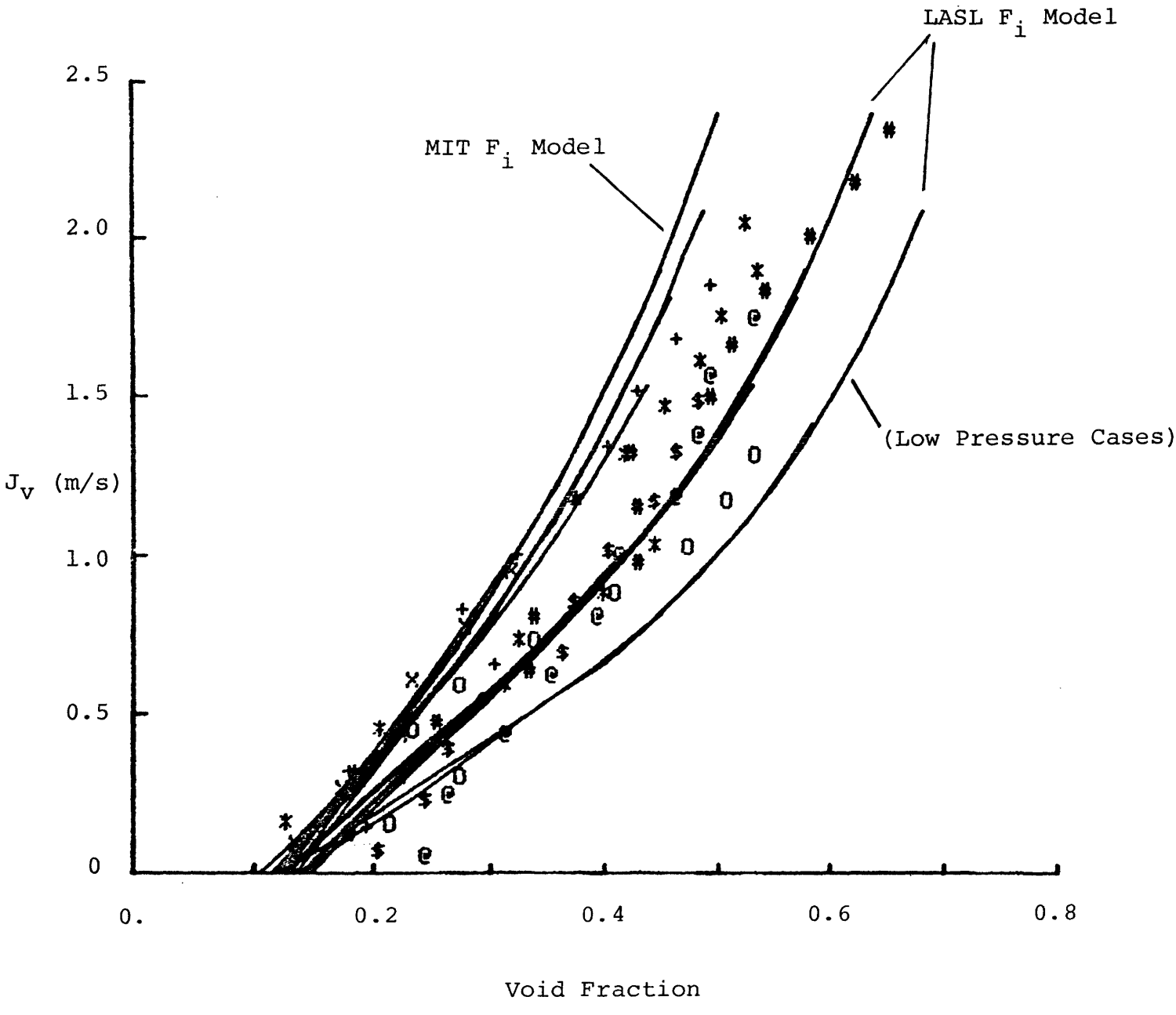

Figure 3.10 Vapor Superficial Velocity versus Void Fraction

Comparison of Data with THERMIT Predictions for Christensen Data.

Over the range of pressures (400 - 1000 psia) of these measurements, the M.I.T. model shows little sensitivity while the LASL model appears to be very sensitive to the pressure. Neither model could predict the scatter in the data, but each could be changed to lie closer to the majority of the data (i.e., the M.I.T. model could be increased or the LASL model decreased).

In summary, the following conclusions can be drawn from the one-dimensional void fraction comparisons. First of all, the vapor generation model is found to accurately predict the point of boiling incipience and the amount of subcooled vapor for the majority of the data. Consequently, this model requires little, if any, improvement. The second conclusion is that improvement is needed in the interfacial momentum exchange model. Either the M.I.T. model should be increased in value or the LASL model decreased in value. On the whole, the void fraction can be accurately predicted with THERMIT over the entire boiling length.

3.2.2 Clad Temperature Comparisons

The verification and assessment of the clad temperature predictive capabilities of THERMIT is the second step in the overall model evaluation strategy. The goal of this effort is to verify that the correlations in the heat transfer model accurately predict the clad temperature distribution when coupled to the fluid dynamics of THERMIT. This coupling arises

from the fact that the heat transfer correlations depend on the specific flow conditions. Hence, if THERMIT is predicting the correct flow conditions for a particular experiment, then the predicted clad temperatures should agree with the measured values provided the heat transfer correlations are valid. Therefore, this heat transfer model evaluation effort relies on the work discussed in the previous section insofar as it can be assumed that the flow conditions are accurately predicted. The THERMIT heat transfer model is a modified form of BEEST heat transfer model (10) which constructs a complete boiling curve. As summarized in Table 3.3, a total of 10 heat transfer regimes are identified which include both pre-CHF and post-CHF conditions. Therefore, measurements over this wide range of conditions are needed to evaluate the heat transfer model.

The predictions of THERMIT have been compared with the data of Bennett (15). These measurements cover both pre-CHF and post-CHF conditions and are, therefore, very useful for the present purposes. The data sets which have been used include a wide range of mass fluxes (0.5 to 3.8 Mlb/hr ft^2) and heat fluxes (0.1 to 0.5 MBtu/hr ft^2). In each case the system pressure is 1000 psia and the test section is a 220 inch tube (D_h = 0.5 inch) which is uniformly heated.

A total of 8 cases have been compared in this study. For each case the clad temperature measurements are compared to the code predictions. The complete set of comparison curves can be found in Appendix D, and only a few examples are discussed below.

TABLE 3.3

SUMMARY OF HEAT TRANSFER REGIMES

ihtr:	regime:	correlation:
1	Forced convection to single-phase liquid	Sieder
2	Natural convection to single-phase liqued	McAdams
3	Subcooled boiling	Chen
4	Nucleate boiling	Chen
5	Transition	Interpolation between q_{CHF} and q_{MSFB}
6	High P, high G film boiling	Groeneveld 5.7
7	Low P, high G film boiling	Modified Dittus-Boelter
8	Low G film boiling	Modified Bromley plus either McAdams vapor or high flow film boiling
9	Forced convection to single-phase vapor	Sieder-Tate
10	Natural convection to single-phase vapor	McAdams

For each case, there are two regions of major interest from the viewpoint of the heat transfer model. These regions are identified in Figure 3.11 for a typical data set. In the first region, I, the type of heat transfer is predominately nucleate boiling and, hence, measurements in this region can be used to validate the nucleate boiling heat transfer correlation. In the second region, II, either film boiling or single phase vapor are present and, consequently, the post-CHF heat transfer models can be evaluated in this region. The CHF correlation can also be verified by noting the location of the temperature excursion. Hence, the heat transfer model can be validated in three parts, i.e., pre-CHF, post-CHF and CHF location.

For example, the data of case 5394 are compared with THERMIT predictions in Figure 3.12. In the pre-CHF regime, the code consistently predicts a slightly larger value for the wall temperature than the data shows. This result indicates that the heat transfer coefficient is too low, but the error is well within the accuracy of the correlation. It is also seen that CHF is predicted to occur closer to the inlet than is actually observed. The difference in location of the CHF points is approximately 10% of the boiling length which again is within the limits of the CHF correlation. In the post-CHF region, the code predictions are in excellent agreement with the data. On the whole, the code can reasonably predict the wall temperatures for this case.

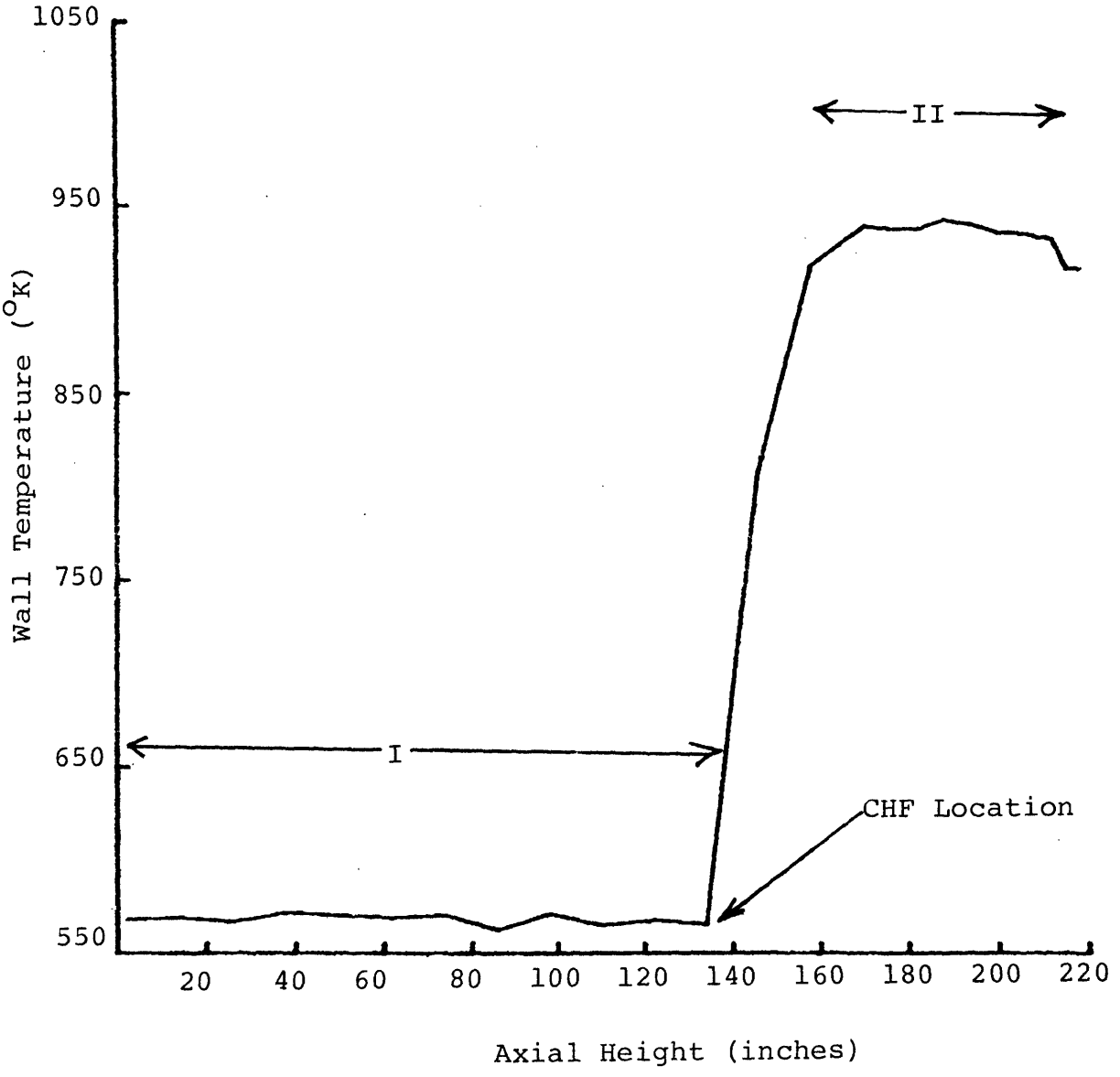

Figure 3.11 Typical Wall Temperature versus Axial Height Curve

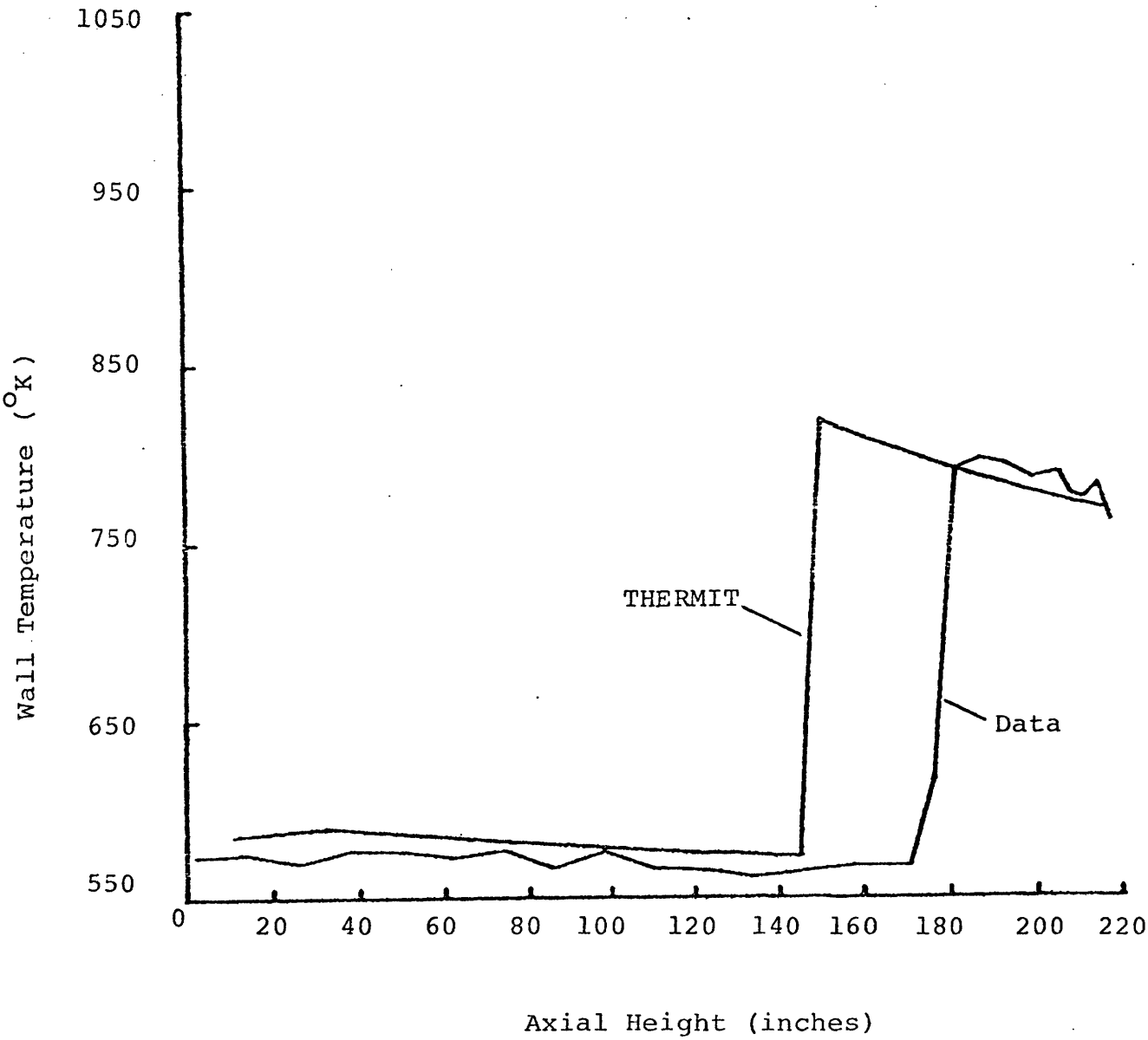

Figure 3.12 Wall Temperature versus Axial Height

Bennett Case 5394

A second comparison case is illustrated in Figure 3.13. Once again, THERMIT predicts both slightly higher wall temperatures in the nucleate boiling regime and an earlier occurrence of CHF. However, in the post-CHF regime the code does not accurately predict the wall temperatures. In this case, the heat transfer coefficient is too large except for a region near the exit. This result indicates that a problem may exist in the model and in particular the choice of the heat transfer correlation in this regime needs further evaluation.

The results of the 8 comparisons can be summarized as follows. In the nucleate boiling regime, the heat transfer model underpredicts the heat transfer coefficient and consequently, the wall temperature predictions are slightly larger than the data. Better agreement is found in this regime for cases with a lower mass flux. The CHF location is consistently predicted to occur earlier than the observed value and the error in this prediction is approximately 10%. An error of this magnitude is not excessive, but improvement can be sought. In the post-CHF regime, good to poor agreement is found between the predictions and the data. At low mass fluxes, the agreement is poor and this problem indicates an area which requires further study.

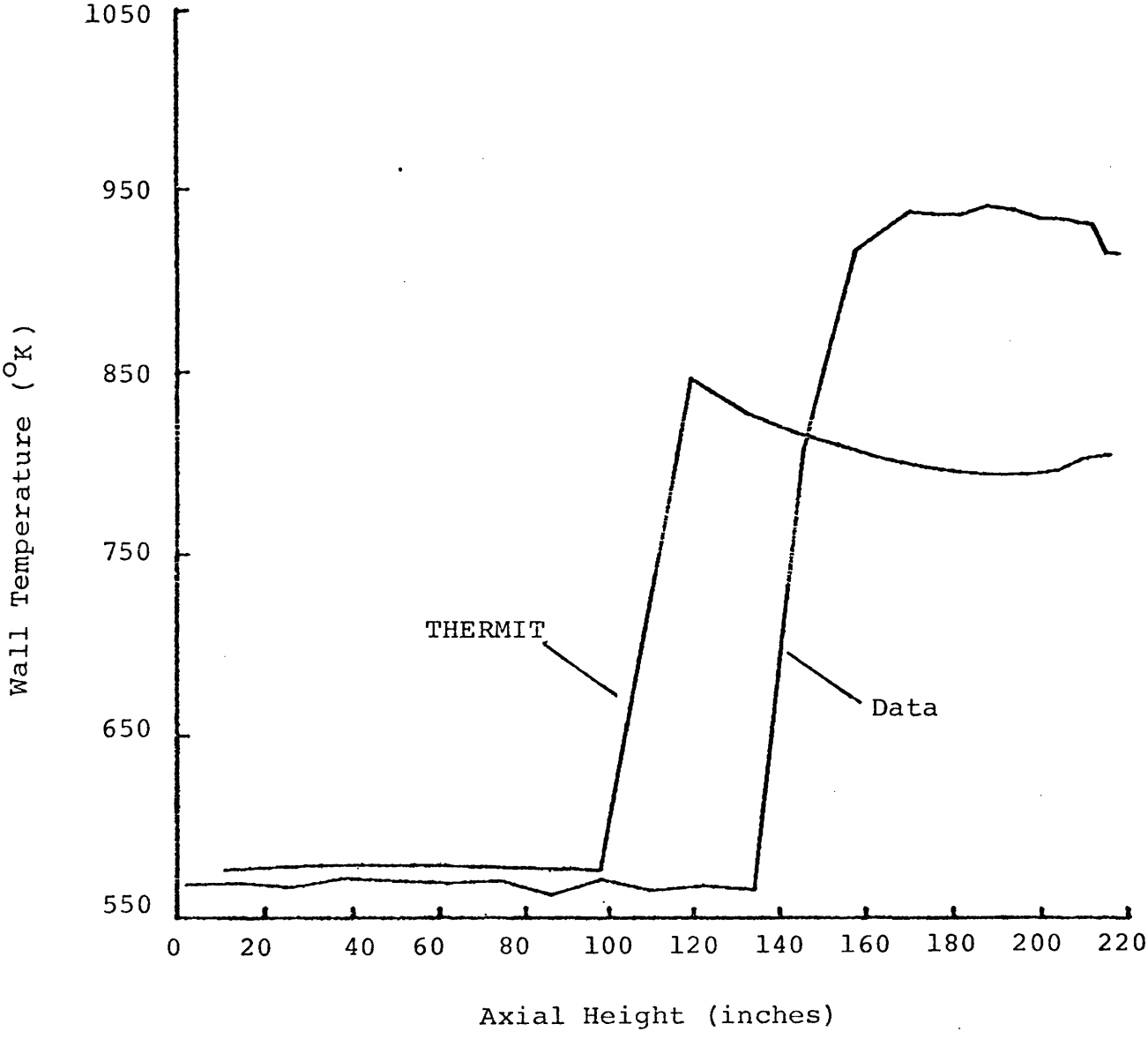

Figure 3.13 Wall Temperature versus Axial Height

Bennett Case 5273

3.3 Steady-State, Three-dimensional Comparisons

3.3.1 Isothermal Subchannel

In the previous section, the validation and assessment efforts using one-dimensional measurements have been discussed. These efforts have been directed towards evaluating the vapor generation model, the interfacial momentum exchange model and the heat transfer model. In this section, the three-dimensional modeling in THERMIT is evaluated using subchannel and core-wide measurements.

The first three-dimensional comparisons made in this evaluation program have been between THERMIT and isothermal subchannel measurements. These measurements consist of flow and pressure drop data for a 9 rod bundle (16). In this bundle, illustrated in Figure 3.14, the exit mass flux distribution as well as the overall pressure drop have been measured. Hence, this data is useful for evaluating the hydraulic modeling in THERMIT.

In these experiments, a uniform inlet velocity would be used and the resulting exit flow distribution and pressure drop would be measured. As seen in Figure 3.14, there are three types of subchannels in the bundle, i.e., edge, corner and center. Since the pressure drops across each channel are approximately equal, the differences in the hydraulic diameters of these channels lead to a driving force for flow redistribution. Opposing this force is the turbulent momentum exchange

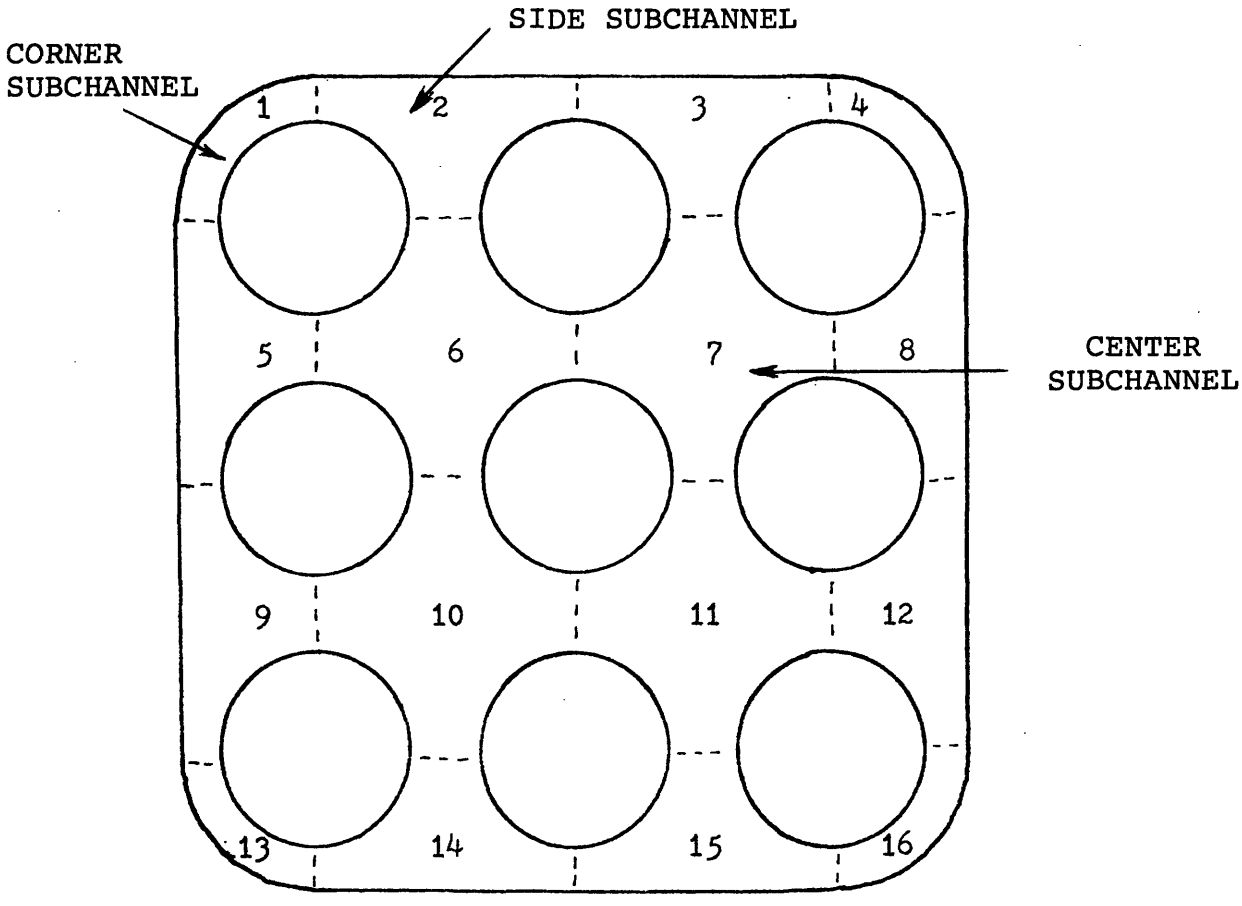

Geometrical Features

Number of Rods	9
Rod Diameter	0.570 inch
Rod-Rod Gap	0.168 inch
Rod-Wall Gap	0.135 inch
Radius of Corner	0.400 inch
Heated Length	72.0 inches

Figure 3.14 Schematic Drawing of 9 Rod Bundle Cross Section

along the channel boundaries which tends to homogenize the flow. Hence, the exit mass flux distribution represents an integration of these effects over the channel length.

Three test cases have been compared in this assessment with each case having a different inlet velocity. For each case, the friction factor has been adjusted in order to predict the correct pressure drop. The reason for performing this adjustment is that spacer pins have been used in the test section and these effectively increase the smooth tube friction by about 20%. With the pressure drop so adjusted, the code predictions of the exit mass flux distribution could be compared with the data.

The initial data comparisons show that THERMIT could not predict the exit flow distribution correctly. This lack of agreement would be expected, though, since THERMIT contains no turbulent mixing model. In fact, the THERMIT predictions are nearly identical to a simple model which can be derived assuming no mixing between subchannels. If equal pressure drops and no mixing are assumed, then the exit mass flux for the ith channel is given by

$$G_i = KD_{h_i}^{2/3} \tag{3.8}$$

The exit mass flux distribution can then be estimated, using the hydraulic diameters. If this distribution is calculated and compared to the THERMIT prediction it is found that the

two are in excellent agreement, but, of course, they do not agree with the data. Hence, the poor agreement between THERMIT and the data could be attributed to the lack of a turbulent mixing model in THERMIT.

In view of this shortcoming, a simple single-phase turbulent mixing model has been added to THERMIT. This model is similar to that found in COBRA IV and is described as follows. The pressure gradient due to turbulent mixing, $\partial P/\partial z)_{tm}$, is given by

$$\left.\frac{\partial P}{\partial z}\right)_{tm_i} = \sum_j w'_{ij}\left(\frac{V_j - V_i}{A_i}\right) \qquad (3.9)$$

where

V_i = axial velocity in channel i

V_j = axial velocity in channel j

A_i = axial flow area in channel i

w'_{ij} = turbulent mixing rate between channels i and j

The mixing rate, w'_{ij}, is then given by

$$w'_{ij} = 2\beta\, S_{ij}\left[\frac{G_i A_i + G_j A_j}{A_i + A_j}\right] \qquad (3.10)$$

Where

S_{ij} = gap width between channels i and j

β = mixing parameter

G = axial mass flux

The mixing parameter, β, is an empirical constant which depends on the geometry and flow conditions. Limiting values for β are zero, which means no mixing, and infinity which means infinite mixing. Typically, though, the values of β range from 10^{-3} to 10^{-1}.

This mixing model has been implemented in order to verify that the discrepancies in the THERMIT predictions were, in fact, due to the lack of a mixing model. Consequently, for each test case, three THERMIT runs have been made. The first run uses $\beta = 0$ (no mixing) which is actually the non-modified version of THERMIT. The second and third runs use $\beta = 0.003$ and $\beta = 0.03$, respectively, so that a range of mixing rates is covered. The results of these runs are compared with the data and the $D_h^{2/3}$ model in Table 3.4.

A number of observations can be made from these comparisons. First of all, it is seen that, without a mixing model, the THERMIT predictions are nearly the same as those calculated using the $D_h^{2/3}$ relationship. Secondly, it is seen that for each case the data lies within the range of the two mixing limits (i.e., $\beta = 0.003$ and $\beta = 0.03$). At lower velocities (cases 1C and 1D) the data shows that the mixing parameter

TABLE 3.4

SINGLE-PHASE DATA COMPARISONS FOR GE 9 ROD BUNDLE

CASE 1C	G_1	Δ%	G_2	Δ%	G_6	Δ%
Data (G_{ave} = 1343)	951	-	1274	-	1560	-
No Mixing ($D_h^{2/3}$)	901	-5%	1251	-2%	1572	+1%
THERMIT (β = 0)	926	-3%	1259	-1%	1607	+3%
THERMIT (β = 0.003)	958	+1%	1266	-1%	1589	+2%
THERMIT (β = 0.03)	1091	+14%	1284	+1%	1506	-3%

CASE 1D	G_1	Δ%	G_2	Δ%	G_6	Δ%
Data (G_{ave} = 2048)	1485	-	1954	-	2292	-
No Mixing ($D_h^{2/3}$)	1374	-8%	1907	-3%	2398	+5%
THERMIT (β = 0)	1399	-6%	1906	-3%	2435	+6%
THERMIT (β = 0.003)	1455	-2%	1916	-2%	2408	+5%
THERMIT (β = 0.03)	1662	+12%	1941	-1%	2270	-1%

CASE 1E	G_1	Δ%	G_2	Δ%	G_6	Δ%
Data (G_{ave} = 2672)	2197	-	2591	-	2970	-
No Mixing ($D_h^{2/3}$)	1792	-19%	2487	-4%	3128	+5%
THERMIT (β = 0)	1829	-17%	2491	-4%	3182	+7%
THERMIT (β = 0.003)	1901	-14%	2497	-4%	3136	+6%
THERMIT (β = 0.03)	2204	+0.3%	2565	-1%	2988	+0.6%

should be near the lower limit while at high velocities (case 1E) the mixing parameter should be near the upper limit. Finally, it is seen that the single-phase data can be correctly predicted by THERMIT if the effects of turbulent mixing are included.

3.3.2 Heated Subchannel Data

The test section illustrated in Figure 3.14 has also been operated with the heated rods. Both uniform and non-uniform radial power distributions have been used and the non-uniform peaking pattern is seen in Figure 3.15. For these tests, the overall pressure drop, exit mass flux distribution, and exit quality distribution have been measured for a variety of flow rates and power levels. These data can be used to evaluate the three-dimensional thermal - hydraulic modeling.

Comparisons have been made between the non-uniform radial power cases and THERMIT predictions. In these cases, measurements have been made in the following five subchannels:

a) hot corner (subchannel 1),

b) hot edge (subchannel 2),

c) hot corner (subchannel 6),

d) cold edge (subchannel 15), and

e) cold corner (subchannel 16).

Two cases have been studied in detail. These are runs 3E1 and 3E2 which have average exit qualities of 0.035 and 0.10, respectively. Hence, both of these cases should yield

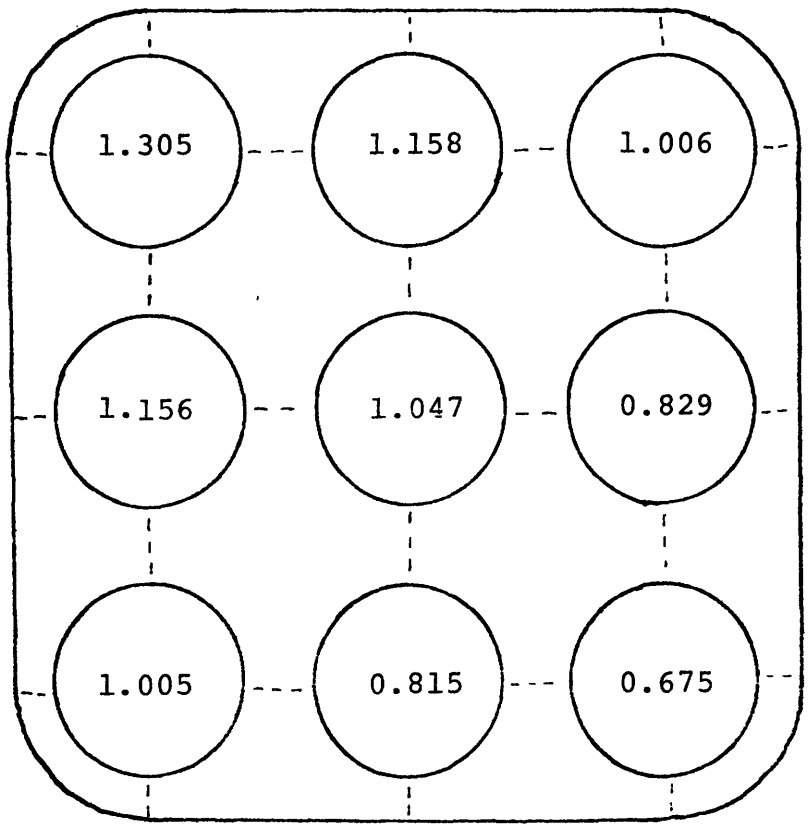

Figure 3.15 Radial Peaking Factors for Non-Uniformly Heated Case

representative data for two-phase flow in a rod bundle which can be used to evaluate THERMIT.

However, since THERMIT does not contain a two-phase mixing model, one would not expect THERMIT to accurately predict the data. The comparisons with tests 3E1 and 3E2 illustrate this point. In each case, the exit mass flux in the hot corner subchannel is too low while the exit quality is too high. Conversely, in the hot center subchannel, the exit mass flux is too high and the exit quality is too low. Deviations in the mass flux distribution are on the order of 10% which indicates the magnitude of the two-phase mixing. Lahey and Moody (17) have discussed the observed data trends and state that the required two-phase mixing must include both the turbulent mixing and vapor diffusion phenomena. Consequently, meaningful comparisons can only be made if a two-phase mixing model is added to THERMIT.

Nevertheless, these experiments have been simulated with THERMIT in order to evaluate the sensitivity of the current models for multi-dimensional applications. This sensitivity becomes an important factor in the effort to develop a two-phase mixing model. This effort is an ongoing activity at present and an adequate two-phase mixing model is expected to be formulated in the second phase of the THERMIT development under this program.

Consequently, for these two cases (3E1 and 3E2) a sensitivity study has been performed. This study has concentrated

on determining the effect of the transverse flow modeling on the exit qualities and flow rates. By varying the geometric and empirical constants used in the transverse flow modeling and, then, observing the net effect, the sensitivity of the predictions to these constants could be determined. A large number of tests have been performed and the results of these are discussed below.

The one parameter with the greatest effect on the exit quantities is the transverse flow area. One choice for these areas would be the actual geometric area between subchannels which is the minimum area in the transverse direction. However, in order to have consistency between the mass equation and the momentum equations, it is necessary that the volume averaged area in the transverse direction be used. If the geometric area is used instead of the average area, then the exit qualities and mass fluxes are greatly different. For example, in case 3E1 with non-averaged areas the exit quality is 58% higher in the hot corner while the exit mass flux is 28% lower in this subchannel. This change is not in the direction of the data. Hence, from both a numerical and a data comparison point of view volume averaged transverse flow areas should be chosen in modeling the transverse flow.

Aside from this parameter, variations in the other modeling have not shown any major effects. For example, the transverse friction factor has been increased by 25% and the net result of this change is to alter the flow and quality

distributions by less than 1%. In another case, the transverse friction has been eliminated which leads to 2% change in the distributions. Neither of these changes provide the driving force needed to predict the data. Hence, the trends in the data cannot be reproduced by simply modifying the transverse momentum equation and, therefore, the axial momentum equation must be modified to include the effects of two-phase mixing.

The overall conclusion which can be drawn from these two-phase comparisons is that, without a two-phase mixing model, THERMIT cannot accurately predict the flow and quality distributions in subchannel geometry. As in the single-phase case, it appears that turbulent mixing effects create a driving force for flow redistribution. An additional redistribution force in the two-phase case is created by the tendency of the vapor to diffuse to the open areas in the test section (i.e., vapor diffusion phenomena). Hence, any mixing model must account for both of these processes.

Additionally, it has been found that the code predictions are very sensitive to the transverse flow areas. However, based on the derivation of the THERMIT equations it is clear that volume averaged transverse flow areas should be used (see Appendix D of reference 1).

A final conclusion of this study is that the code predictions are only slightly sensitive to the transverse friction modeling. This result is most likely due to the fact that the

rod to rod gap spacing is relatively large in BWR bundles. Consequently, transverse pressure gradients are essentially non-existant. Nevertheless, the effects of this modeling may become important when a two-phase mixing model is included in THERMIT.

3.3.3 Core Exit Temperature Measurements

A measured exit temperature distribution of the Maine Yankee reactor has been compared to the predictions of THERMIT. For this case, core-wide modeling has been used in THERMIT so that each assembly is modeled as a single channel. Due to symmetry, only 1/8 of the core has been analyzed. Typical values for the power distribution and geometrical data have also been used. With this modeling, the calculated exit temperatures in each assembly could be compared with the measured values in order to further assess the three-dimensional predictive capabilities of THERMIT.

Comparisons of the data and code predictions can be seen in Figure 3.16. The measured versus predicted core temperature rises are in fairly good agreement. Since a uniform inlet temperature is assumed, these temperature rises are directly related to the exit temperatures. It is seen that a majority of the data lie within 5 °F of the corresponding predictions. Considering the accuracy of the thermocouple measurements and uncertainties in the power distribution, this agreement is quite good. Hence, THERMIT is able to accurately predict the core-wide exit temperature distribution.

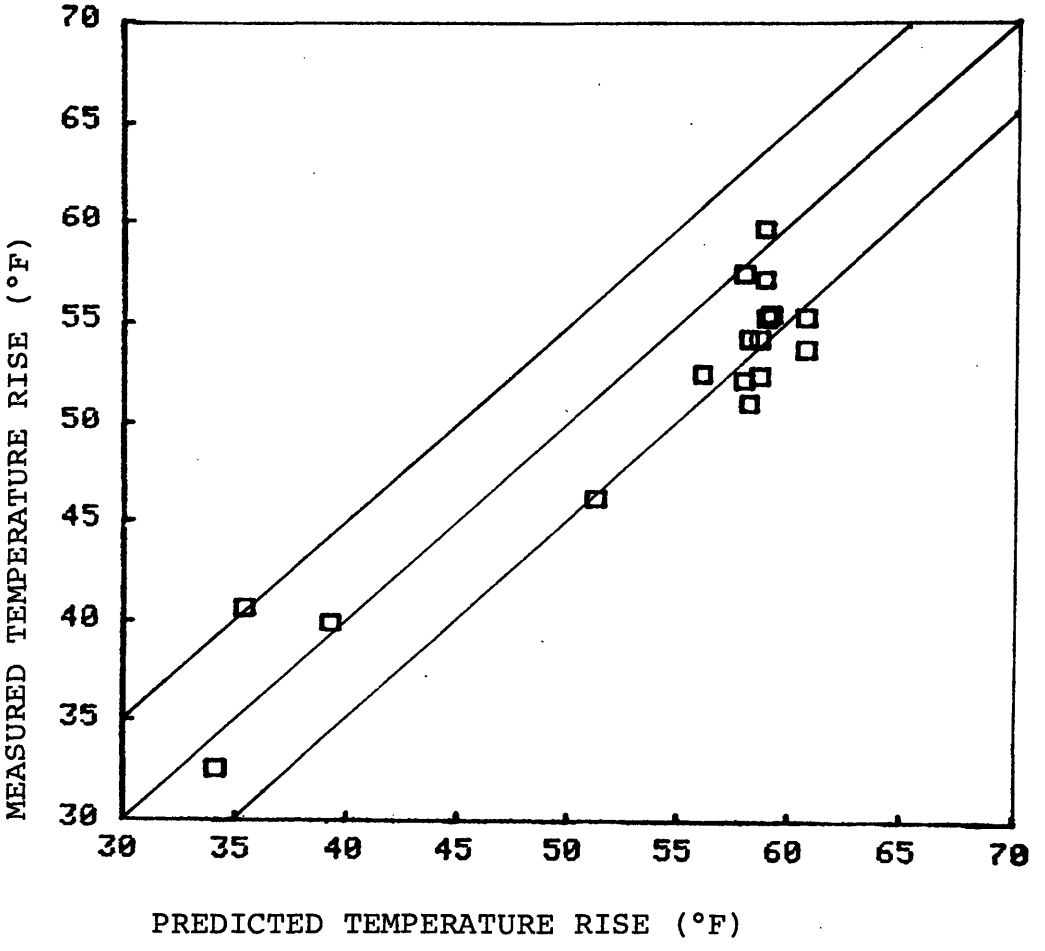

Figure 3.16 Measured Versus Predicted Coolant Temperature Rises Maine Yankee 1/8 Core Analysis.

For this case, COBRA IV has also been used to analyze the data and its predictions are compared to THERMIT. As seen in Figure 3.17, the agreement between the two codes is quite good. A maximum difference of 3 °F between the predictions of the two codes is found and 90% of the differences are less than 2 °F. Since COBRA IV is thought to accurately predict single-phase flow conditions, the good correspondence between the two codes illustrates that THERMIT can accurately predict single-phase flow conditions.

3.4 Transient One-Dimensional Comparisons

The first test of the transient capabilities of THERMIT has been performed using a one-dimensional blowdown test. In this test, Edwards (18) has measured the pressure-time history in a horizontal pipe during rapid depressurization. The pipe has an inner diameter of 0.0732 m and a length of 4.1 m and initially contains subcooled water (T = 504 °K) at 6.9 MPa. At time t = 0, one end of the pipe is rapidly opened and the water depressurizes. Pressure measurements at seven locations along the pipe have been taken during the course of the transient (0.6 sec in duration).

These measurements have been compared with THERMIT predictions for this blowdown test. In modeling this problem with THERMIT the following features have been employed. First of all, the Nigmatulin vapor generation model is used in this analysis. This model predicts vapor generation due to flashing

				567.3 568.5 -1.2	574.4 574.6 -0.2
	566.1 567.3 -1.2	576.7 576.0 +0.7	583.3 582.2 +1.1	591.3 587.9 +3.4	589.4 587.2 +2.2
571.1 571.1 0.0	587.6 584.1 +3.5	588.2 586.0 +2.2	587.5 586.3 +1.2	591.6 589.6 +2.0	589.5 588.3 +1.2
589.2 588.3 +1.1	590.8 589.0 +1.8	589.3 588.2 +1.1	591.3 589.3 +2.0	589.0 588.2 +0.8	591.0 589.3 +1.7
	590.0 589.1 +0.9	592.9 591.0 +1.9	588.9 588.2 +0.7	591.9 589.8 +2.1	588.7 587.8 +0.9
		588.7 587.5 +1.2	589.9 588.4 +1.5	587.9 587.3 +0.6	591.1 589.2 +1.9
			587.3 586.3 +1.0	590.3 588.4 +1.9	587.6 586.8 +0.8
				587.2 586.3 +0.9	590.0 588.2 +1.8
					587.1 586.0 +1.1

KEY

THERMIT
COBRA IV
DIFFERENCE

Temperatures in °F

Figure 3.17 Comparison of THERMIT and COBRA IV Exit Temperature Predictions - Maine Yankee 1/8 Core Analysis.

which is the type of boiling in this test. The second feature concerns the modeling of the frictional loss in the tube. No specific break-flow multiplier is used as is required in other codes. A rough tube friction factor correlation is also used since at very high Reynold's numbers ($>10^6$) the smooth tube correlation is not accurate. The Levy two-phase flow multiplier is employed for two-phase conditions. The final feature of the modeling concerns the nodal representation of the pipe. Twenty-three non-uniform nodes have been used as can be seen in Figure 3.18. The location of each measuring station is at the center of its corresponding node.

With these modeling features, THERMIT has been used to calculate the pressure-time history for this blowdown case. In the actual measurements, two time periods of interest are identified. The first is the 0 - 15 msec period in which the pressure wave propagates along the pipe. The second period is the 15 - 600 msec period in which the pressure decreases in a more or less smooth manner. Comparisons of THERMIT during the short time period indicate that the pressure wave is propagated too rapidly. This trend has also been observed by Rivard & Torrey (9) who suggest that the vapor generation model controls the pressure wave propagation velocity. With the Nigmatulin model, they find the same behavior as observed here, but with a conduction controlled model better agreement is found. This conduction controlled model has not been implemented into THERMIT, since the short term behavior is not as critical as the long term behavior.

Figure 3.18

Schematic Drawing of Edwards' Blowdown Pipe

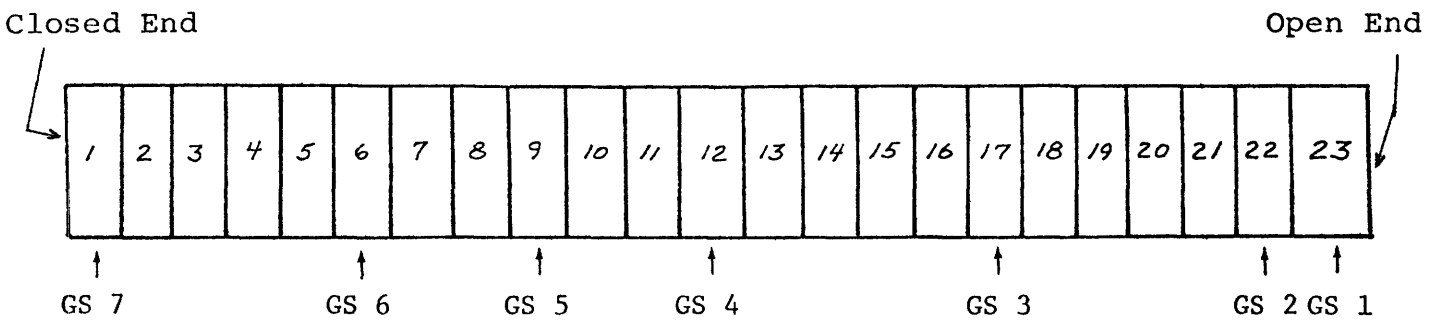

Notes:

1. Pipe Diameter = 0.073 m
2. Pipe Length = 4.1 m
3. Initial Pressure = 6.9 MPa
4. Initial Temperature = 504 K
5. Break Area reduced by 10-15% over nominal area
6. Pressure Transducers located at each Gauge Station (GS 1 - 7)
7. Noding Deatils:

Node Length (m)	Node Number
0.158	1, 6, 9, 12, 17, 22
0.16295	2, 3, 4, 5, 18, 19, 20, 21
0.18825	13, 14, 15, 16
0.1985	7, 8, 10, 11
0.247	23

The comparisons for the long term behavior (illustrated in Figure 3.19) show that THERMIT can predict reasonably well the pressure distribution. The agreement is very good in the middle of the pipe (GS 4 and GS 5) but is only adequate at either the closed end (GS 7) or near the open end (GS 2). The effect of using a smooth tube friction factor correlation is also illustrated. It is seen that the depressurization rate is overpredicted when the smooth tube correlation is used. With the rough wall correlation the rate of depressurization is in much better agreement with measurements.

In these comparisons, the sensitivity of the code predictions to the node sizes or to the inlet temperature distribution have not been investigated. These modeling changes would certainly have some impact on the code predictions and would probably improve the results. However, the intent of this analysis has been to assess the transient capabilities of THERMIT. Consequently, perfect agreement between the code and measurements is not an immediate goal. Rather this analysis has attempted to show that THERMIT can analyze depressurization transients provided proper models are selected. In particular, the vapor generation model is important for calculating the pressure wave propagation and the axial friction model controls the long term rate of depressurization.

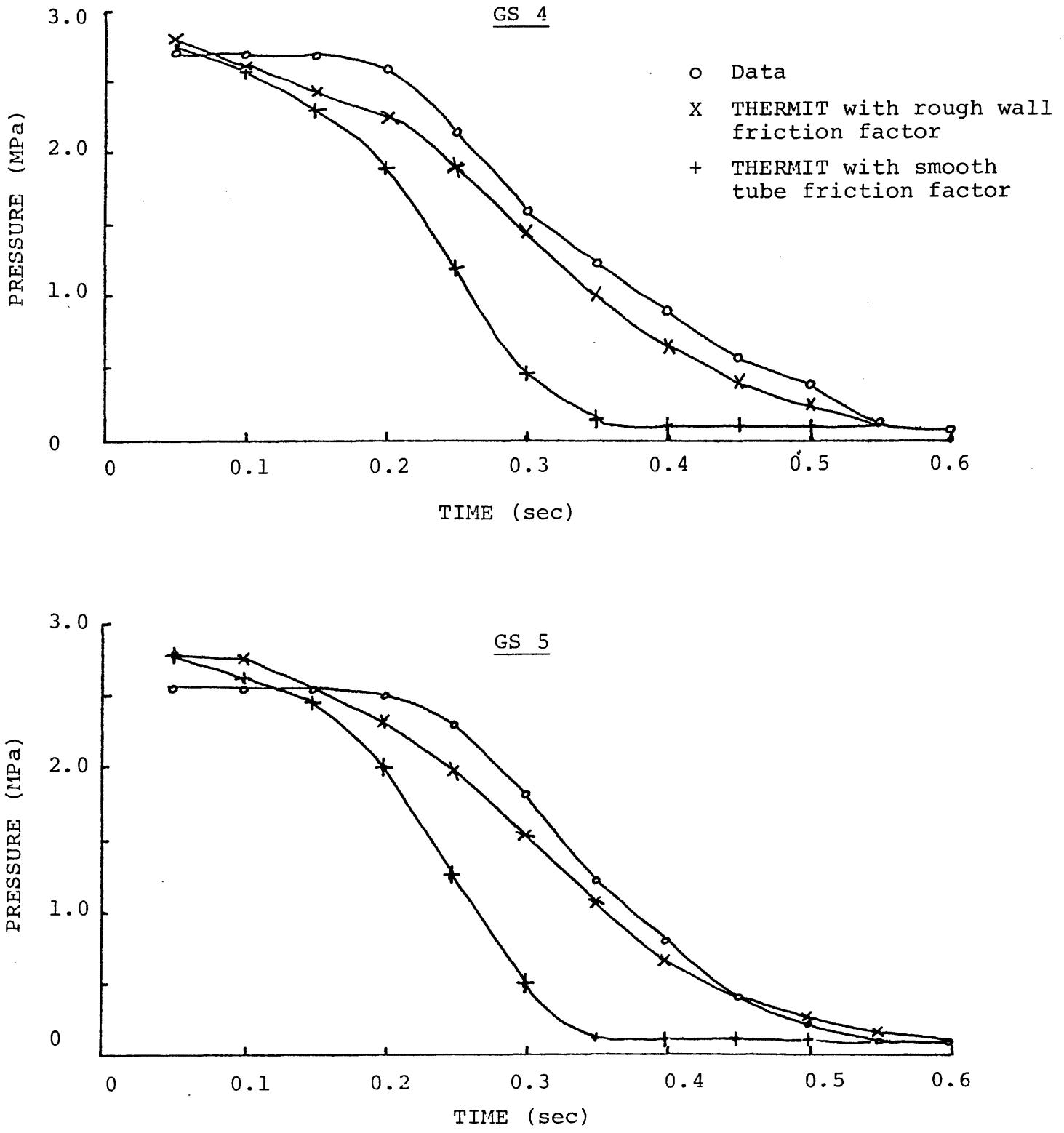

Figure 3.19 Pressure-Time Histories for Edwards Pipe Blowdown Test. (a - GS 4, b - GS 5, c - GS 7, d - GS2)

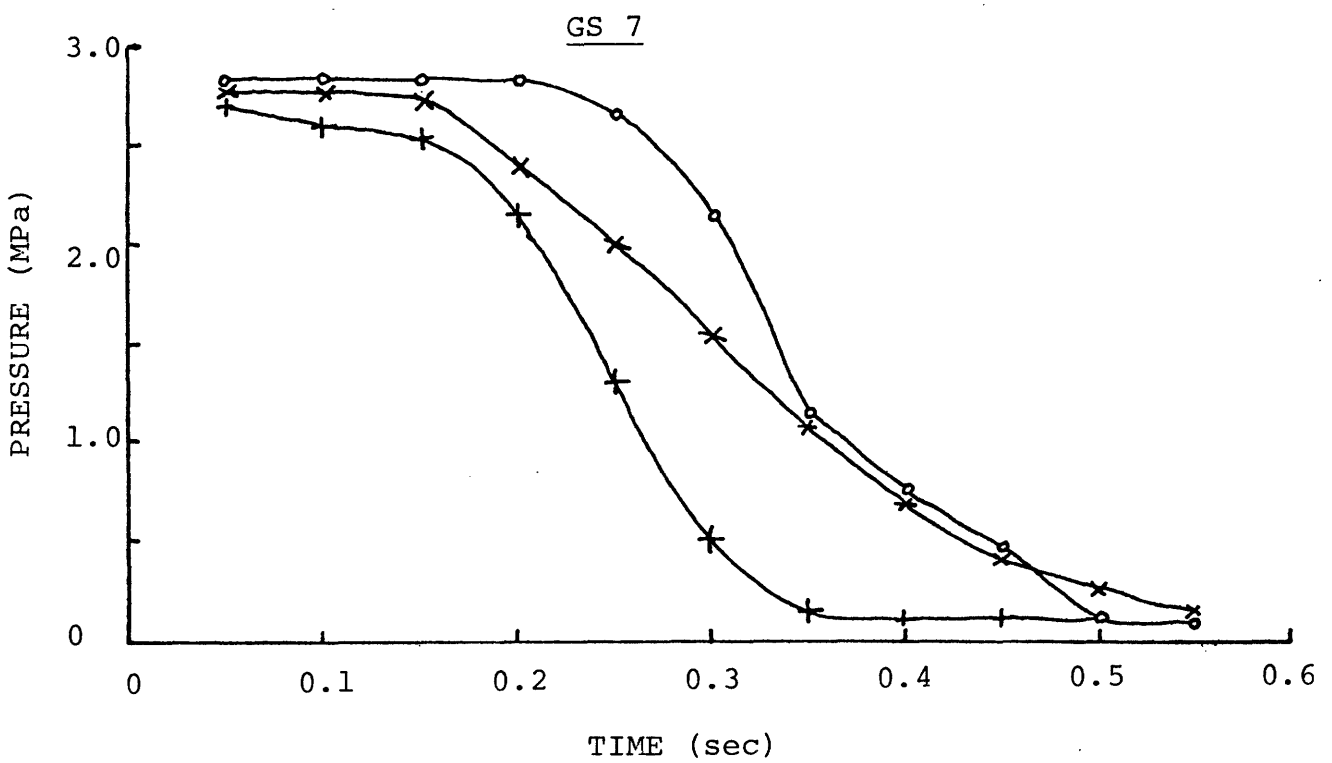

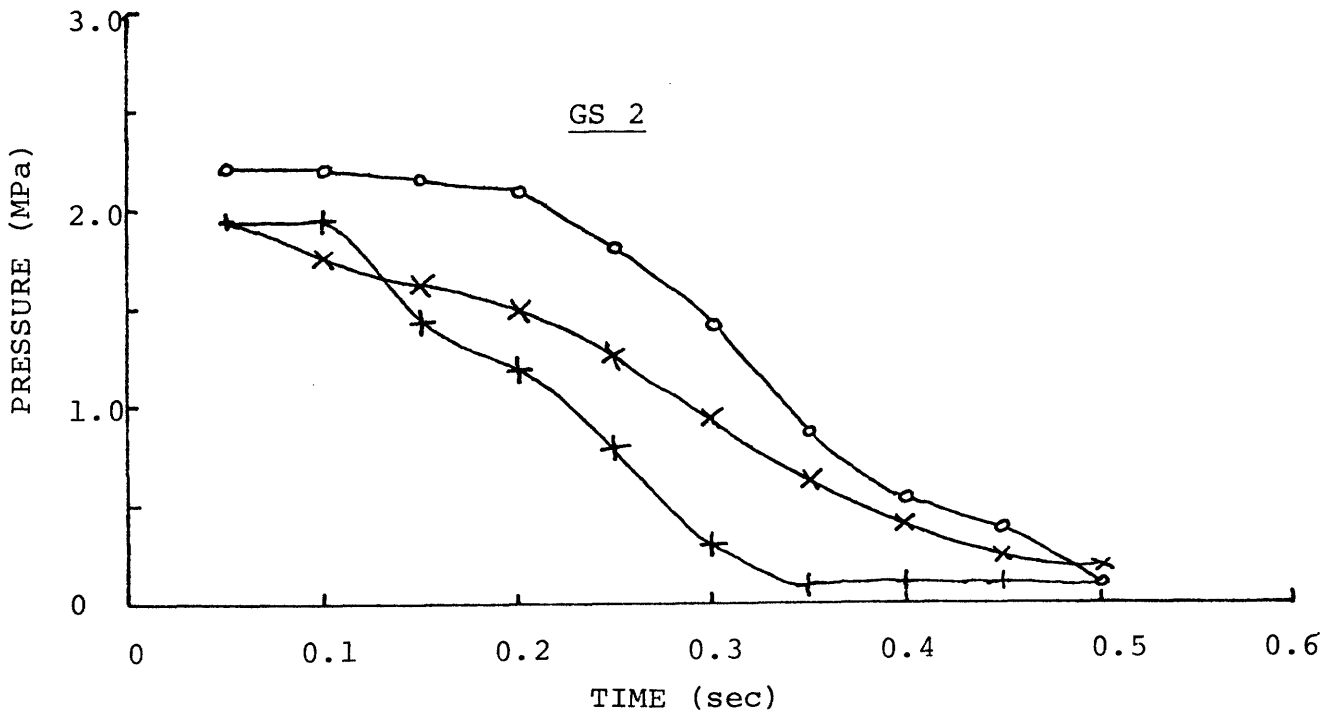

Figure 3.19 (Continued)

3.5 Transient Multidimensional Comparisons

3.5.1 Rod Ejection Accident

Since very few experimental measurements are available for multidimensional transient experiments, alternative means for evaluating the multi-dimensional transient capabilities of THERMIT are needed. One possible way to assess these capabilities is to compare the predictions of THERMIT with those of another code (e.g., COBRA-IV). This method has been used by making comparisons between THERMIT and COBRA-IV for simplified transients simulating rod ejection events in LWR's.

Two such transients have been analyzed with both COBRA-IV and THERMIT. In these cases, two assemblies, each modeled as a channel, with large radial peaking (3:1) between the channels and a uniform axial power distribution have been used. The initial conditions are different for each case with the first case starting from a Hot Zero Power (HZP) condition and the second starting from a low flow, low power condition. The transient is initiated by rapidly increasing the power (heat generation rate) which simulates the rod ejection and, then, due to Doppler feedback effects the power is shut off. The power-time history is illustrated in Figure 3.20 and the initial conditions for each case are summarized in Table 3.5. These two transients have been analyzed with both THERMIT and COBRA IV and their predictions are compared in the following sections.

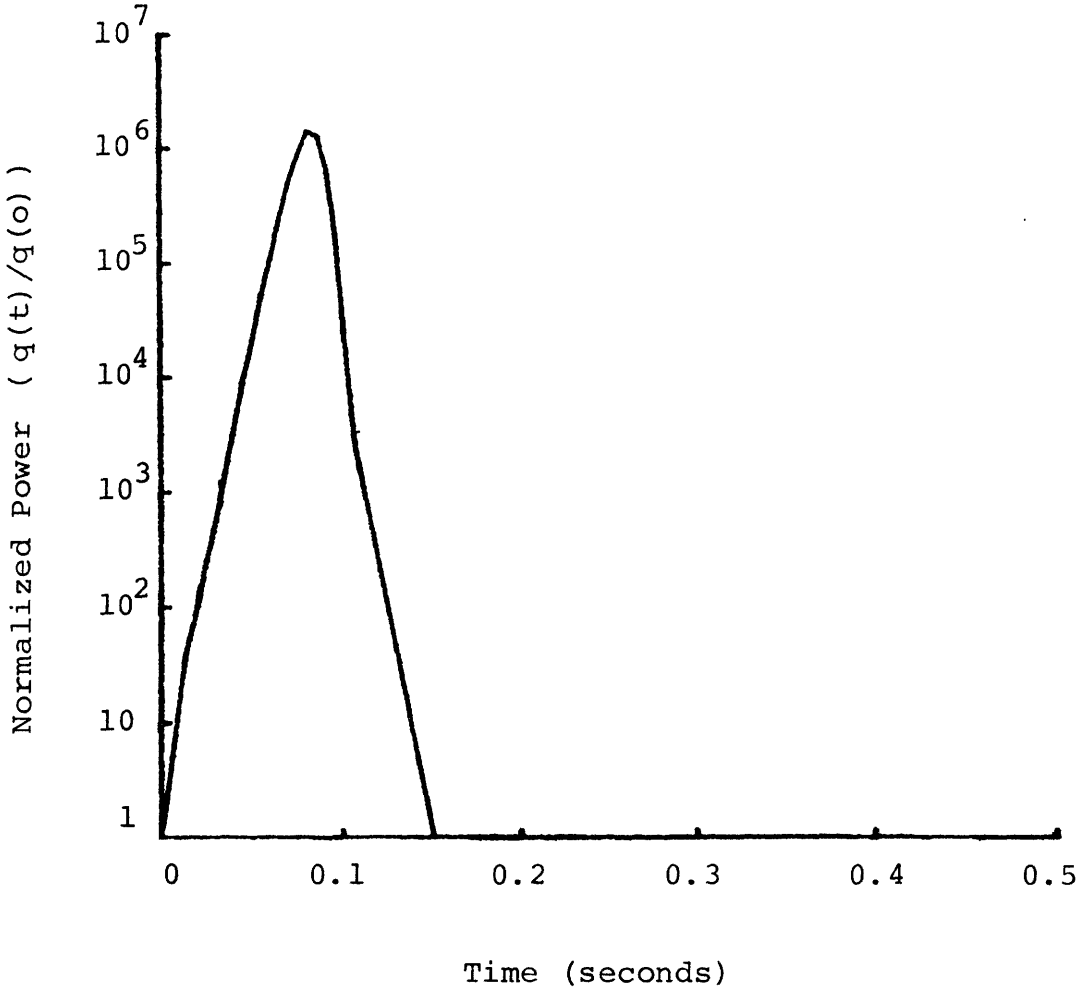

Figure 3.20 Normalized Transient Power Distribution Used in Rod Ejection Accident Cases.

TABLE 3.5

INITIAL CONDITIONS FOR ROD EJECTION TRANSIENTS

	Hot Zero Power Case	Low Flow Low Power Case
Initial Power per Assembly (kw)	8.05	29.2
Inlet Mass Flux (kg/m^2 sec)	3363.	272.
Inlet Temperature (K)	608.3	608.3
System Pressure (MPa)	144.8	144.8
Flow Area per Assembly (m^2)	0.0209	0.0209

3.5.2 Hot Zero Power Initial Condition Case

The first comparison of the two codes is for the rod ejection transient initiated from a hot zero power condition. For this case, the initial power is essentially zero, but the flow rate is the full power value.

The power excursion does not lead to flow reversal and overall the transient is not very severe. The clad temperatures increase slightly and subcooled boiling is predicted to occur during the transient. The COBRA-IV (implicit) and THERMIT predictions of these parameters have been compared and are discussed below.

The maximum clad temperature predictions during the transient are compared in Figure 3.21. It is seen that, in the first part of the transient, the two codes are in excellent agreement. However, during the later stages, there is a difference of about 7 °F between the predictions of the two codes. These differences are due to the fact that the heat transfer and fuel pin models are not the same in both codes. Consequently, some differences would be expected so that the above differences are not excessive

The void fraction predictions during this transient are illustrated in Figure 3.22. THERMIT predicts boiling to occur earlier than COBRA-IV. Overall, the two codes are in good agreement. This good agreement occurs in spite of the fact that the void fraction calculational methods are different in each

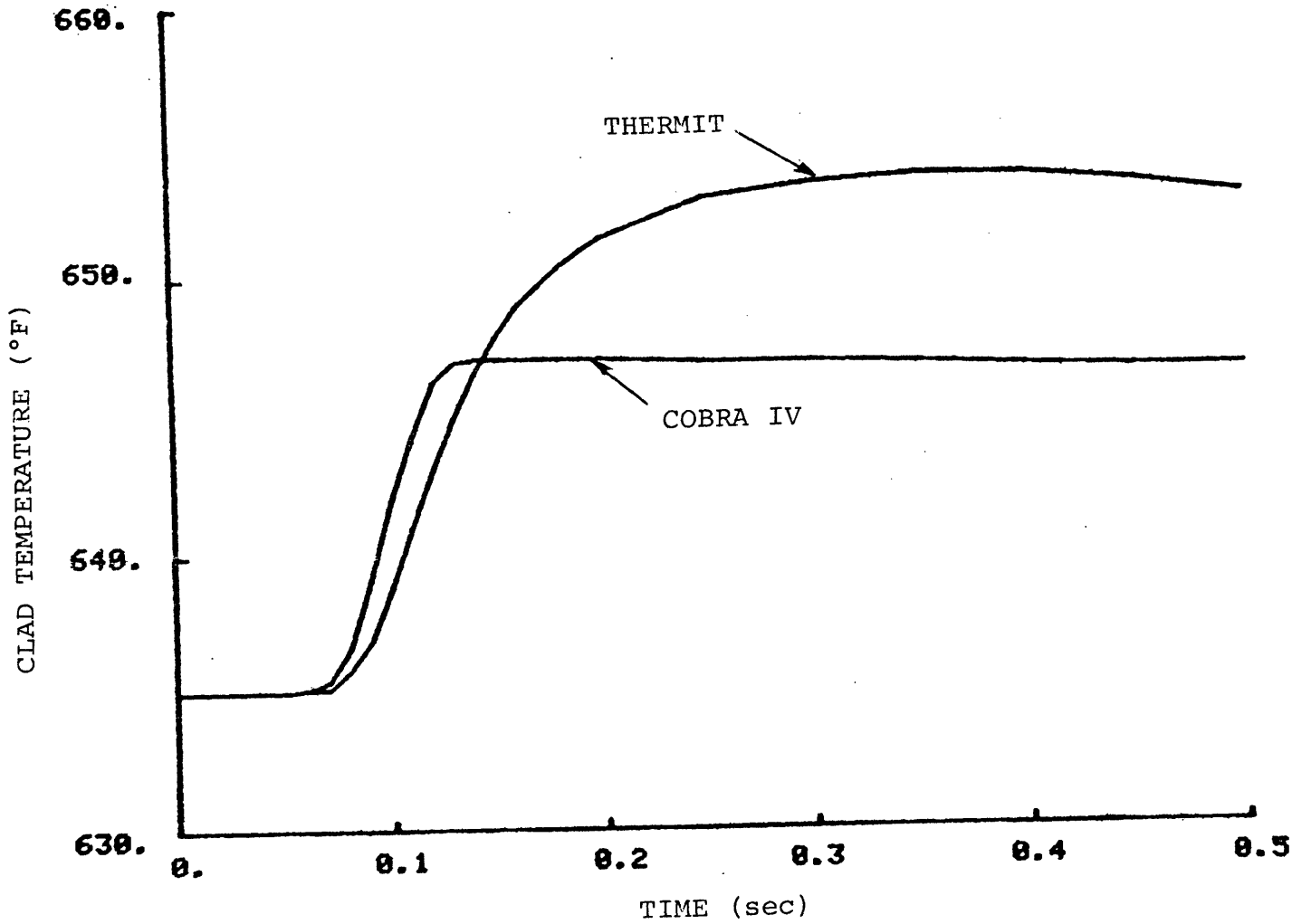

Figure 3.21 Clad Temperature Versus Time - Rod Ejection Accident from HZP Condition.

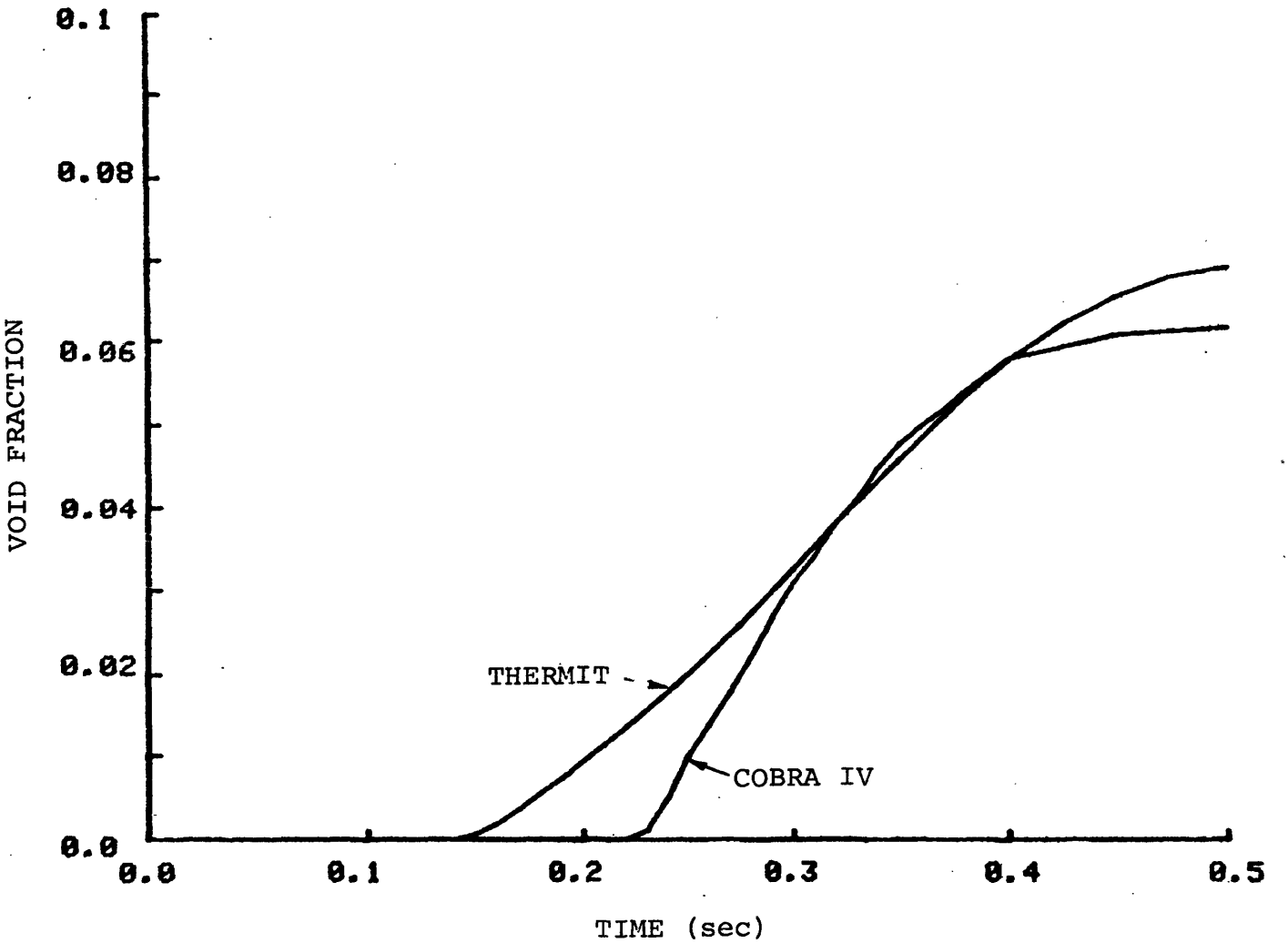

Figure 3.22 Void Fraction Versus Time - Rod Ejection Accident from HZP Condition.

code. In COBRA-IV (implicit), the Levy subcooled boiling model is used while in THERMIT the modified Ahmad model (see Appendix A) is used. Hence, for this transient the two codes are in fairly good agreement irrespective of modeling differences.

3.5.3 Low Flow, Low Power Initial Condition Case

The rod ejection transient initiated from a low flow, low power condition has been designed so that flow reversal and coolant expulsion from the inlet would occur. In order to simulate these effects, it is necessary to use a pressure-pressure boundary condition (i.e., both the inlet and outlet pressures are specified as boundary conditions). Consequently, the explicit method of COBRA-IV, which allows this type of boundary condition, has been compared with THERMIT for this transient.

Before discussing the results of the comparisons, two major differences between these codes should be discussed. First, the explicit method of COBRA-IV uses a strict homogeneous equilibrium model which does not account for either subcooled boiling or slip between the phases. On the other hand, THERMIT uses a non-equilibrium two-phase model which explicitly accounts for these effects. The second difference is in their heat transfer models. COBRA-IV has a RELAP-4 type model while THERMIT uses the BEEST heat transfer model. Both of these heat transfer models attempt to predict the same heat transfer behavior although each model contains different heat transfer correlations. These modeling differences in the codes would be

expected to lead to differences in their predictions.

For this rod ejection transient both flow reversal and coolant expulsion are found to occur. The flow reversal and coolant expulsion are governed by the rate of density change. This, in turn, is coupled to the rate of vapor generation (i.e., void fraction). Hence, the void fraction is an important parameter for this transient.

The void fraction predictions of each code are illustrated in Figures 3.23 and 3.24. It is seen that THERMIT predicts boiling to occur earlier due to the fact that THERMIT can predict subcooled boiling. Additionally, the space-time void fraction distributions are significantly different which is also due to the differences in the two-phase modeling.

These void fraction differences lead to significantly different flow behavior during this transient. The inlet and outlet mass flux predictions of each code are illustrated in Figures 3.25 and 3.26. THERMIT predicts a sudden flow reversal at the point where subcooled boiling begins and,after reaching a maximum, the flow rate stabilizes. On the other hand, COBRA-IV predicts an initial flow reversal at the same time as THERMIT and then a second flow reversal when saturated boiling begins. The initial flow reversal, common to both codes, is caused by the power deposited in the fuel finally being transported into the coolant. The density is rapidly decreased in both codes, but more so in THERMIT since subcooled boiling begins immediately. This is why the THERMIT coolant expulsion is larger in magnitude. The

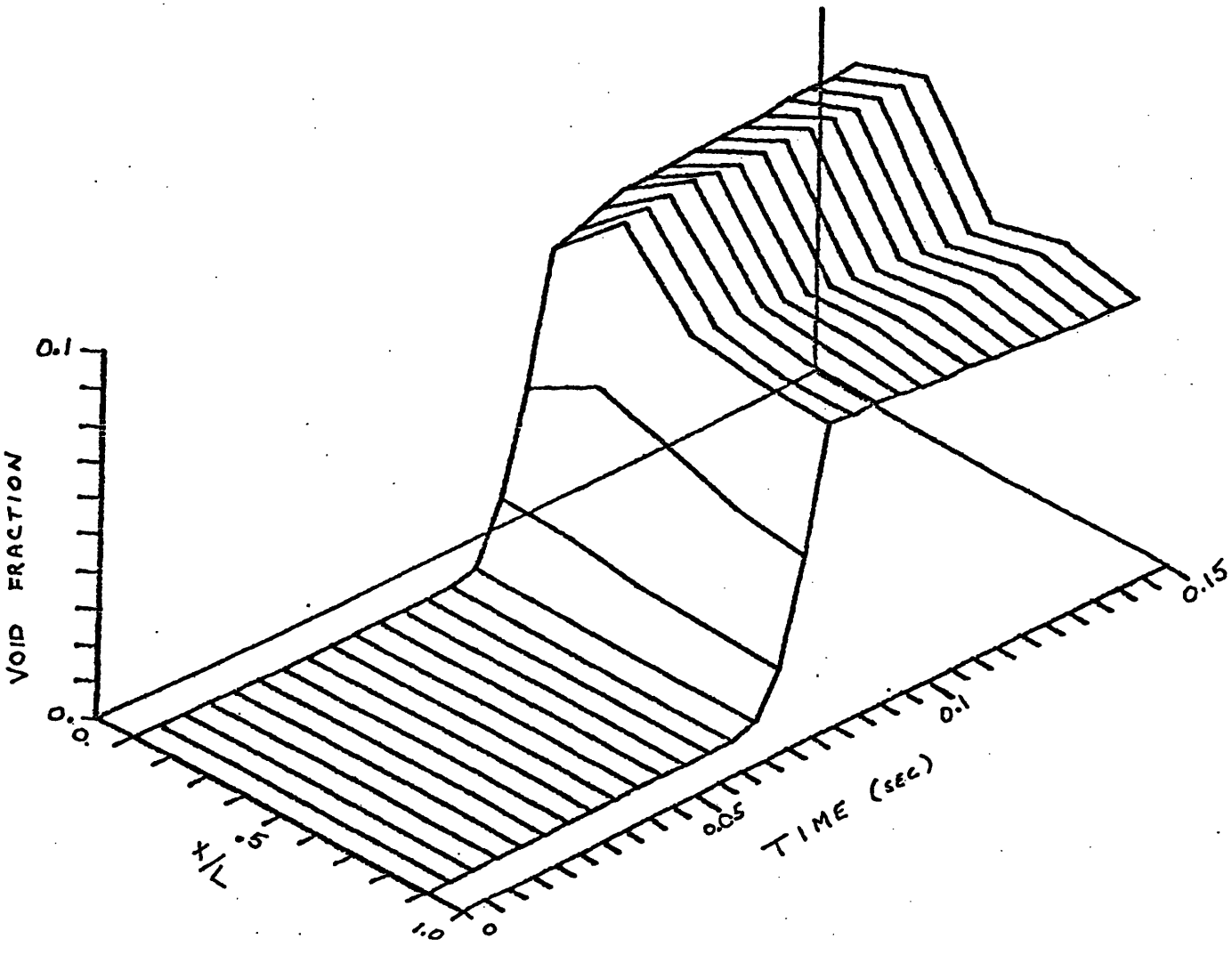

Figure 3.23 THERMIT Space-Time Void Fraction Distribution-Rod Ejection Transient from Low Flow, Low Power Condition.

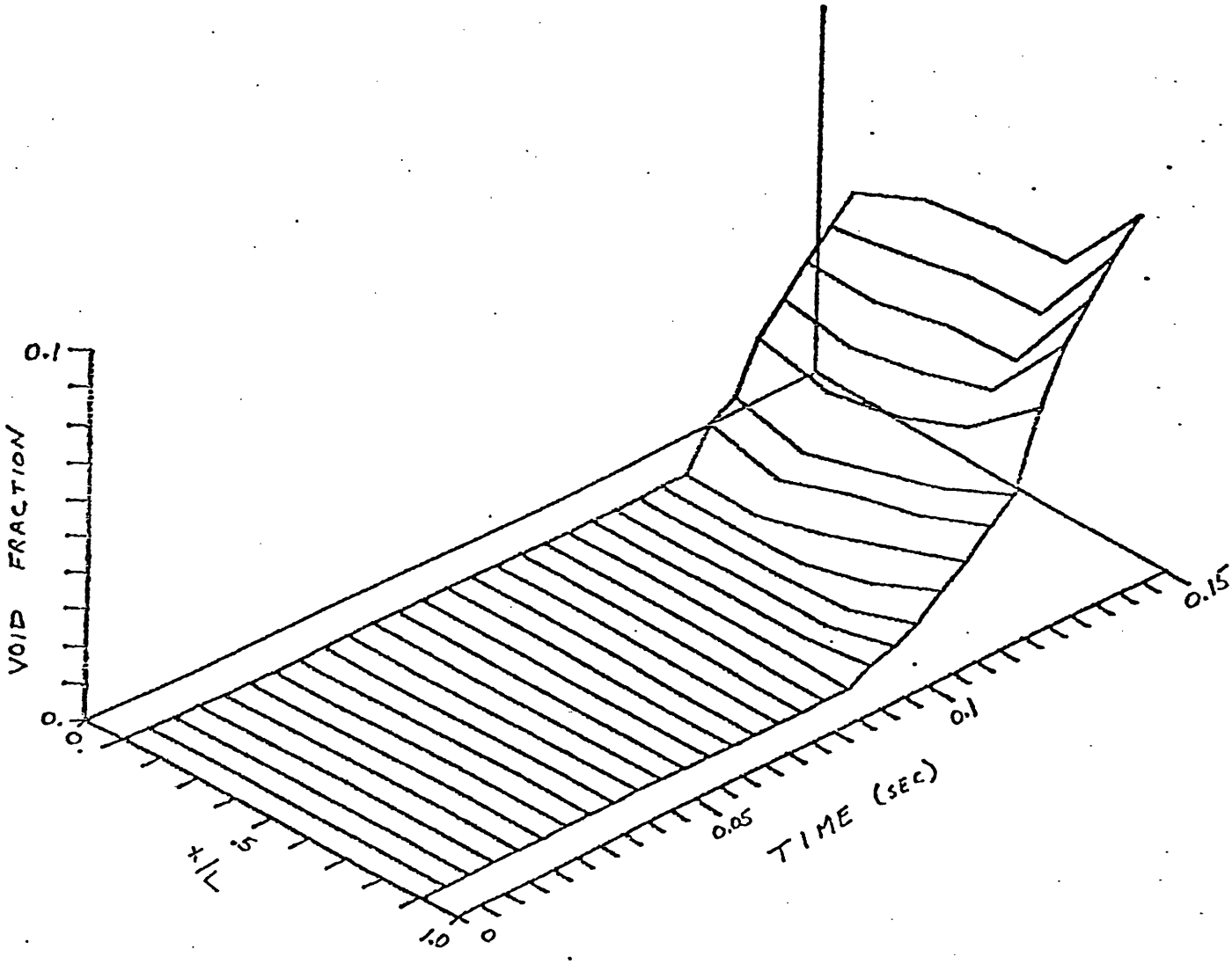

Figure 3.24 COBRA IV Space-Time Void Fraction Distribution-Rod Ejection Accident from Low Flow, Low Power Condition.

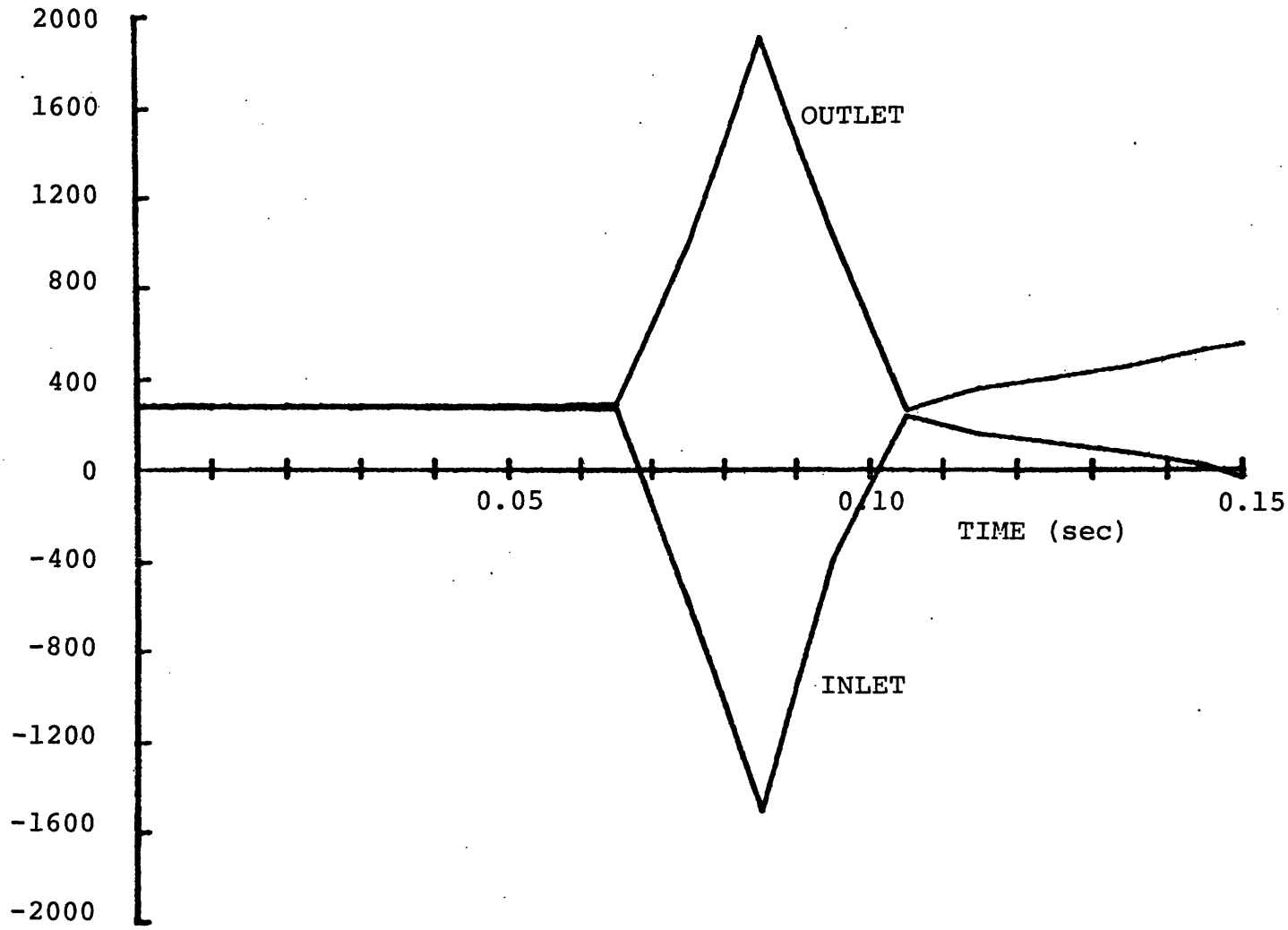

Figure 3.25 THERMIT Inlet and Outlet Mass Flux Distributions Versus Time-Rod Ejection Accident from Low Flow, Low Power Condition.

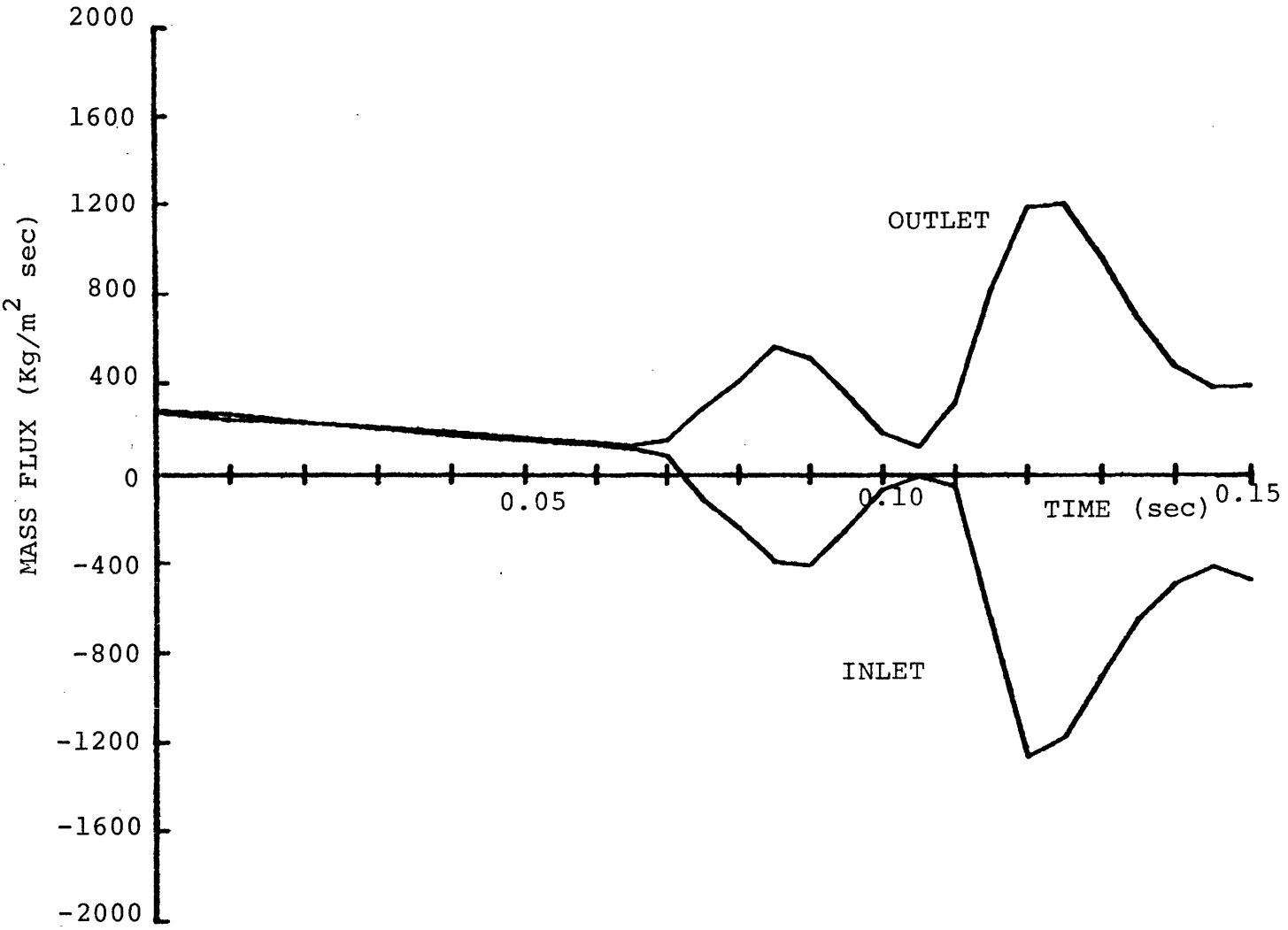

Figure 3.26 COBRA IV Inlet and Outlet Mass Flux Distribution Versus Time-Rod Ejection Accident from Low Flow, Low Power Condition.

second flow reversal, predicted by COBRA-IV, coincides with the start of saturated boiling which leads to another density decrease in the COBRA-IV case. However, since THERMIT has already predicted boiling to occur, no new flow reversal is predicted. Therefore, it is clear that the flow behavior is coupled to the void fraction predictions.

In spite of these significant differences in the predicted flow, the clad temperature predictions of each code are found in good agreement. As seen in Figure 3.27, the clad temperature rapidly increases for both codes at approximately the same time. This indicates that CHF is predicted to occur at nearly the same time. Furthermore, the post-CHF clad temperatures exhibit the same trends so that the heat transfer calculations seem nearly independent of the fluid dynamics.

These comparisons serve to illustrate the multi-dimensional, transient capabilities of THERMIT. For this very severe transient, both flow reversal and coolant expulsion can be predicted by THERMIT. The differences between the COBRA-IV and THERMIT predictions can be explained in terms of the differences in their respective two-phase models. Hence, if the THERMIT two-fluid model were forced to simulate a homogeneous equilibrium model, then it would be expected that better agreement between the two codes would be obtained. This type of simulation is planned in the ongoing effort to assess THERMIT.

Furthermore, it is important that some test cases for the voiding dynamics be developed such that THERMIT predictions are checked against either analytic solutions or experimental evidence.

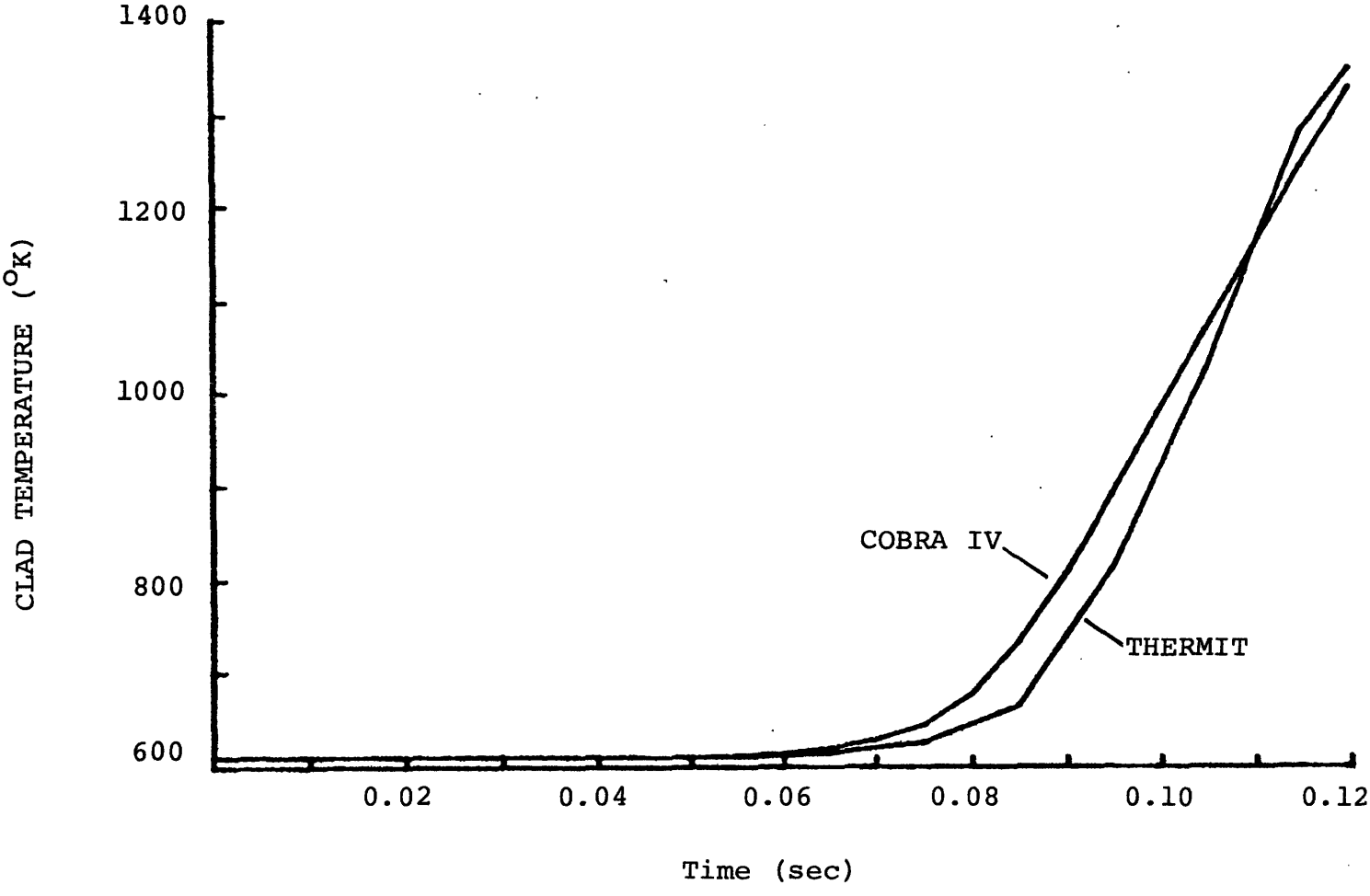

Figure 3.27 Clad Temperature versus Time
Rod Ejection Accident from
Low Flow, Low Power Condition

4. DIRECTIONS FOR FURTHER DEVELOPMENT

The results of this research have identified a number of areas which require further investigation. For subchannel applications, the most important area for future work lies in the development of a turbulent mixing model. This model is required so that the flow and enthalpy distributions can be accurately predicted. Both single-phase and two-phase mixing must be considered in this model. For single-phase conditions many mixing models are available, but for two-phase conditions very few models have been proposed. The two-phase mixing is complicated by the vapor diffusion phenomena which at present can not be represented solely on theoretical grounds. Hence, the required turbulent mixing model must be valid for both single-phase and two-phase conditions and must account for both turbulent mixing and vapor diffusion.

A second area which requires further study is the heat transfer model. In particular, two parts of this model need to be investigated. The first is the post-CHF model which showed relatively poor agreement with the data and should be improved. The second is the CHF model used for BWR conditions. At present, a critical power correlation is available for these conditions, but the way in which this correlation is being used may not be strictly valid and needs to be improved.

Another model which could be improved is the interfacial momentum exchange model. Although this model produced fairly accurate results for a wide range of conditions, some improvement could be obtained. Specifically, for fast transients, this model must account for virtual mass effects which are currently not considered in this model.

For all THERMIT applications, a useful improvement would be the addition of a flow regime identification system (flow map). This scheme could be used in conjunction with the interfacial exchange models to more realistically define these exchange processes.

Further investigation is also needed in developing techniques for obtaining steady-state solutions. Although many features have been added to THERMIT to reduce the computational requirements, improvement is still needed. For example, it might be possible to develop a special numerical scheme which would only be used to obtain steady-state solutions.

Another aspect of the numerical method which could be improved is the inner iteration scheme. The current scheme is found to converge very slowly when small radial mesh sizes are used. Some improvement in this scheme may be obtained by changing the iterative sweeping technique which is currently in the code.

Investigations into the possibility of using variable radial mesh spacings in THERMIT would also be warranted. The

motivation for this type of research is to determine whether or not THERMIT can be used for "single-pass" type design analysis. In order to perform this type of analysis, some modifications of the code will be needed, but the extent of these changes is not known and needs further study.

In addition to investigating the above topics, further testing of THERMIT is required. Specifically, the transverse flow coupling for subchannel applications needs to be verified and the transient capabilities of the code need to be assessed.

REFERENCES

1. W.H. Reed and H.B. Stewart, "THERMIT: A Computer Program for Three-Dimensional Thermal-Hydraulic Analysis of Light Water Reactor Cores," M.I.T. Report prepared for EPRI (1978).

2. D.R. Liles and W.H. Reed, "A Semi-Implicit Method for Two-Phase Fluid Dynamics," Journal of Computational Physics, 26, p. 390, (1978).

3. F.H. Harlow and A.A. Amsdem, "A Numerical Fluid Dynamics Calculation Method for All Flow Speeds," Journal of Computational Physics, 8, p. 197, (1971).

4. R.W. Bowring and P. Moreno, "COBRA-IIIC/MIT Computer Code Manual," M.I.T. Department of Nuclear Engineering Report (1976).

5. C.W. Stewart, C.L. Wheeler, et. al., "COBRA-IV: The Model and the Method," BNWL-2214, Battelle Pacific Northwest Laboratories, (1973).

6. H.B. Stewart, "Stability of Two-Phase Flow Calculations Using Two-Fluid Models," private communication.

7. S.Y. Ahmad, "Axial Distribution of Bulk Temperature and Void Fraction in a Heated Channel With Inlet Subcooling," Journal of Heat Transfer, 92, p. 595, (1970).

8. H.B. Stewart, private communication.

9. W.C. Rivard and M.D. Torrey, "Numerical Calculation of Flashing from Long Pipes Using a Two-Fluid Model," LA-6104-MS, Los Alamos Scientific Laboratory, (1975).

10. T.A. Bjornard and P. Griffith, "PWR Blowdown Heat Transfer," Thermal and Hydraulic Aspects of Nuclear Reactor Safety - Vol. 1, Light Water Reactors ASME Symposium, (1977).

11. L. Wolf and A. Schor, private communication.

12. G.W. Maurer, "A Method of Predicting Steady-State Boiling Vapor Fractions in Reactor Coolant Channels," WAPD-BT-19, (1960).

13. H. Christensen, "Power-to-Void Transfer Functions," ANL-6385, (1961).

14. J.F. Marchaterre, et. al., "Natural and Forced-Circulation Boiling Studies," ANL-5735, (1960).

15. A.W. Bennett, et. al., "Heat Transfer To Steam-Water Mixtures Flowing In Uniformly Heated Tubes In Which The Critical Heat Flux Has Been Exceeded," AERE-R-5373, (1967).

16. R.T. Lahey, B.S. Shiralkar, and D.W. Radcliffe, "Subchannel and Pressure Drop Measurements in a Nine-Rod Bundle for Diabatic and Adiabatic Conditions," GEAP-13049, (1970).

17. R.T. Lahey and F.J. Moody, The Thermal Hydraulics of a BWR, ANS Monograph, (1975).

18. A.R. Edwards and T.P. O'Brien, "Studies of Phenomena Connected With the Depressurization of Water Reactors," Journal of the British Nuclear Energy Society, 9, p. 125, (1970).

19. L.S. Tong, Boiling Crisis and Critical Heat Flux, TID-25887, AEC Critical Review Series, (1972).

20. S. Bertoletti, et. al., "Heat Transfer Crisis with Steam-Water Mixtures," Energia Nucleare, 12, p. 121, (1965).

APPENDIX A

DESCRIPTION OF THE SUBCOOLED VAPOR GENERATION MODEL

In the two-fluid liquid and vapor mass equations, the transfer of mass across the liquid-vapor interfaces is represented by the interfacial mass transfer rate, Γ. This term is also referred to as the vapor generation rate since boiling conditions are usually analyzed. For typical reactor conditions, subcooled boiling is an important phenomena. Hence, the model for Γ must be capable of predicting vapor generation even for subcooled liquid conditions.

In the current version there are two models for the vapor production rate. The first model, referred to as the Nigmatulin model, has been discussed in reference 1. This model can predict vapor generation due to rapid depressurization, but it cannot predict subcooled boiling. The second model, referred to as the subcooled boiling model, is discussed in this Appendix. This model accounts for subcooled boiling, but cannot predict vapor generation due to flashing. Hence, this model would not be used during depressurization transients.

The subcooled boiling model for Γ is represented as the sum of two terms:

$$\Gamma = \frac{1}{h_v - h_\ell} \left[\dot{q}_v + \dot{q}_c \right] \qquad \text{(A.1)}$$

where

h_v = vapor enthalpy

h_ℓ = liquid enthalpy

$\dot{q}_v$ = heat from the wall which produces vapor

$\dot{q}_c$ = heat from vapor which goes into liquid

The first term, $\dot{q}_v$, represents the amount of heat per unit volume which would produce vapor bubbles neglecting non-equilibrium effects. The second term, $\dot{q}_c$, represents the amount of heat per unit volume which is either lost or gained by the vapor bubbles due to non-equilibrium condensation or vaporization. The sum of these two terms represents the total heat deposited into the vapor phase and, when divided by the latent heat of vaporization, the vapor generation rate is obtained. Hence, the difficulty in formulating this model lies in the determination of $\dot{q}_v$ and $\dot{q}_c$. The analysis of Ahmad (7) is used to determine the appropriate functional dependence of these two terms and these models are discussed below.

The term $\dot{q}_v$ can be related to the total power through the following equation:

$$\dot{q}_w = \dot{q}_v + \dot{q}_\ell \qquad \text{(A.2)}$$

The term $\dot{q}_w$ is the total power per unit volume and is related to the wall heat flux by

$$\dot{q}_w = q''_w A_H \qquad \text{(A.3)}$$

where

q''_w = wall heat flux

A_H = heated surface area per unit volume

The term $\dot{q}_\ell$ is the amount of heat per unit volume deposited in the channel which increases the liquid temperature. Hence, it is seen that the total power is divided into two components: one which increases the liquid temperature and one which produces vapor.

The ratio, χ, defined as

$$\chi \equiv \dot{q}_v/\dot{q}_w \tag{A.4}$$

represents the fraction of the total power which produces vapor. This ratio assumes two limiting values. For liquid temperatures below the bubble departure temperature, T_d, no vapor is generated so that χ equals zero. Once the liquid becomes saturated (i.e., $T_\ell = T_s$), all the wall heat produces vapor so that χ equals 1.0. A simple linear relationship is used for temperatures between Td and Ts so that χ is given by

$$\chi = \begin{cases} 0 & T_\ell \leq T_d \\ \dfrac{T_\ell - T_d}{T_s - T_d} & T_d < T_\ell < T_s \\ 1.0 & T_\ell \geq T_s \end{cases} \tag{A.5}$$

Hence, if the value for T_d can be determined, then $\dot{q}_v$ can be obtained using

$$\dot{q}_v = \begin{cases} 0 & T_\ell \leq T_d \\ \dot{q}_w \dfrac{T_\ell - T_d}{T_s - T_d} & T_d < T_\ell < T_s \\ \dot{q}_w & T_\ell \geq T_s \end{cases} \quad (A.6)$$

The temperature difference $T_s - T_d$ can be obtained using the Ahmad correlation, i.e.,

$$T_s - T_d = q''_w / H \quad (A.7)$$

where

$$H = \frac{k}{D_h}\left[2.44 \left(\frac{GD_h}{\mu} \right)^{1/2} \left(\frac{C_p \mu}{k} \right)^{1/3} \left(\frac{h_{in}}{h_f} \right)^{1/3} \left(\frac{h_{fg}}{h_f} \right)^{1/3} \right] \quad (A.8)$$

Then, after some algebraic manipulation the expression for $\dot{q}_v$ in the subcooled boiling regime (i.e., $T_d < T_\ell < T_s$) is given as

$$\dot{q}_v = \dot{q}_w - H(T_s - T_\ell)A_H \quad (A.9)$$

The second term, $\dot{q}_c$, is modeled using the following expression

$$\dot{q}_c = S/V \; k_t(T_\ell - T_v) \quad (A.10)$$

where S/V is the ratio of the vapor-liquid interfacial surface area to the total fluid volume; and k_t is the effective conductivity. For bubbly flow one finds

$$S = 4\pi R_b^2 \; N \tag{A.11}$$

$$V = \frac{4}{3}\pi R_b^3 \; \frac{N}{\alpha} \tag{A.12}$$

where R_b is the average bubble radius and N is the bubble number density. The ratio S/V can then be calculated to find

$$S/V = \frac{3\alpha}{R_b} \tag{A.13}$$

The model for R_b is

$$R_b = \begin{cases} R_{bo} & \alpha < 0.10 \\ R_{bo}\left[\frac{9\alpha}{1-\alpha}\right]^{1/3} & \alpha \geq 0.10 \end{cases} \tag{A.14}$$

where

$$R_{bo} = R_{bo,pool}\left[1 + 1.34V_{\ell E}^{1/3}\right]^{-1} \tag{A.15}$$

$$V_{\ell E} = (1-\alpha)\, V_\ell \tag{A.16}$$

$$R_{bo,pool} = 0.45\sqrt{\frac{\sigma}{(\rho_\ell - \rho_v)}} \tag{A.17}$$

The effective conductivity k_t is given by

$$k_t = \begin{cases} \dfrac{k_\ell}{0.015\, R_{bo}} & T_v \leq T_\ell \\ \dfrac{k_v k_\ell}{0.01\, R_{bo} k_\ell + 0.015\, R_{bo} k_v} & T_v > T_\ell \end{cases} \tag{A.18}$$

With these expression, values for both $\dot{q}_c$ and $\dot{q}_v$ can be determined. Then using equation A.1 the vapor generation rate can be calculated.

APPENDIX B

DESCRIPTION OF INTERFACIAL MOMENTUM EXCHANGE MODELS

A unique feature of the two-fluid equations is that interactions between the two phases within a control volume must be modeled explicitly. These interactions arise from the fact that, within a control volume, there are liquid-vapor interfaces across which mass, energy and momentum may be exchanged. In view of their nature, these interactions are commonly referred to as interfacial exchange terms.

In the two-fluid momentum equations, momentum transfer between the liquid and vapor is modeled using the term called the interfacial momentum exchange rate, F_i. This term models the total amount of interfacial shear stress within a given control volume. Consequently, it will depend on a number of parameters including the interfacial surface area, the velocities of each phase, the density of each phase and the viscosity of each phase. Since the physical properties are functions of pressure and temperature, the functional dependence of F_i may be written as:

$$F_i = F_i(V_\ell, V_v, P, T_\ell, T_v, \alpha) \qquad (B.1)$$

The correct form of this function is not well known, but from one-dimensional studies a dependency on the relative velocity $(V_v - V_\ell)$ is found to occur. Hence, F_i may be written as

$$F_i = K_i \, (V_v - V_\ell) \qquad (B.2)$$

where the value of K_i is determined from a correlation.

Analyzed from a physical point of view, it may be seen that the function representing K_i will depend on the flow regime. In bubbly flow K_i will have a very large value so that the value of $(V_v - V_\ell)$ is near zero (i.e., slip ratio equals 1.0). In annular flow, there will be a non-zero relative velocity so that value of K_i is reduced. Furthermore, the interfacial surface area will also depend on the flow regime. Hence the model for K_i must depend on the flow regime.

In THERMIT, the model for K_i is continuous for all flow regimes and is given as

$$K_i = K_1 + K_2 \, |V_v - V_\ell| \qquad (B.3)$$

The first term accounts for the drag of vapor bubbles moving through the liquid and, hence, this term predominates in the bubbly flow regime. The second term represents a form loss resulting from the motion of two continuous streams. Consequently, this second term dominates in the annular flow regime.

In THERMIT, there are currently two models for the constants K_1 and K_2. The first model, referred to as the MIT model, has been developed using void fractions which are typical of a BWR.

In this model the functions for K_1 and K_2 are

$$K_1 = \left(\frac{1.01 - \hat{\alpha}}{\hat{\alpha}\ D_h}\right)^2 \mu_\ell \tag{B.4}$$

$$K_2 = \left(\frac{1.01 - \hat{\alpha}}{\hat{\alpha}\ D_h}\right) \frac{\rho_v}{2} \tag{B.5}$$

where

$$\hat{\alpha} = \max\ (\alpha,\ 0.1) \tag{B.6}$$

Hence, this model for F_i is given by

$$F_i = \left(\frac{1.01 - \hat{\alpha}}{\hat{\alpha}\ D_h}\right) \left[\frac{1.01 - \hat{\alpha}}{\hat{\alpha}\ D_h} \mu_\ell + \frac{\rho_v\ |V_v - V_\ell|}{2}\right] (V_v - V_\ell) \tag{B.6}$$

It is seen that this model yields a positive value for K_i even if there is no vapor present. This is required in order to prevent a singularity in solution method.

The second model for K_1 and K_2 is that used in similar codes at Los Alamos Scientific Laboratory and is referred to as the LASL model (9). The functions for K_1 and K_2 in this model are:

$$K_1 = \frac{9}{2} \frac{\bar{\mu}}{r} \; a \tag{B.8}$$

$$K_2 = \frac{3}{16} \bar{\rho} \; a \tag{B.9}$$

where

$$\bar{\rho} = \alpha \; \rho_v + (1 - \alpha) \; \rho_\ell \tag{B.10}$$

$$\bar{\mu} = (\alpha \; \mu_v/\rho_v + (1 - \alpha) \; \mu_\ell/\rho_\ell) \bar{\rho} \tag{B.11}$$

$$a = a_n^{1/3} \; \tilde{\alpha}^{2/3} \tag{B.12}$$

$$r = (\tilde{\alpha}/a_n)^{1/3} \tag{B.13}$$

$$a_n = \frac{4\pi N}{3} \tag{B.14}$$

$$N \equiv 10^7/m^3 \tag{B.15}$$

$$\tilde{\alpha} = \begin{cases} \alpha & \text{if } \alpha \leq 0.5 \\ 1-\alpha & \text{if } \alpha > 0.5 \end{cases} \tag{B.16}$$

Hence, this model for F_i is given by

$$F_i = \frac{3}{8} \; a \left[\frac{12\bar{\mu}}{r} + \frac{\bar{\rho} \; |V_v - V_\ell|}{2} \right] \; (V_v - V_\ell) \tag{B.17}$$

A comparison of these two models shows that the LASL model predicts a higher value for F_i. The relative magnitude of this difference can be seen by taking the ratio of F_i models

and assuming the same velocity profiles and that the K_1 terms can be ignored. Then, one finds

$$F_i^{LASL} / F_i^{MIT} \approx K_2^{LASL} / K_2^{MIT} \tag{B.18}$$

$$= \frac{3}{16} a \bar{\rho} \Big/ \frac{(1.01 - \alpha)}{\alpha D_h} \frac{\rho_v}{2} \tag{B.19}$$

After simplifying, one obtains

$$K_2^{LASL} / K_2^{MIT} = 130 D_h \tilde{\alpha}^{5/3} \left[\alpha + (1 - \alpha) \rho_\ell / \rho_v\right] / (1.01 - \alpha) \tag{B.20}$$

Then, for BWR conditions one may use

$$D_h \approx 0.01 \text{ m}$$

$$\rho_\ell / \rho_v \approx 20$$

to obtain

$$K_2^{LASL} / K_2^{MIT} = 1.3 \tilde{\alpha}^{5/3} \left[\alpha + 20 (1 - \alpha)\right] / (1.01 - \alpha) \tag{B.21}$$

The expression has been evaluated for void fractions greater than 0.4 and the following results are obtained

α	K_2^{LASL} / K_2^{MIT}
0.4	5.8
0.5	8.6
0.6	11.9
0.7	16.0
0.8	21.3
0.9	30.7

Hence, it is seen that the LASL F_i model predicts a larger value for F_i in the high void fraction regime (annular flow).

Each of the above models is currently included in THERMIT as a separate option. The choice of which model is used is controled by the user through an input option.

APPENDIX C

DESCRIPTION OF CHF CORRELATIONS

C.1 Background

The heat transfer model in THERMIT is capable of predicting both pre-CHF and post-CHF heat transfer conditions. Of the many correlations involved in this model, the CHF correlation is probably the most important. For steady-state and operational transients, the predictions of this correlation provide an estimation of the safety margin. Furthermore, in very severe transients, such as blowdown, the time at which CHF occurs is controlled by this correlation. Hence, an accurate CHF correlation is required in the overall heat transfer model.

In the original THERMIT heat transfer model (i.e., the BEEST model (10)) only one CHF correlation was included: the Biasi correlation. This correlation had a very large data base and was thought to be well-suited for blowdown applications. However, for operational transients it was not clear whether or not this correlation would be applicable. In particular, this correlation could not predict DNB type CHF and, furthermore, the effects of a non-uniform axial power distribution would not be accounted for. Hence, other CHF correlations were investigated for inclusion in the THERMIT heat transfer model.

Two correlations have been added to the heat transfer model. The first is the W-3 correlation (19). This correla-

tion is to be used for PWR steady-state and operational transient analysis. The widespread acceptance of this correlation as a standard design tool makes it easier to assess the heat transfer model when this correlation is included.

The second correlation which has been added is the CISE correlation (20). This correlation would be used for BWR steady-state and operational transient analysis. The critical power, calculated by this correlation is an integral parameter and presumably accounts for the effects of non-uniform heat flux distributions. This critical power cannot be directly related to a critical heat flux, since upsteam effects are integrated into the correlation. Hence, it is difficult to compare a critical power correlation with a critical heat flux correlation. Nevertheless, both types of correlations should predict burnout for the same conditions, so that the inclusion of the CISE correlation for BWR conditions is a good choice.

These three CHF correlations are described in this appendix. The Biasi correlation is presented first followed by the W-3 correlation and then the CISE correlation.

C.2 Biasi Correlation

The Biasi critical heat flux correlation is a function of the pressure, hydraulic diameter, mass flux and quality. Two expressions are given for the critical heat flux. These are

$$q_{CHF,1} = 2.764 \times 10^7 \ (100\ D)^{-n} G^{-1/6} \left[1.468F\ G^{-1/6} - x \right] \frac{w}{m^2} \qquad (C.1)$$

$$q_{CHF,2} = 7.086 \times 10^{7} \, (100D)^{-n} \, G^{-0.6} \, H \left[1 - X\right] \frac{w}{m^2} \qquad (C.2)$$

where

$$F = 0.7249 + 0.099 \, P_{bar} \exp\left[-0.032 \, P_{bar}\right] \qquad (C.3)$$

$$H = -1.159 + 0.149 \, P_{bar} \exp\left[-0.019 \, P_{bar}\right] + 8.99 \, P_{bar} \, (10 + P_{bar}^{2})^{-1} \qquad (C.4)$$

$$P_{bar} = 10^{-5} \, P \qquad (C.5)$$

$$n = \begin{cases} 0.4 & D > 0.01 \text{ m} \\ 0.6 & D \leq 0.01 \text{ m} \end{cases} \qquad (C.6)$$

The second expression (C.2) is used for $G < 300$ kg/m^2-sec. For higher G the larger of two is used.

The range of applicability of this corrleation is given as:

$P = 2.7 \times 10^{5}$ to 1.4×10^{7} Pa

$G = 100$ to 6000 kg/m^2-sec

$D = 0.003$ to 0.0375 m

$X > 0$

$L = 0.2$ to 6.0 m

C.3 W-3 Correlation

The W-3 correlation for a uniform heat flux is a function of the pressure, hydraulic diameter, mass flux, quality and inlet subcooling. This correlation is given as

$$(1)\quad \frac{q''_c}{10^6} = \left\{(2.022 - 0.0004302P) + (0.1722 - 0.0000984P) \times \mathrm{EXP}\left[(18.177 - 0.004129P)X\right]\right\} \times \left[(0.1484 - 1.596X + 0.1729X|X|)(G/10^6) + 1.037\right] \times (1.157 - 0.869X) \times \left[0.2664 + 0.8357\ \mathrm{EXP}(-3.151D_E)\right] \times \left[0.8258 + 0.000794\ (h_f - h_{IN})\right] \quad \mathrm{Btu/hr\ ft^2} \tag{C.7}$$

For a non-uniform heat flux the critical heat flux is given as

$$q^{NU}_{CHF} = q^{u}_{CHF}/F \tag{C.8}$$

where

$$F = \frac{c}{q(\ell)(1 - \exp(-c\ell))} \int_0^{\ell} q(z)\ \exp\ -c(\ell - z)\ dz \tag{C.9}$$

and

$$C = \frac{0.15\ (1 - X_c)^{4.31}}{(G/10^6)^{4.78}} \quad \mathrm{in^{-1}}$$

ℓ is the channel location and X_c and $q(\ell)$ are the quality and heat flux at the location ℓ.

This correlation is valid within the following parameter ranges.

P = 1000 to 2000 psia

G = 1.0×10^6 to 5.0×10^6 lb/hrft^2

D = 0.2 to 0.7 inch

X = -0.25 to 0.15

L = 10 to 144 inches.

C.4 CISE Correlation

The CISE correlation, which is used to calculate the critical power, depends on the pressure, hydraulic diameter, mass flux and boiling length. The correlation is given as

$$\frac{Q_c}{GA\,h_{fg}} = \frac{aL_b}{b + L_b} \qquad \text{(C.10)}$$

where

$a = (1 - P/P_c)\,(G/1000)^{1/3}$

$b = 0.199\ (P_c/P - 1)^{.4}\ G\ D_h^{1.4}$

L_b = boiling length (m)

Q_c = critical power (w)

The quoted range of applicability of this correlation is for the following parameter ranges

$P = 4.4 \times 10^6$ to 1.47×10^7 Pa

$G = 1000$ to 4000 kg/m^2 sec

$D > 0.007$ m

$X > 0.$

APPENDIX D

THERMIT COMPARISONS WITH STEADY-STATE, ONE-DIMENSIONAL DATA

In this appendix, all of the THERMIT comparisons with the steady-state, one-dimensional tests are presented. These include the void fraction comparisons with the data of Maurer, Christensen, and Marchaterre, as well as the wall temperature comparisons with the data of Bennett. For the void fraction comparisons, the subcooled boiling model and the MIT F_i model have been used in each case. Additionally, for the Christensen and Marchaterre cases, THERMIT predictions using the LASL F_i model are also included. The test conditions for these void fraction cases are summarized in Table D.1, and the comparisons with the data are illustrated in Figures D.1 - D.21.

For the wall temperature comparisons, the Nigmatulin boiling model and the MIT F_i model have been used. The test conditions for these cases are summarized in Table D.2 and the comparisons with the data are illustrated in Figures D.22 - D.29.

Table D.1 Summary of Test Conditions for Void Fraction Data

Case	Figure Number	Pressure (psia)	Mass Flux Mlb/hrft^2	Heat Flux MBtu/hrft^2	Inlet Subcooling Btu/lb	D_h (in)
Maurer 214-3-5	D.1	1200	0.902	0.600	144.4	0.16
Maurer 214-3-4	D.2	1200	0.589	0.347	63.8	0.16
Maurer 214-9-3	D.3	1600	0.409	0.097	78.5	0.16
Maurer 214-10-2	D.4	1600	0.595	0.197	81.4	0.16
Christensen 9	D.5	400	0.473	0.067	4.7	0.7
Christensen 10	D.6	400	0.478	0.067	16.8	0.7
Christensen 11	D.7	600	0.694	0.112	29.2	0.7
Christensen 12	D.8	600	0.685	0.112	14.6	0.7
Christensen 13	D.9	600	0.680	0.112	6.4	0.7
Christensen 15	D.10	800	0.669	0.157	26.8	0.7
Christensen 16	D.11	1000	0.648	0.157	27.4	0.7
Marchaterre 184	D.12	263	0.621	0.068	17.2	0.44
Marchaterre 185	D.13	263	0.636	0.050	12.8	0.44
Marchaterre 224	D.14	263	0.596	0.050	13.0	0.44
Marchaterre 226	D.15	263	0.577	0.016	4.9	0.44
Marchaterre 235	D.16	264	0.604	0.016	4.9	0.44
Marchaterre 159	D.17	613	0.626	0.085	26.9	0.44
Marchaterre 163	D.18	613	0.440	0.015	9.3	0.44
Marchaterre 168	D.19	613	0.621	0.076	25.0	0.44
Marchaterre 296	D.20	613	1.074	0.067	13.5	0.44
Marchaterre 298	D.21	613	1.075	0.076	14.7	0.44

Table D.2 Summary of Test Conditions for Wall Temperature Data

Bennett Case Number	Figure Number	Heat Flux MBtu/hr ft^2	Mass Flux Mlb/hr ft^2	Inlet Subcooling Btu/lb
5325	D.22	0.181	0.49	63
5332	D.23	0.205	0.49	59
5336	D.24	0.253	0.49	58
5266	D.25	0.222	0.74	51
5276	D.26	0.251	0.75	52
5273	D.27	0.292	0.76	46
5391	D.28	0.524	3.82	33
5394	D.29	0.555	3.82	31

Pressure = 1000 psia

D_h = 0.497

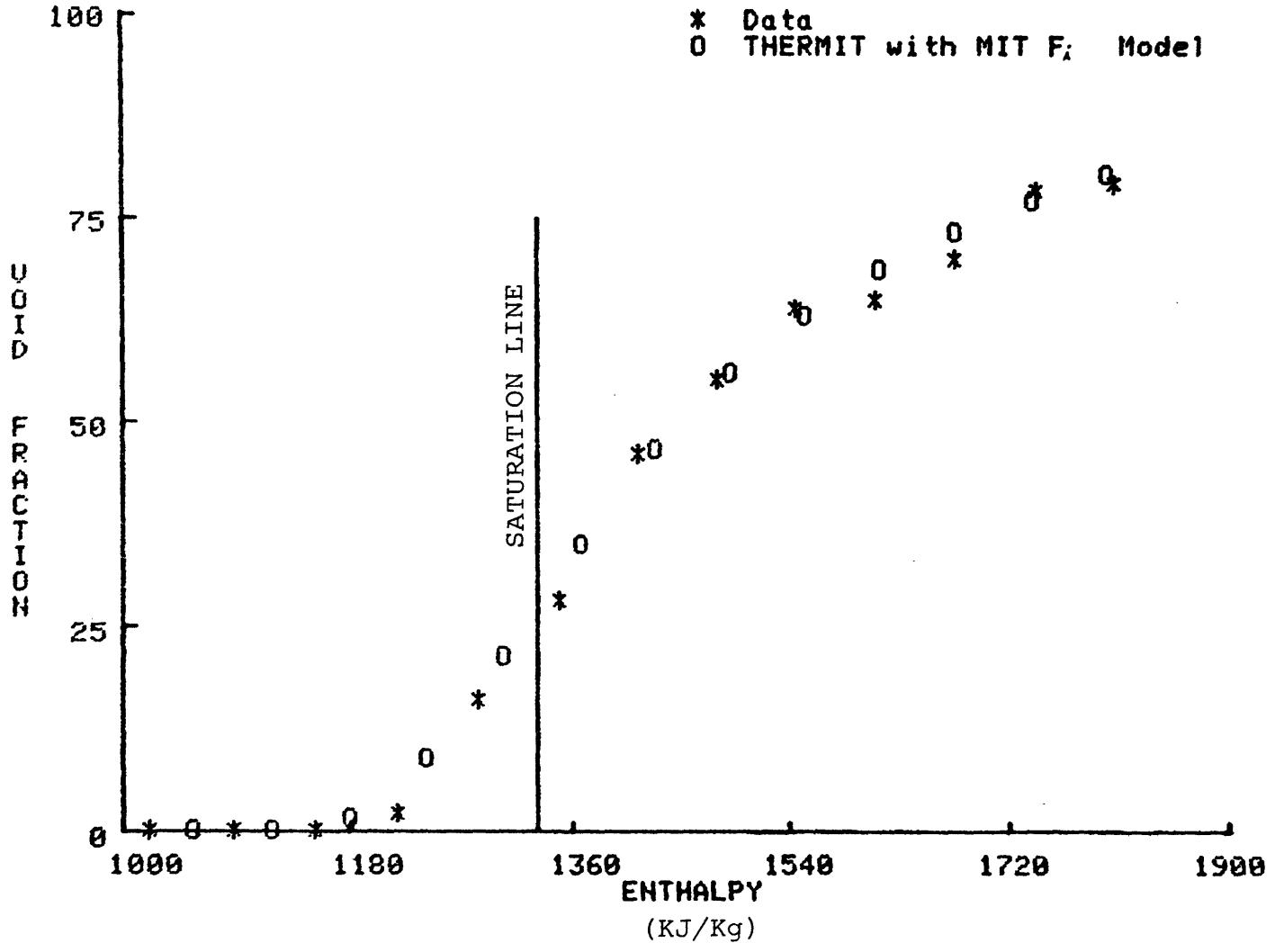

Figure D.1 Void Fraction Versus Enthalpy - Maurer Case 214-3-5

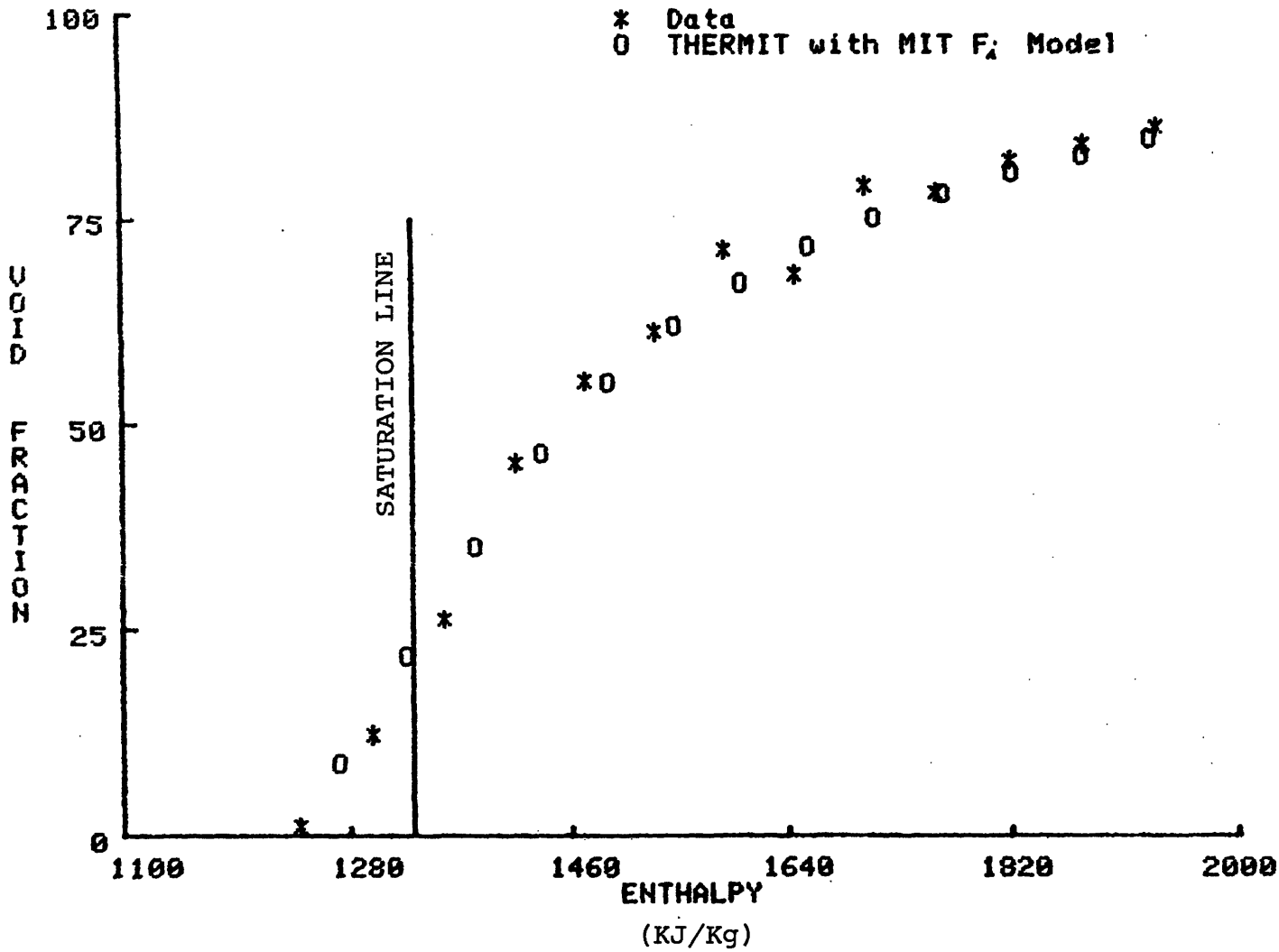

Figure D.2 Void Fraction Versus Enthalpy - Maurer Case 214-3-4

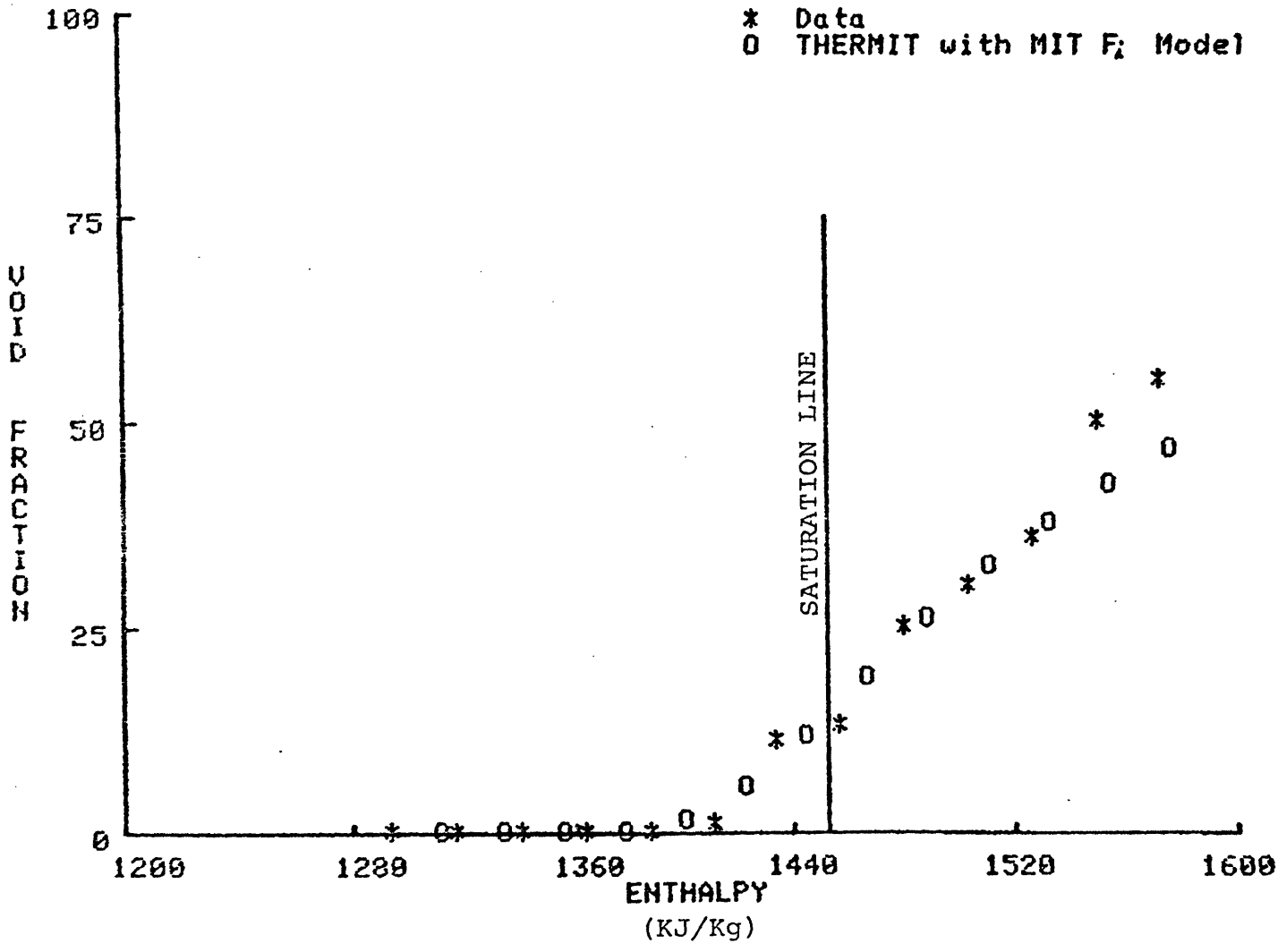

Figure D.3 Void Fraction Versus Enthalpy - Maurer Case 214-9-3

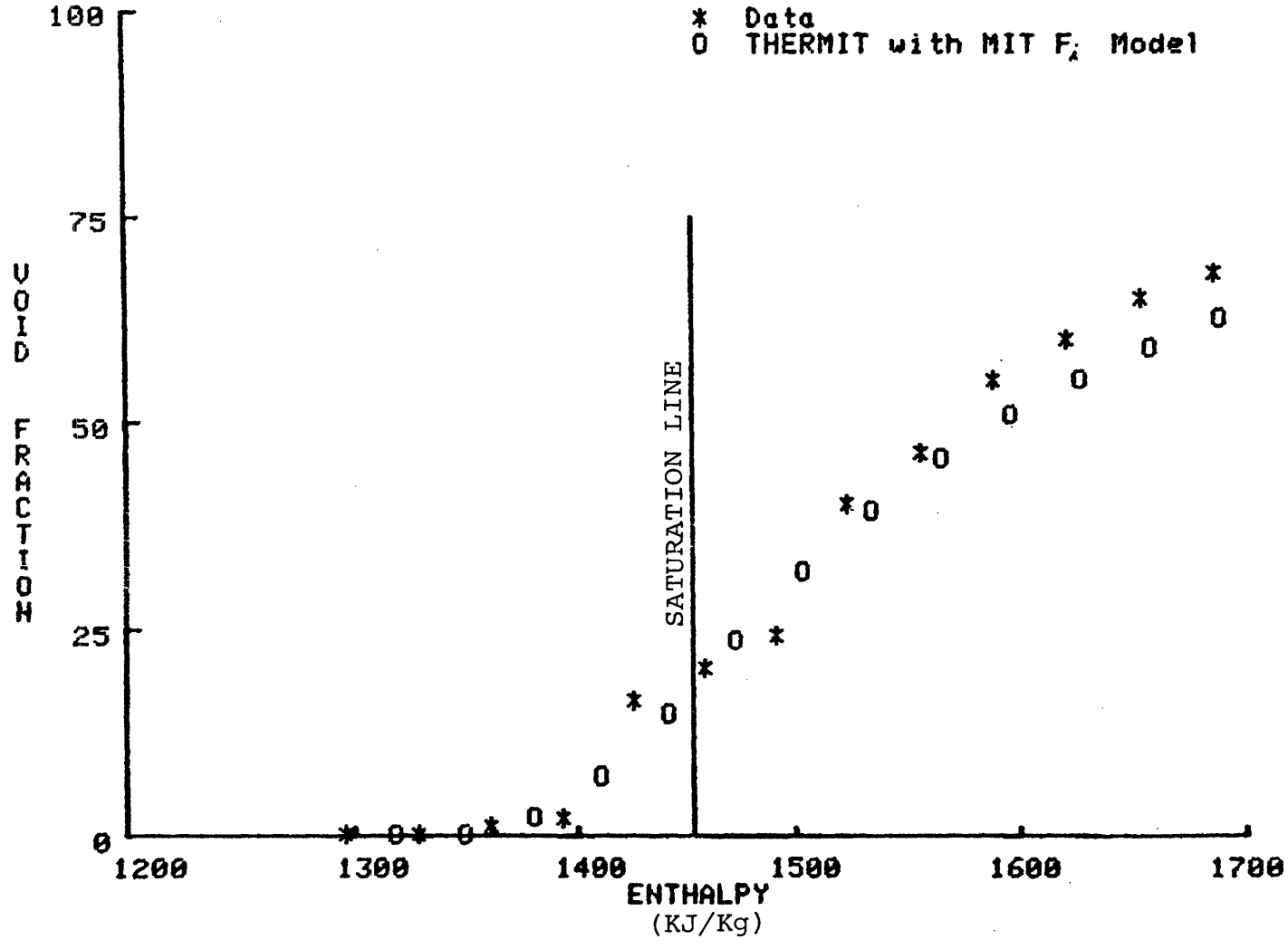

Figure D.4 Void Fraction Versus Enthalpy - Maurer Case 214-10-2

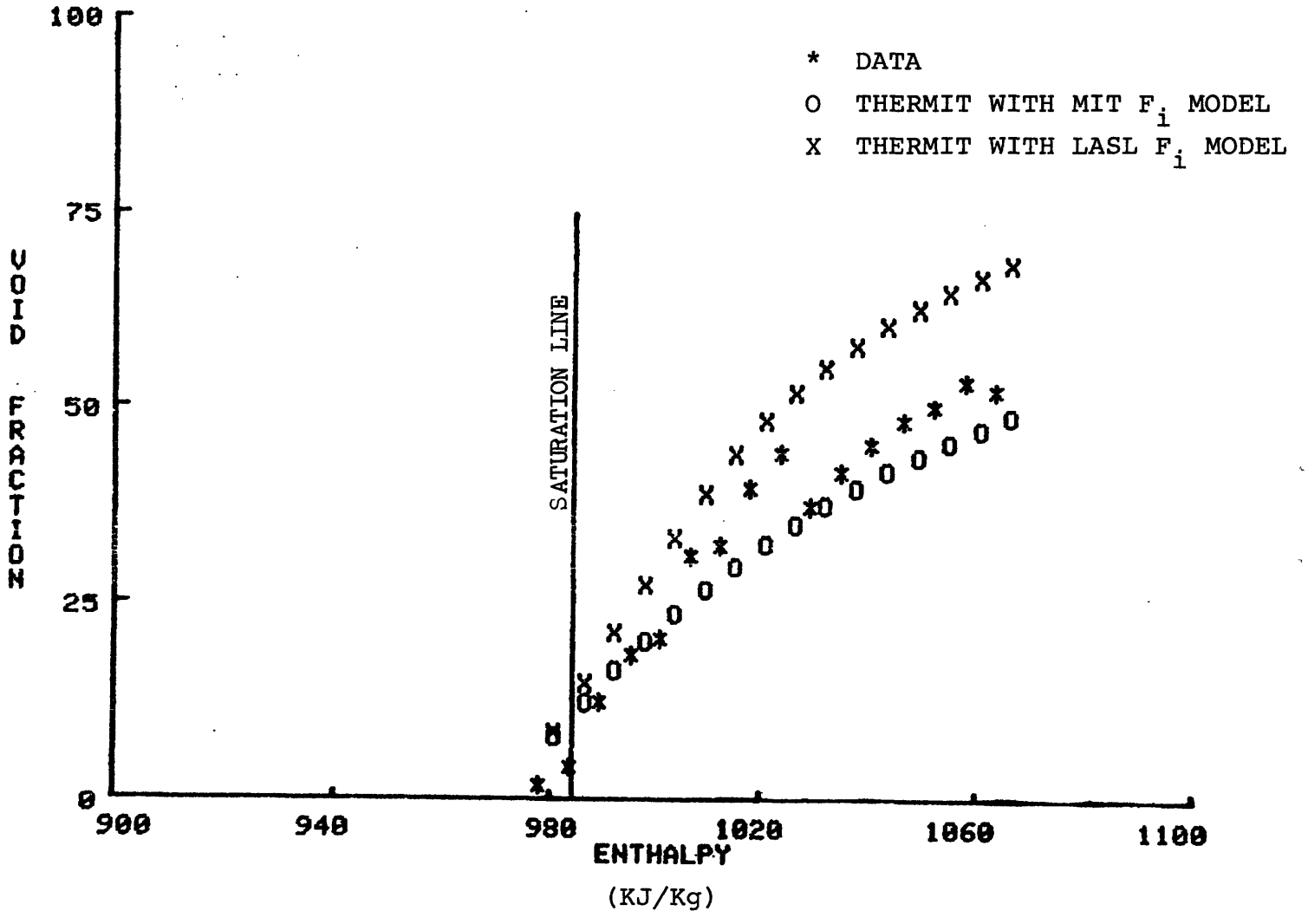

Figure D.5 Void Fraction Versus Enthalpy - Christensen Case 9

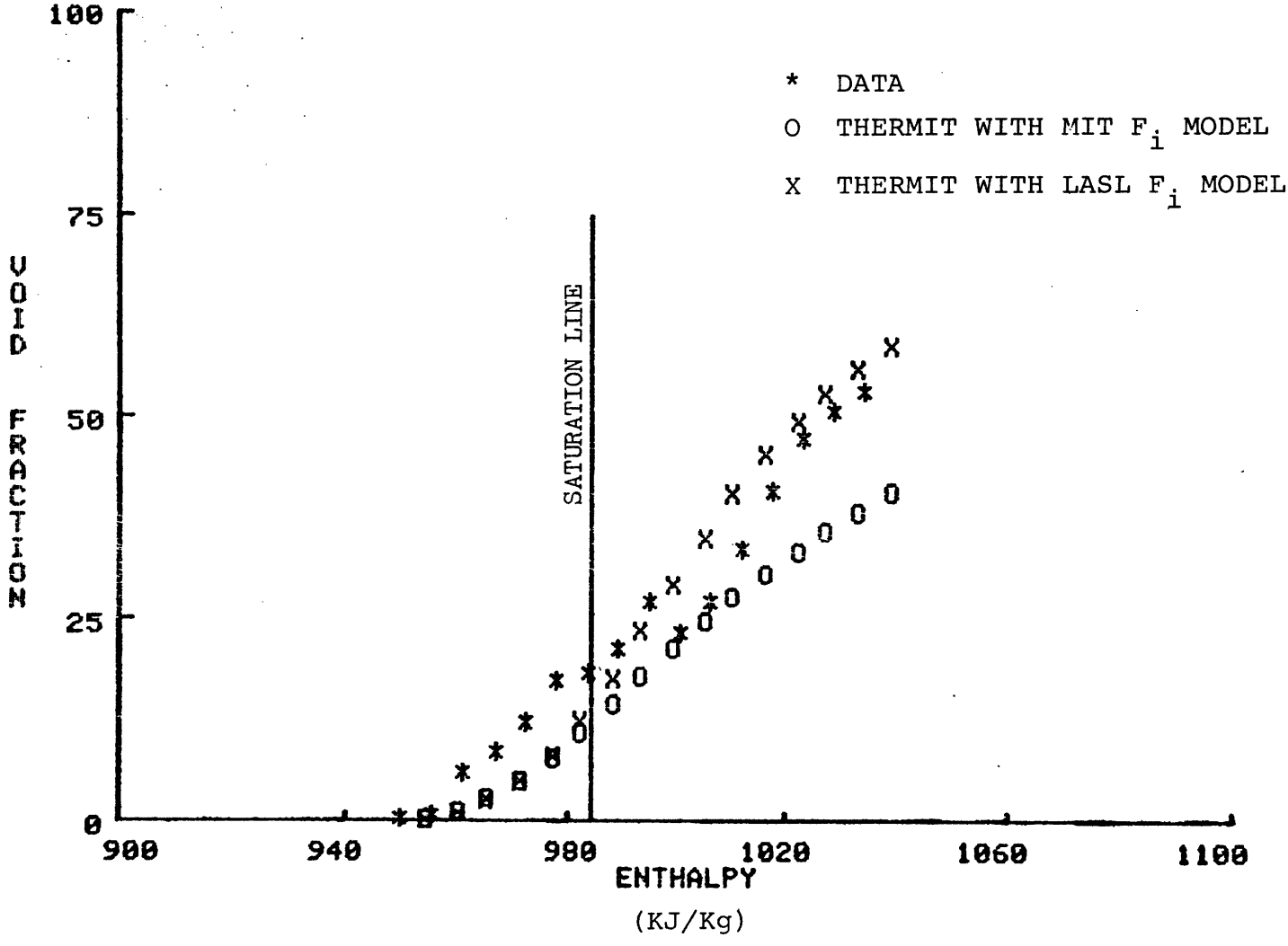

Figure D.6 Void Fraction Versus Enthalpy - Christensen case 10

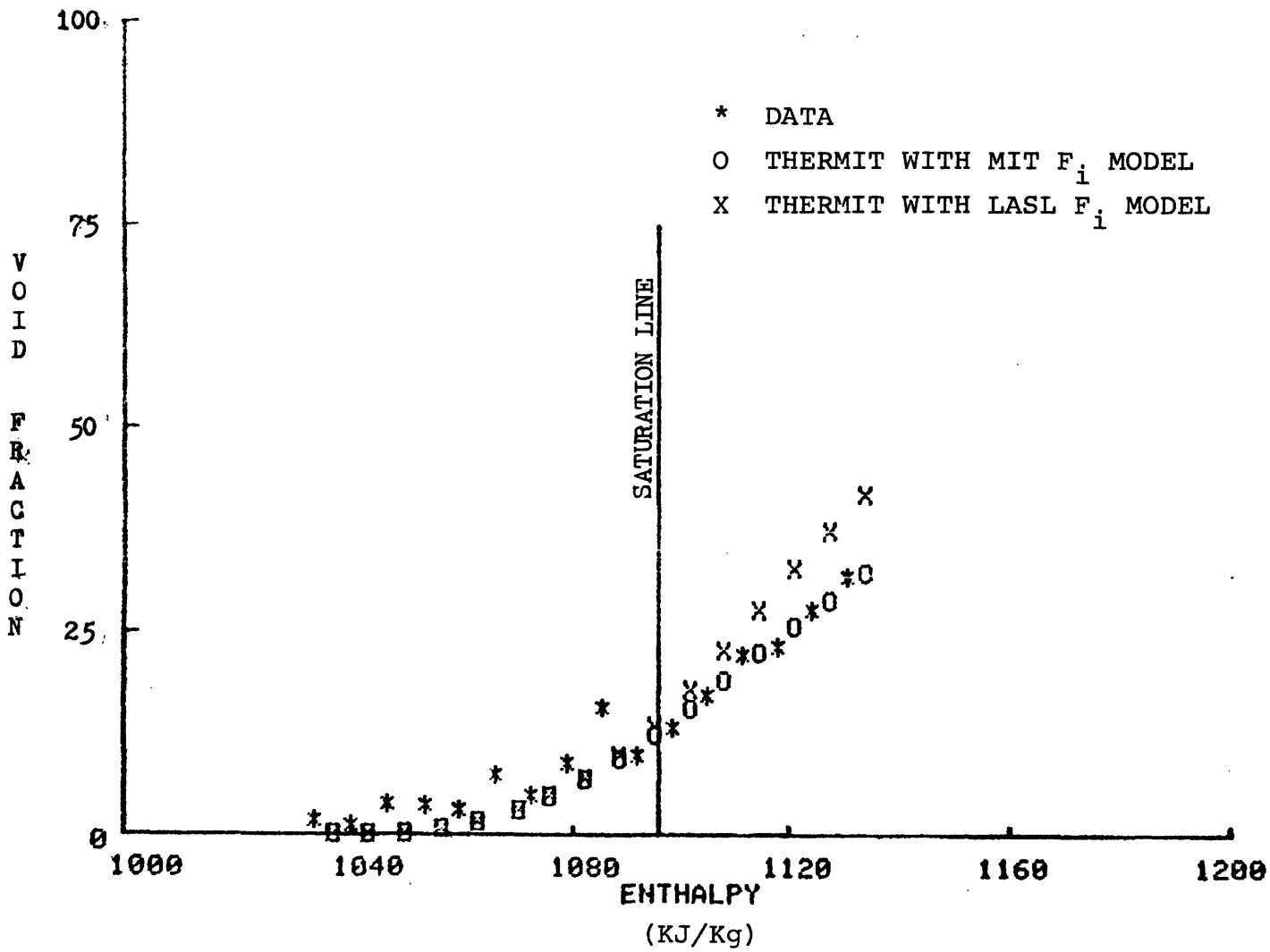

Figure D.7 Void Fraction Versus Enthalpy - Christensen case 11

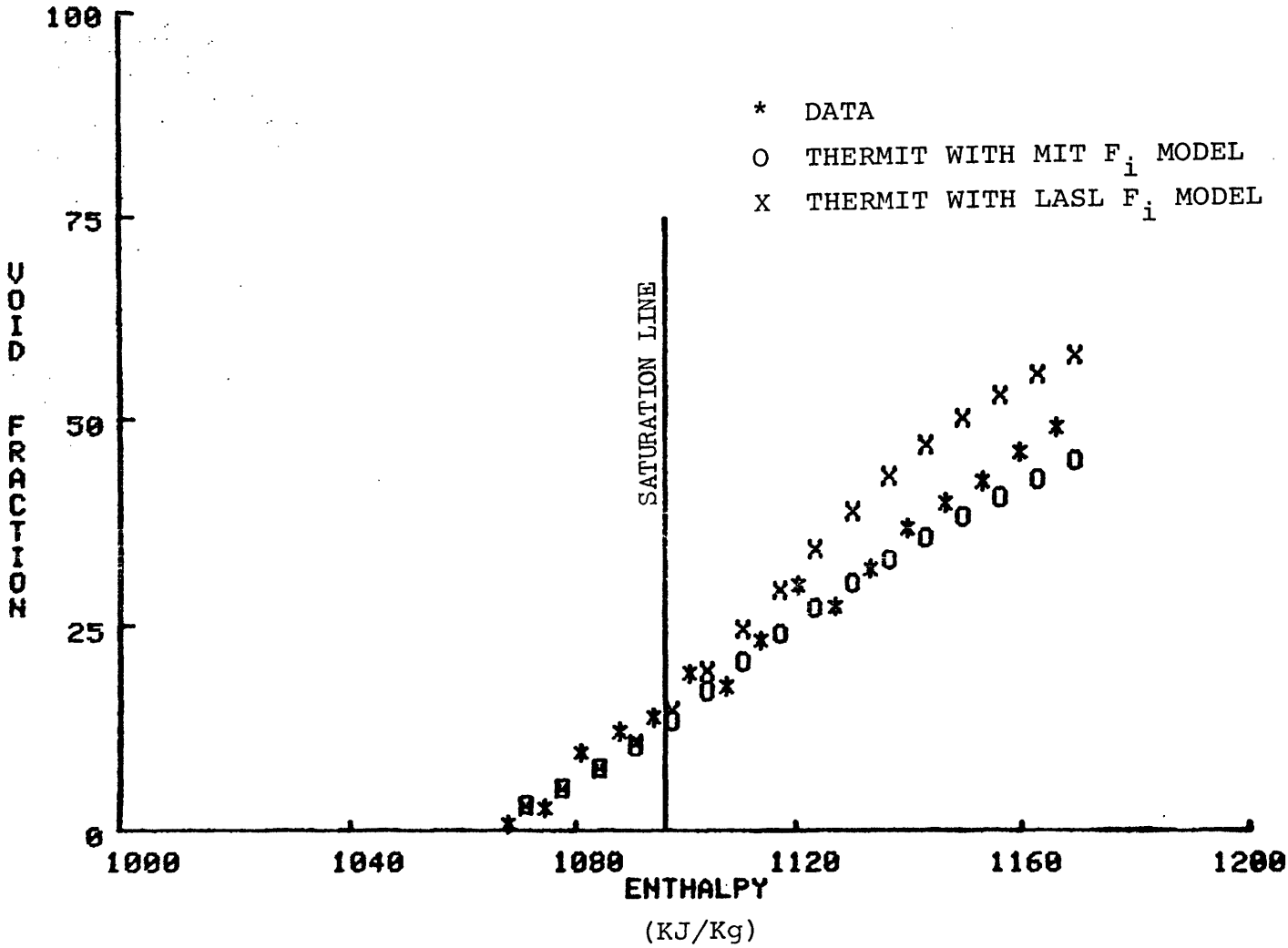

Figure D.8 Void Fraction Versus Enthalpy - Christensen Case 12

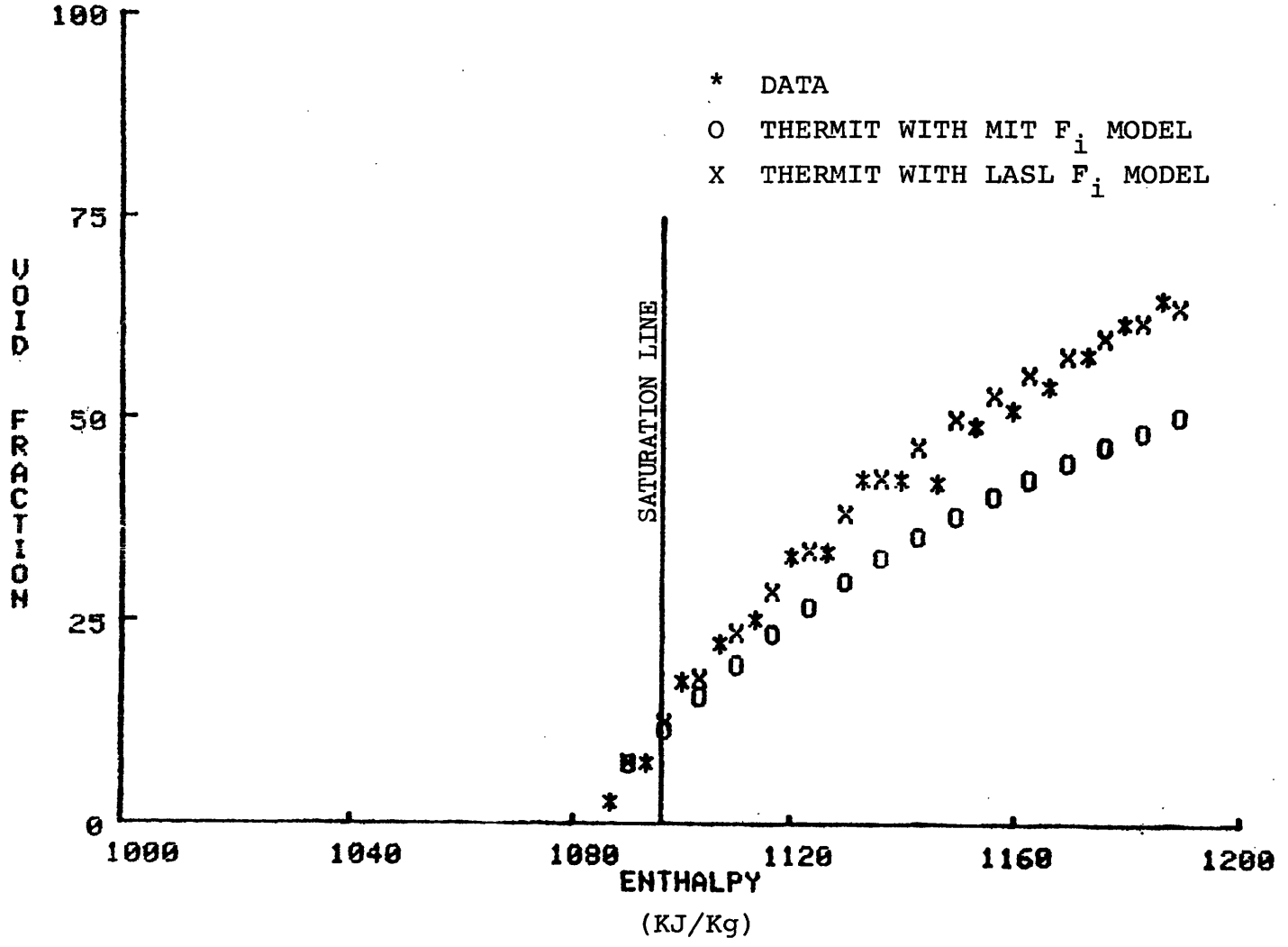

Figure D.9 Void Fraction Versus Enthalpy - Christensen Case 13

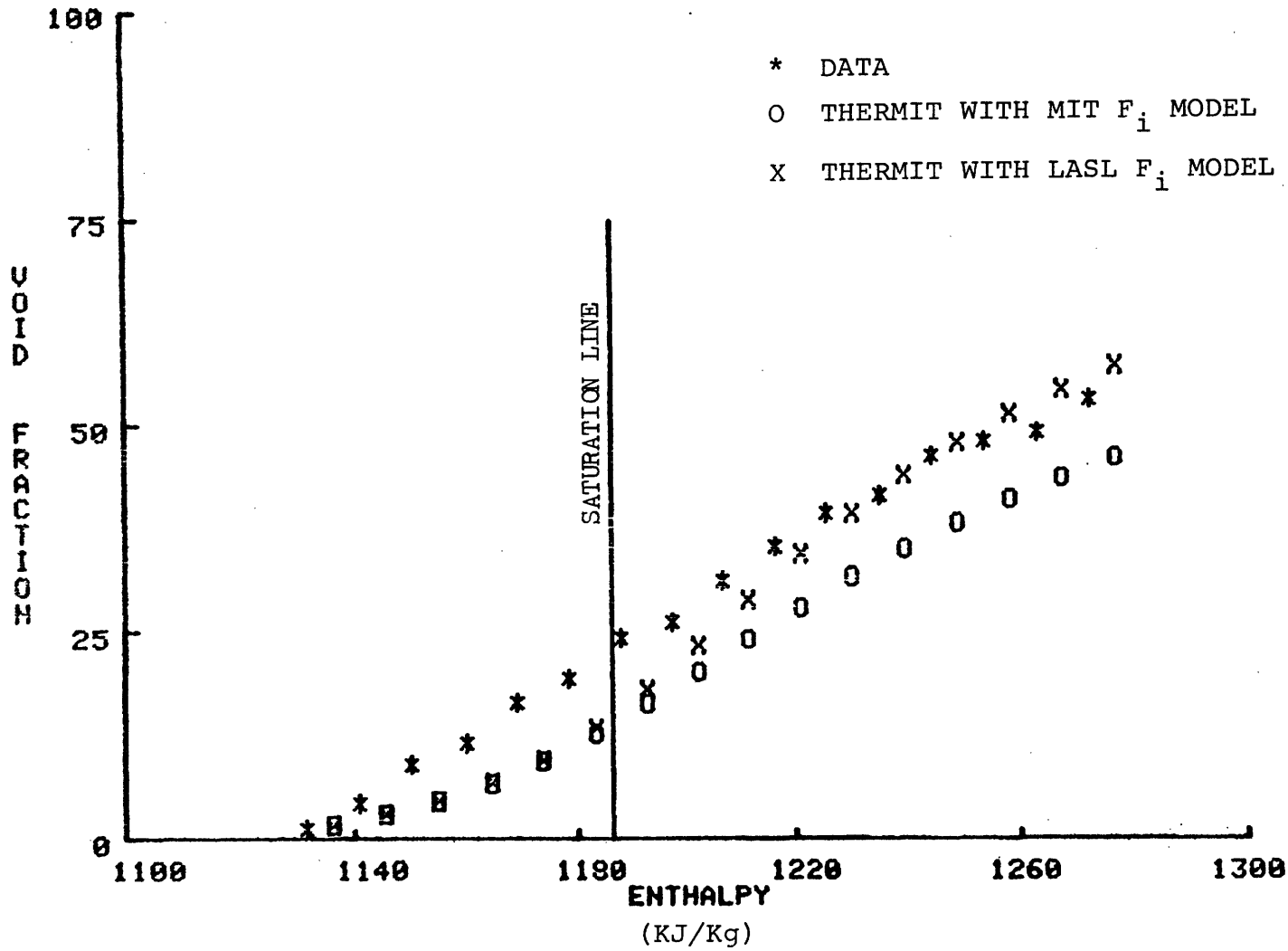

Figure D.10 Void Fraction Versus Enthalpy - Christensen Case 15

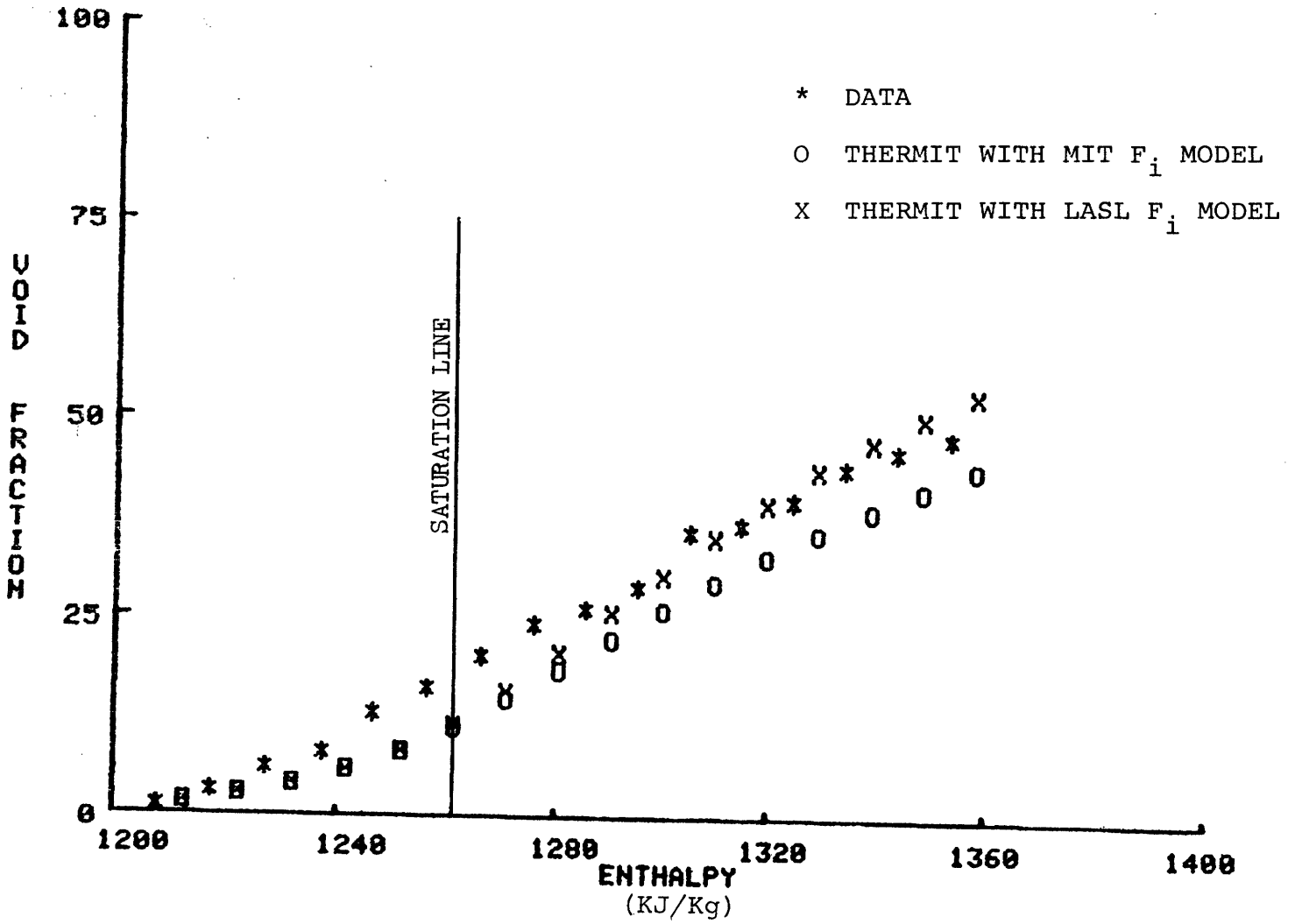

Figure D.11 Void Fraction Versus Enthalpy - Christensen Case 16

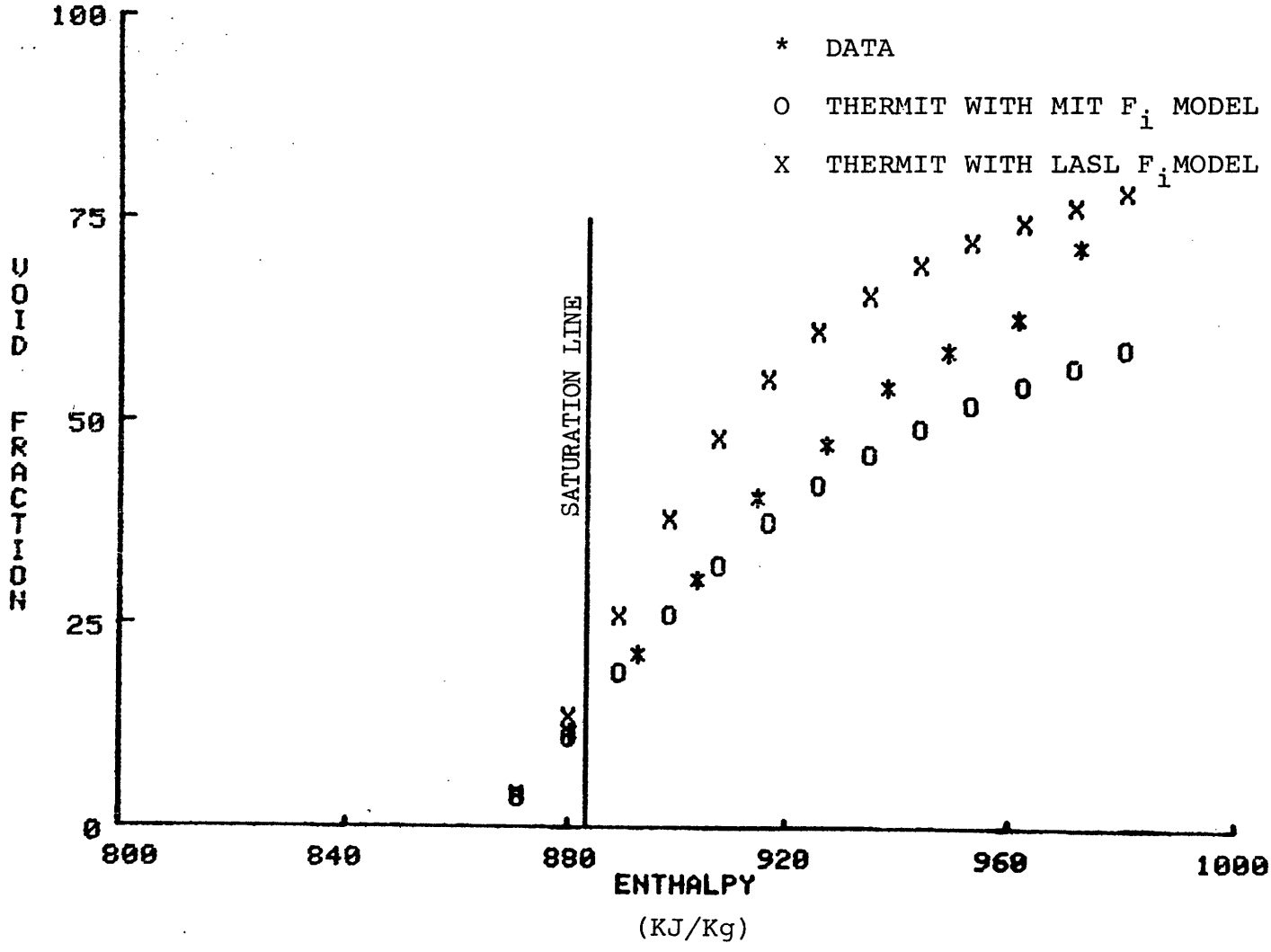

Figure D.12 Void Fraction Versus Enthalpy - Marchaterre Case 184

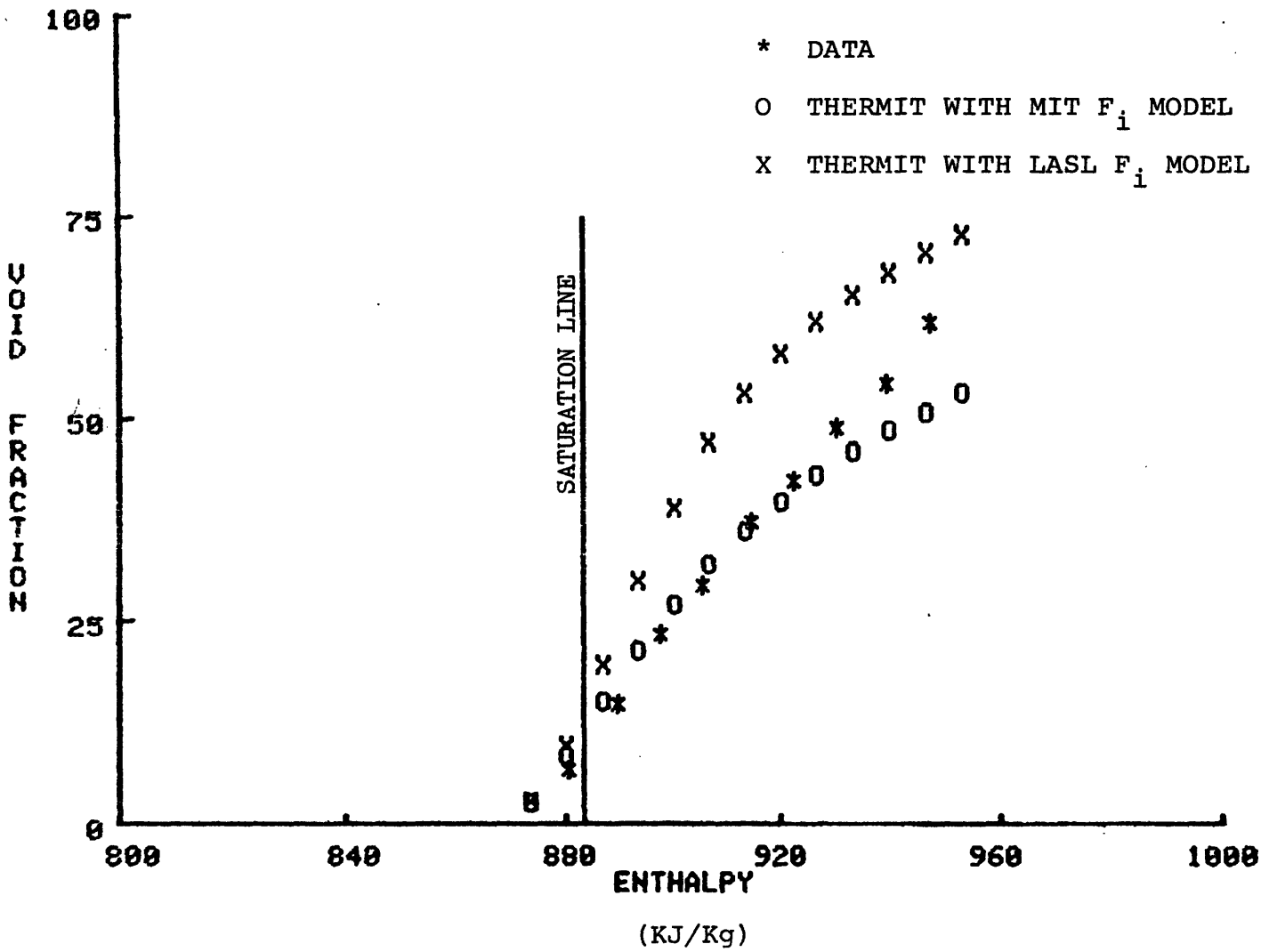

Figure D.13 Void Fraction Versus Enthalpy - Marchaterre Case 185

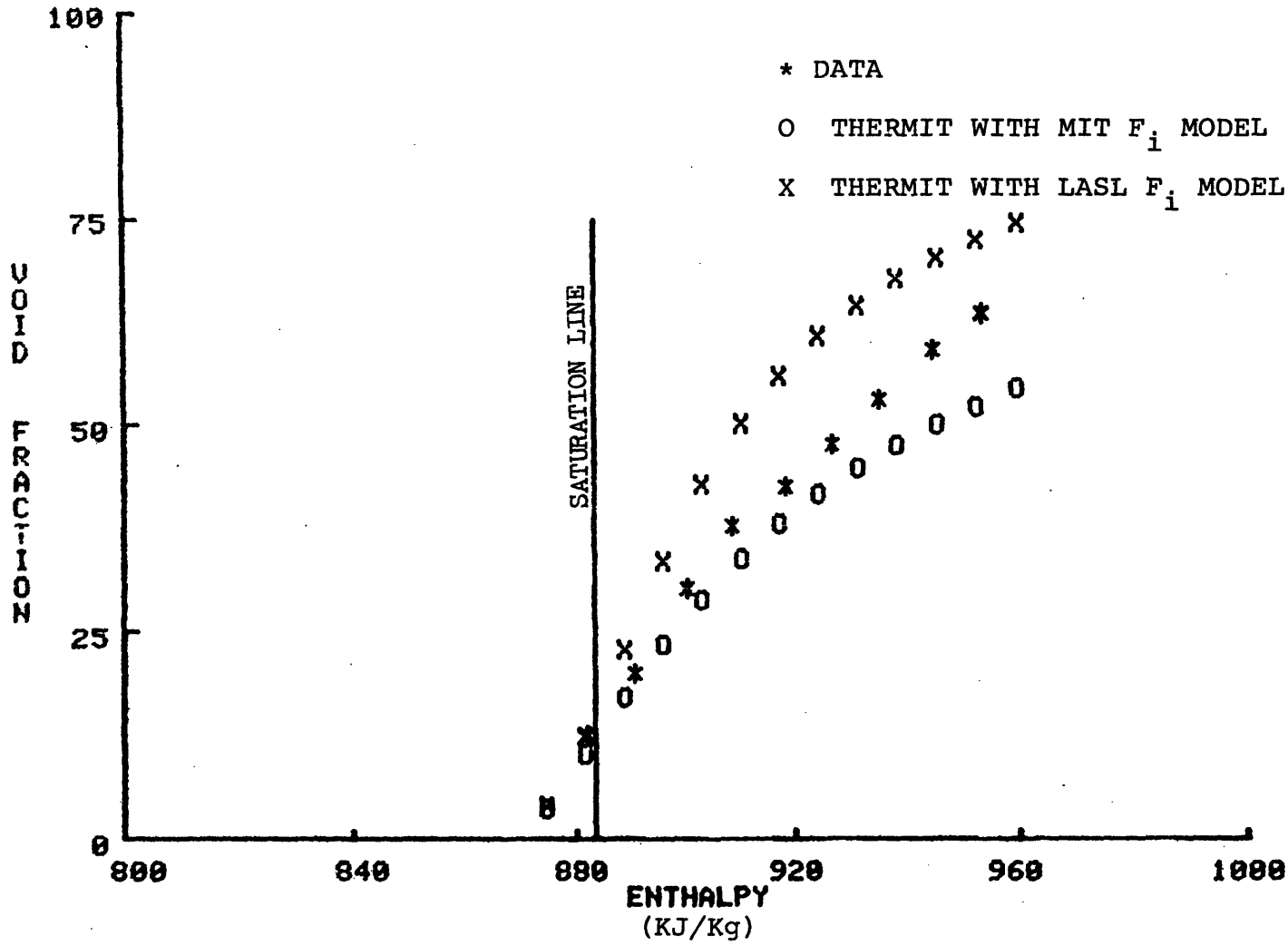

Figure D.14 Void Fraction Versus Enthalpy - Marchaterre Case 224

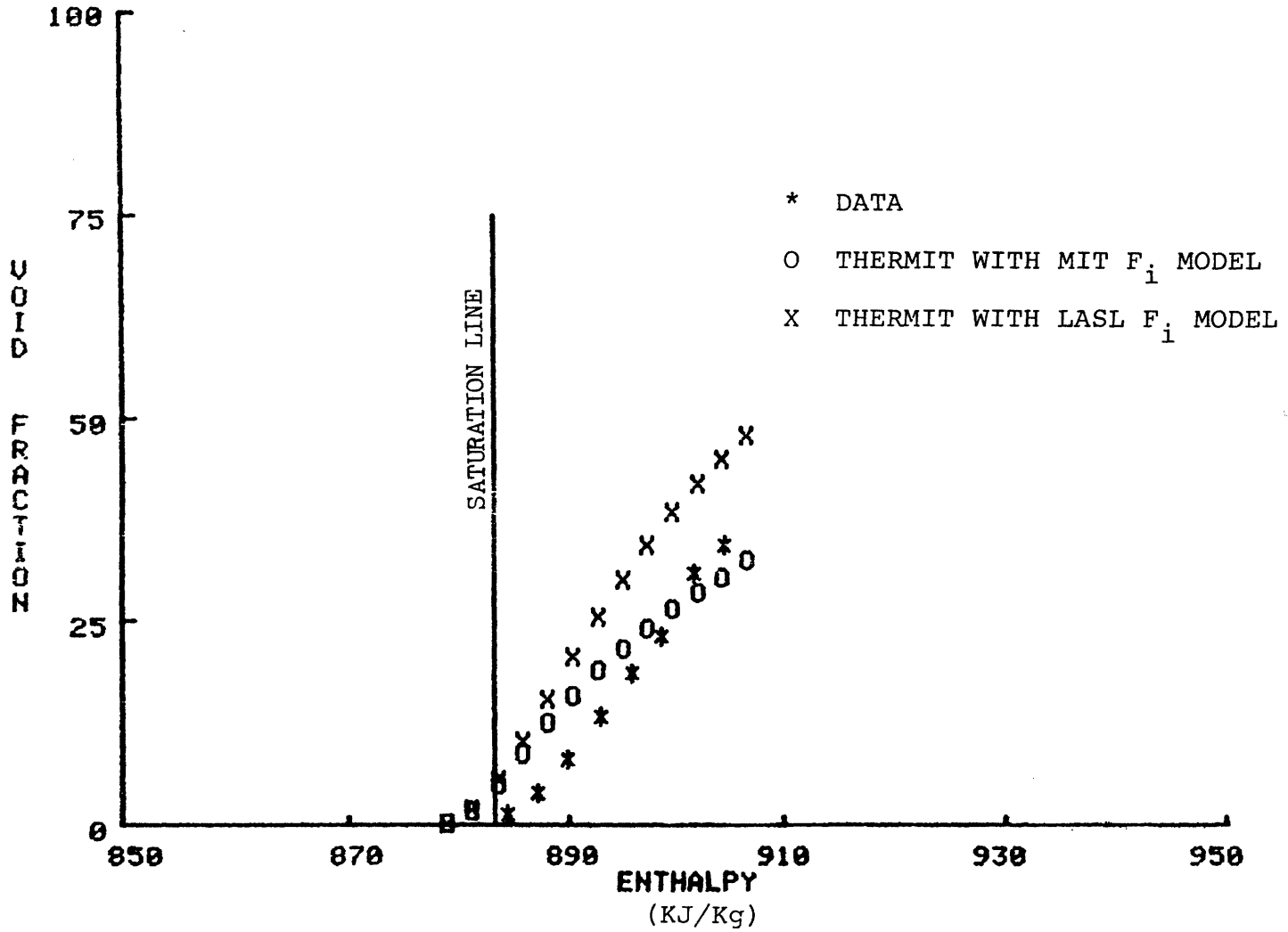

Figure D.15 Void Fraction Versus Enthalpy - Marchaterre Case 226

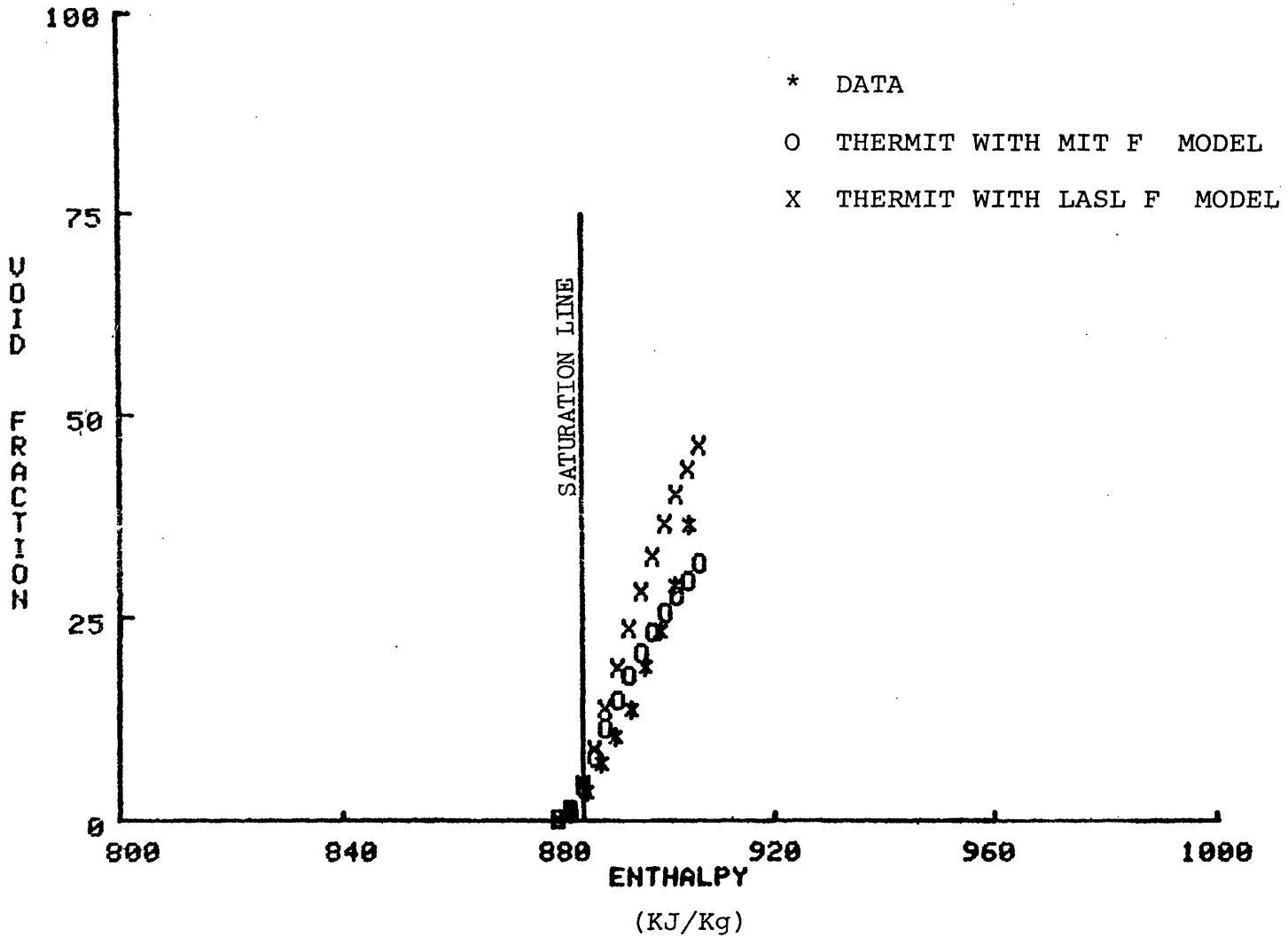

Figure D.16 Void Fraction Versus Enthalpy - Marchaterre Case 235

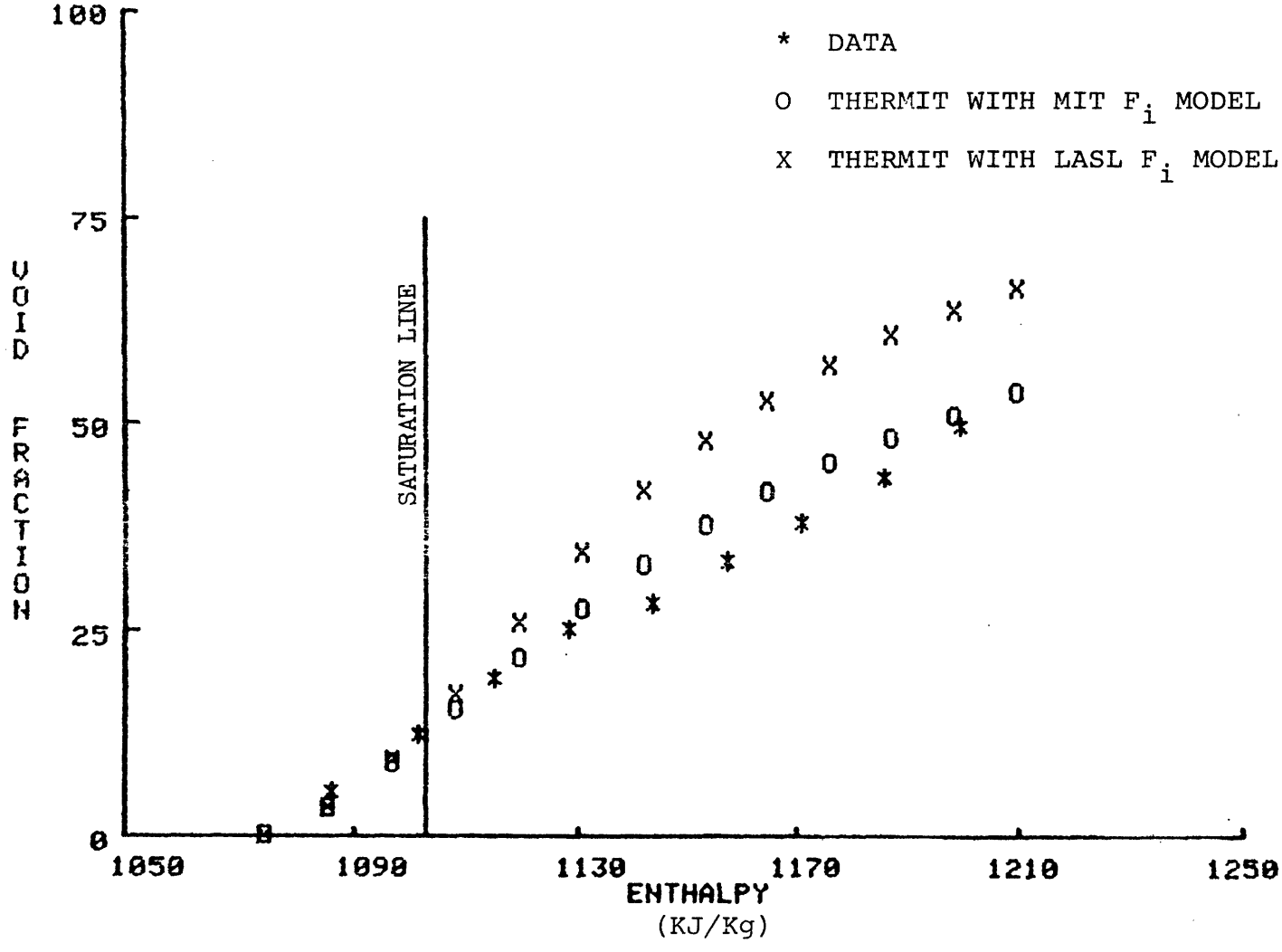

Figure D.17 Void Fraction Versus Enthalpy - Marchaterre Case 159

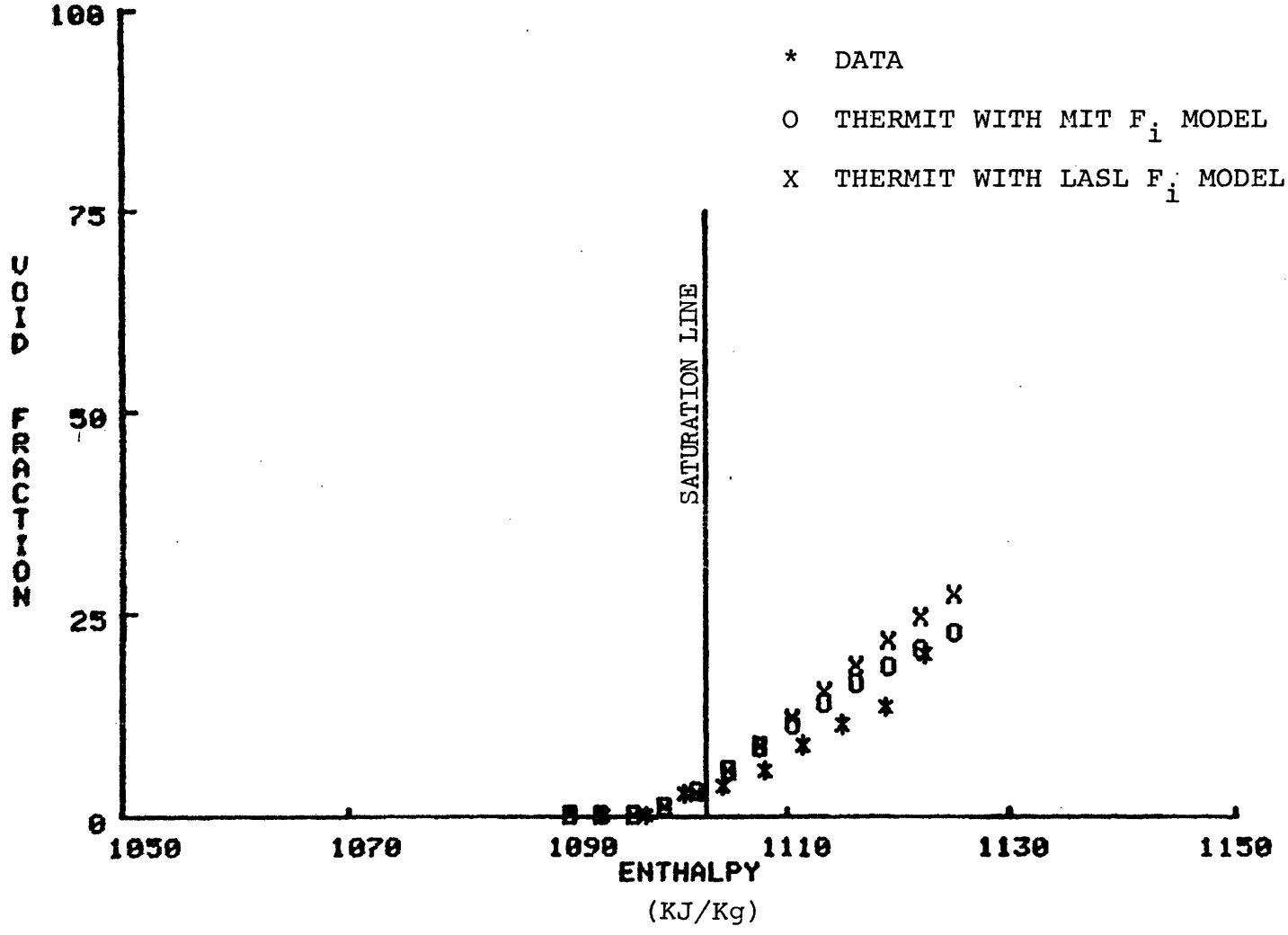

Figure D.18 Void Fraction Versus Enthalpy - Marchaterre Case 163

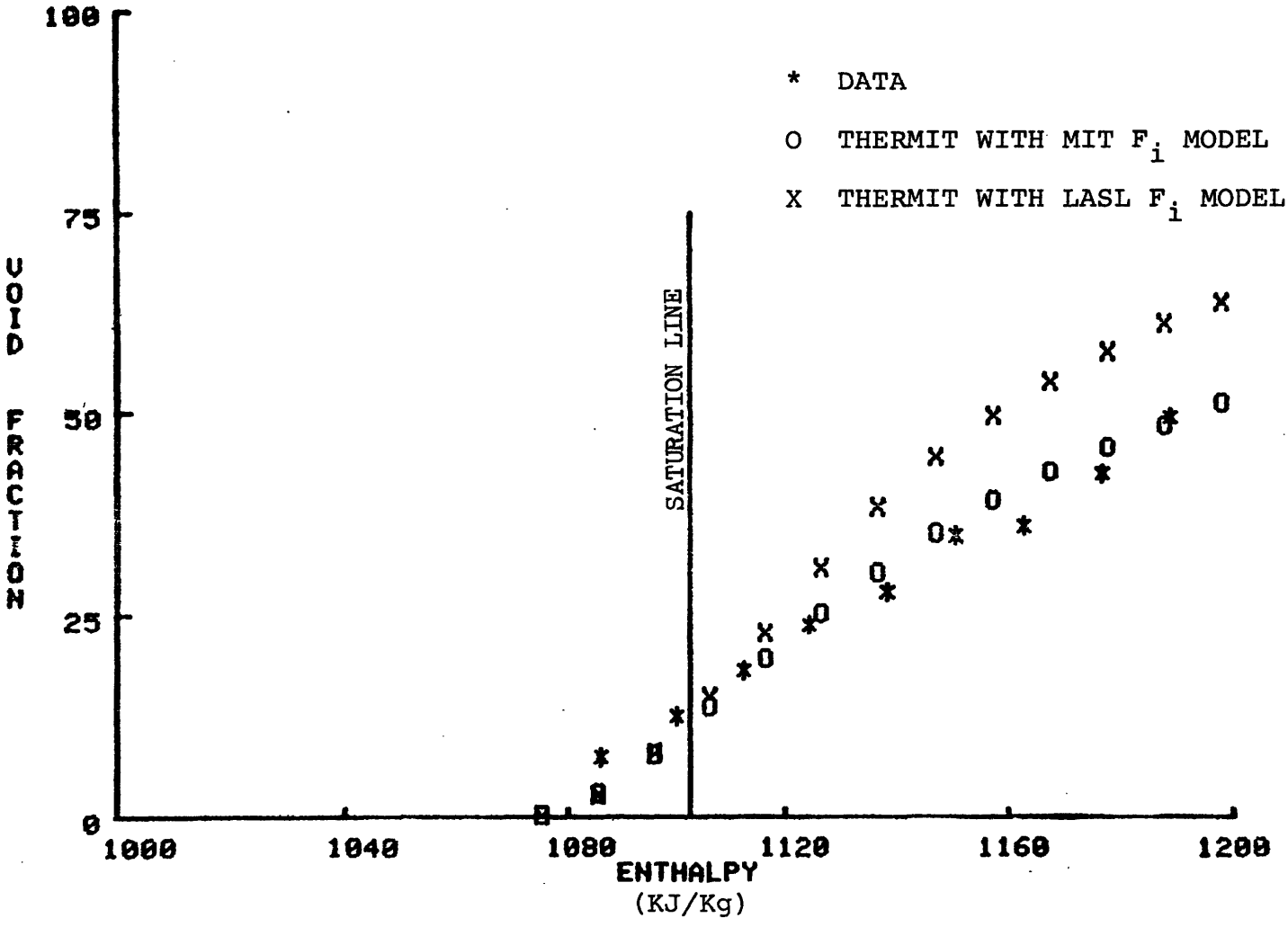

Figure D.19 Void Fraction Versus Enthalpy - Marchaterre Case 168

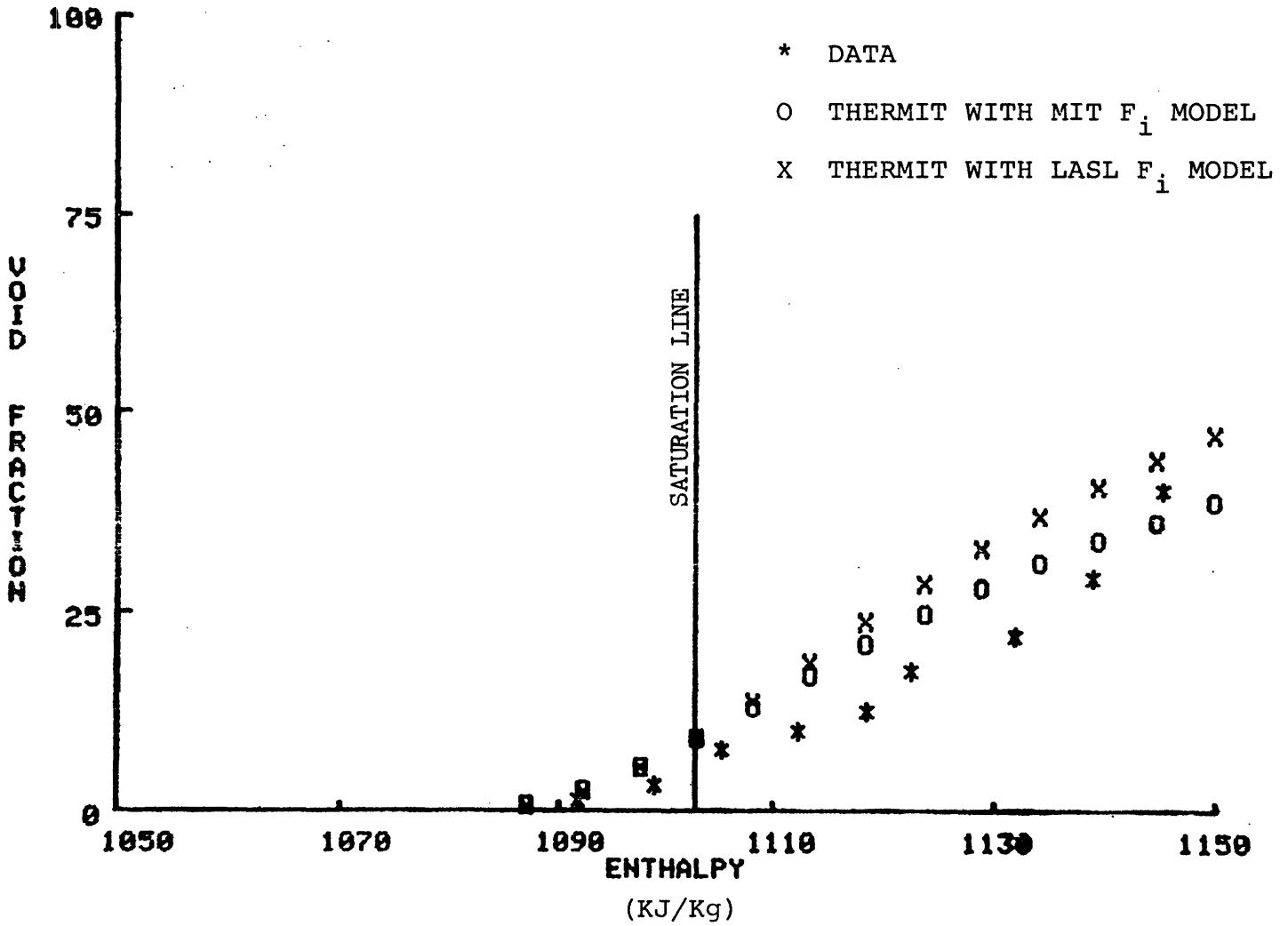

Figure D.20 Void Fraction Versus Enthalpy - Marchaterre Case 296

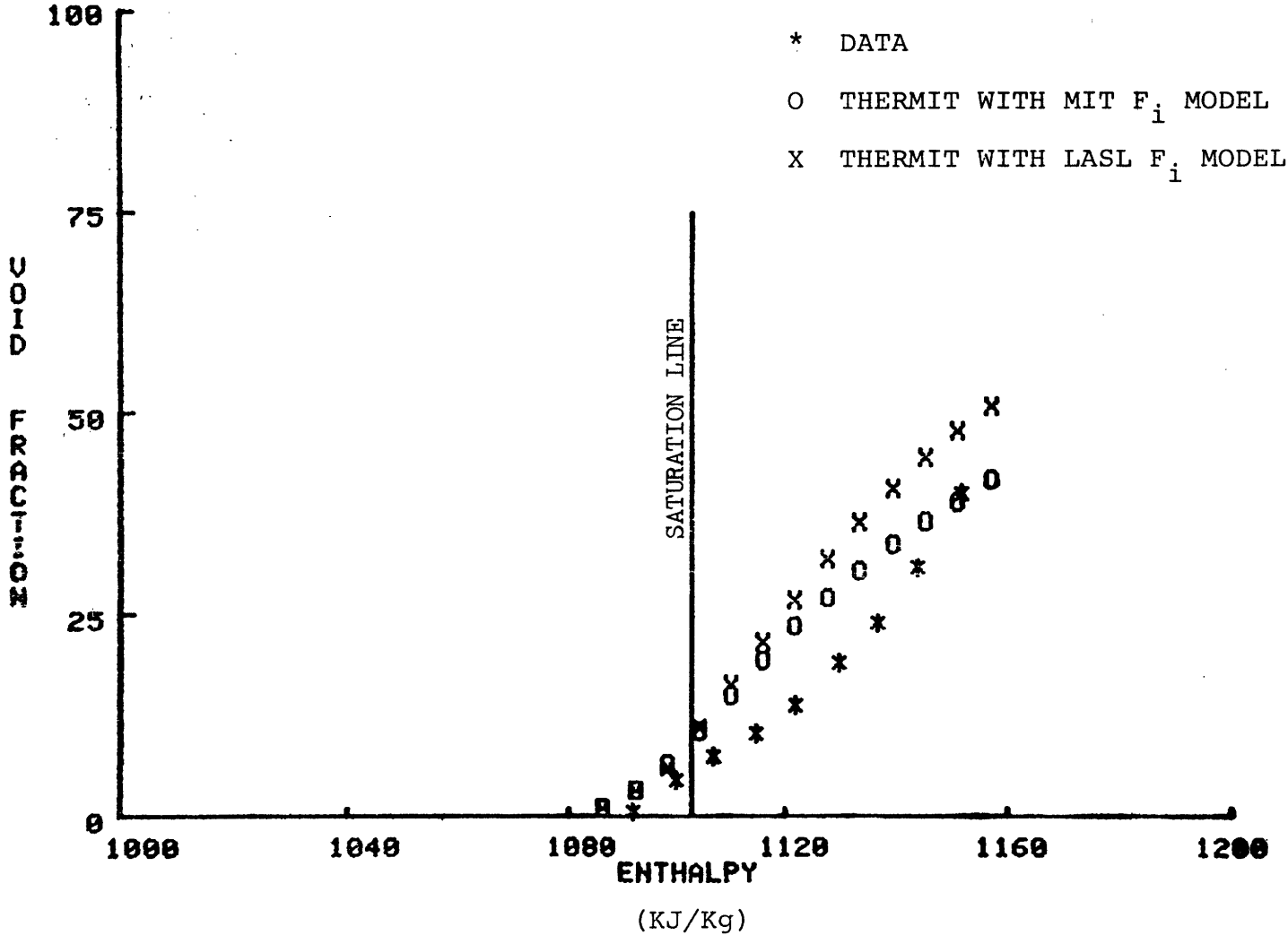

Figure D.21 Void Fraction Versus Enthalpy - Marchaterre Case 298

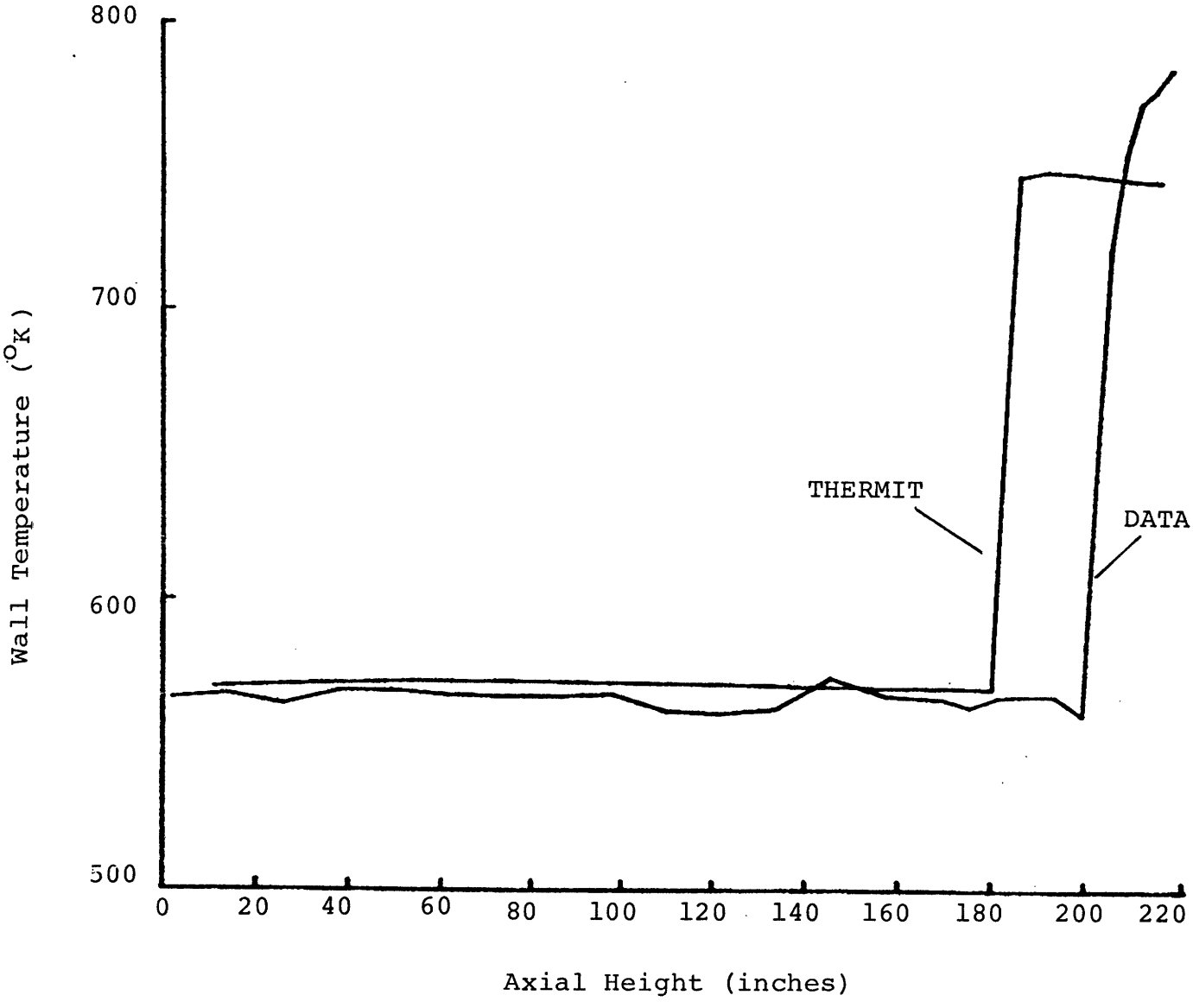

Figure D.22 Wall Temperature versus Axial Height

Bennett Case 5325

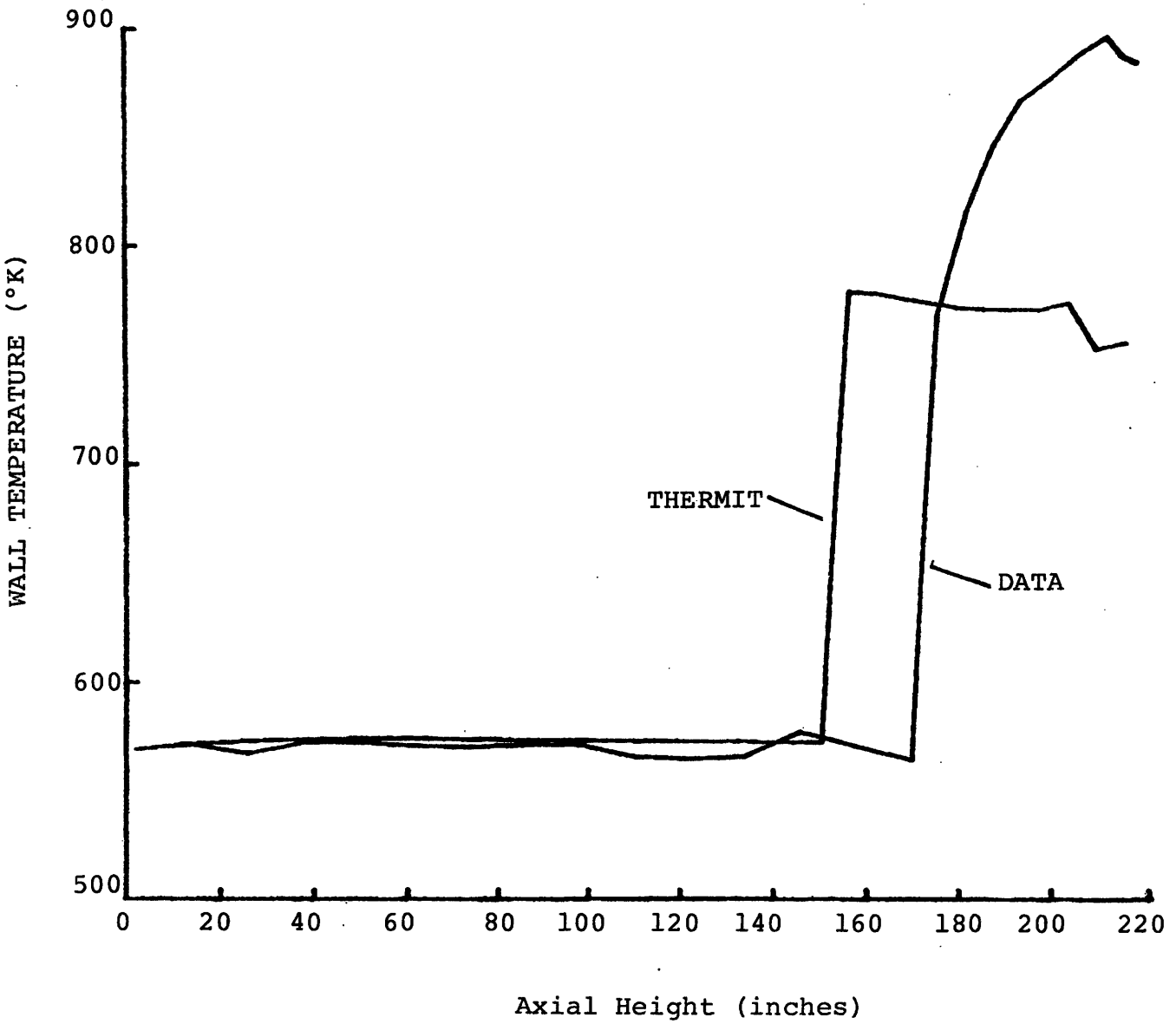

Figure D.23 Wall Temperature versus Axial Height

Bennett Case 5332

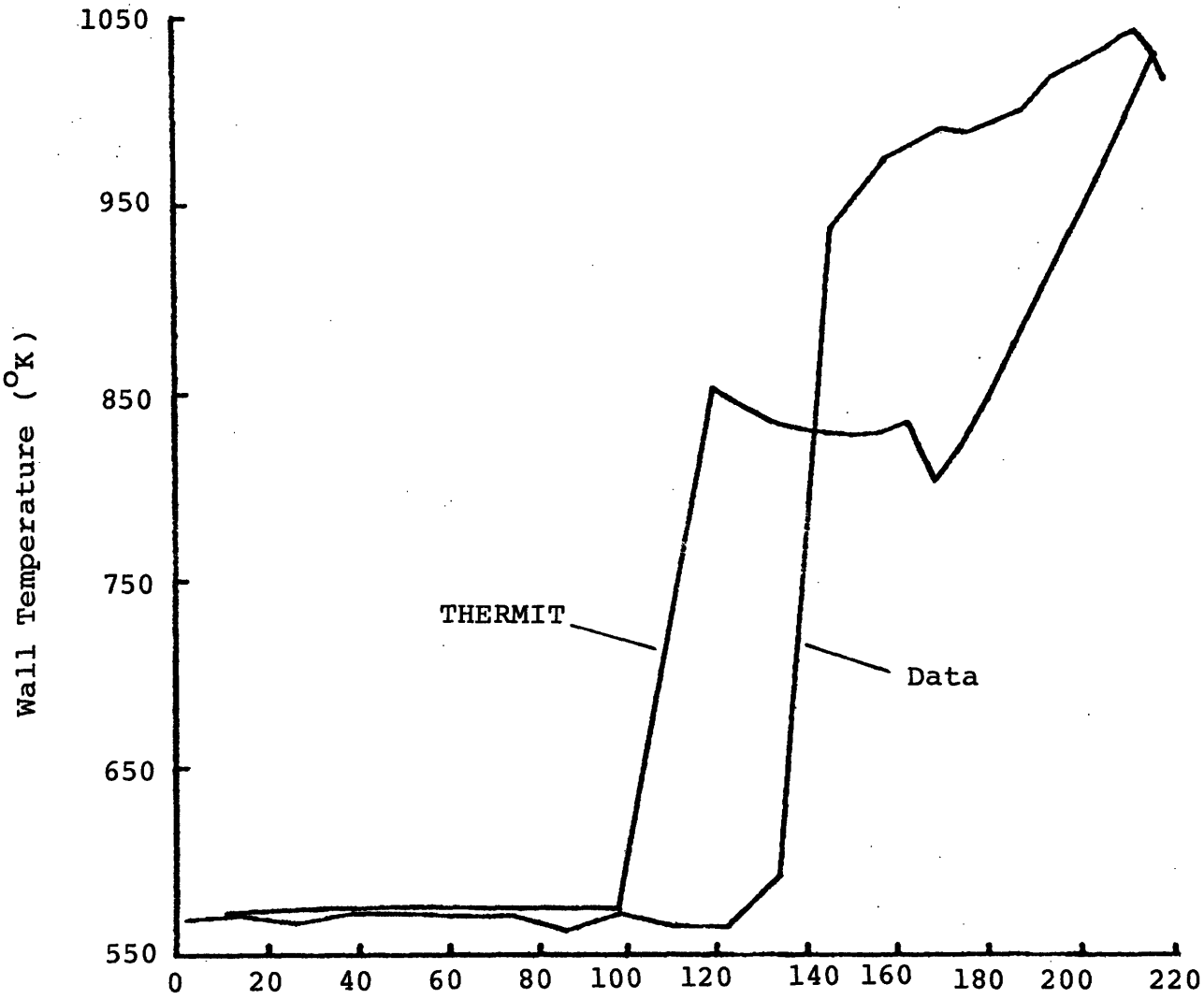

Figure D.24 Wall Temperature versus Axial Height

Bennett case 5336

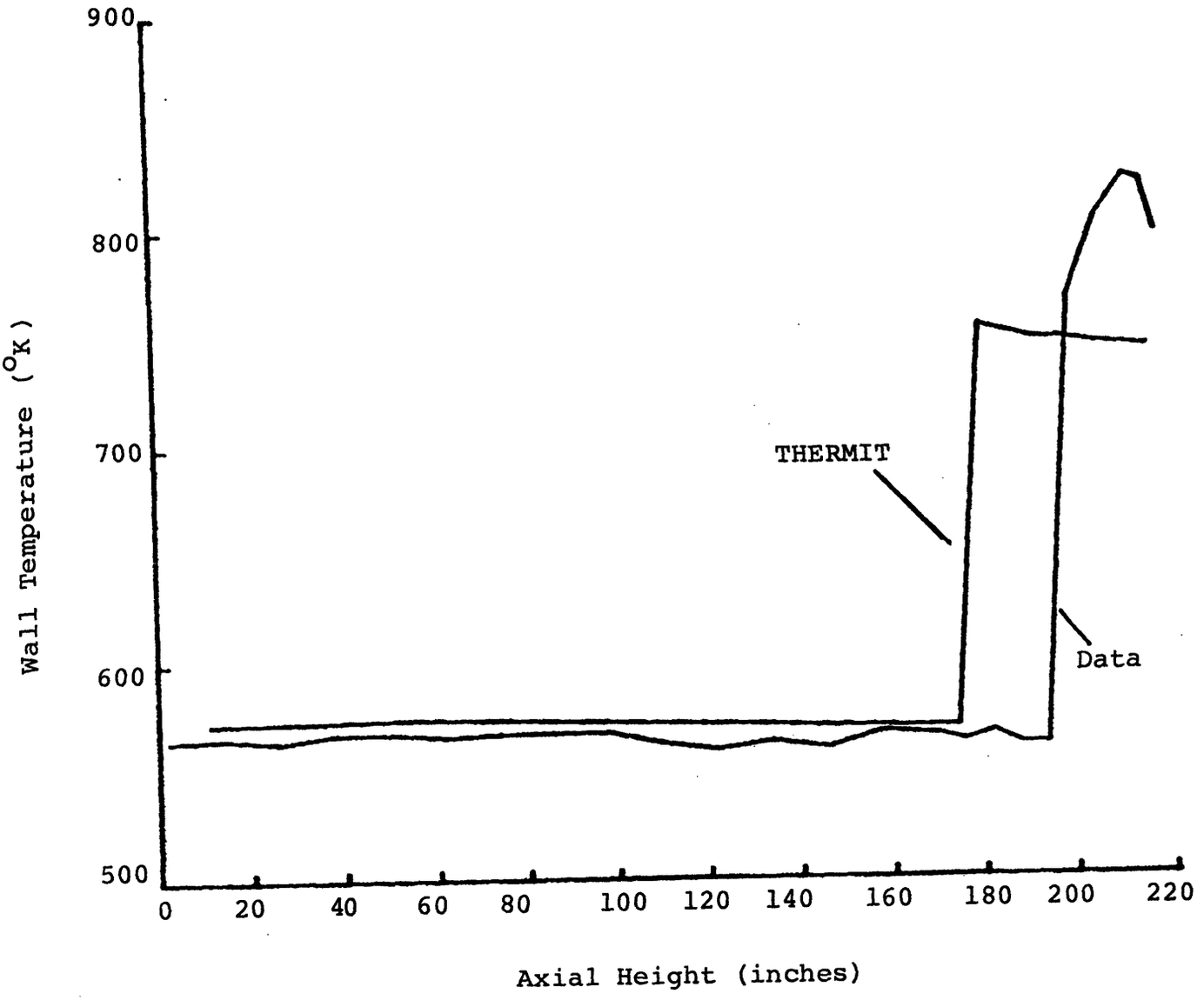

Figure D.25 Wall Temperature versus Axial Height

Bennett Case 5266

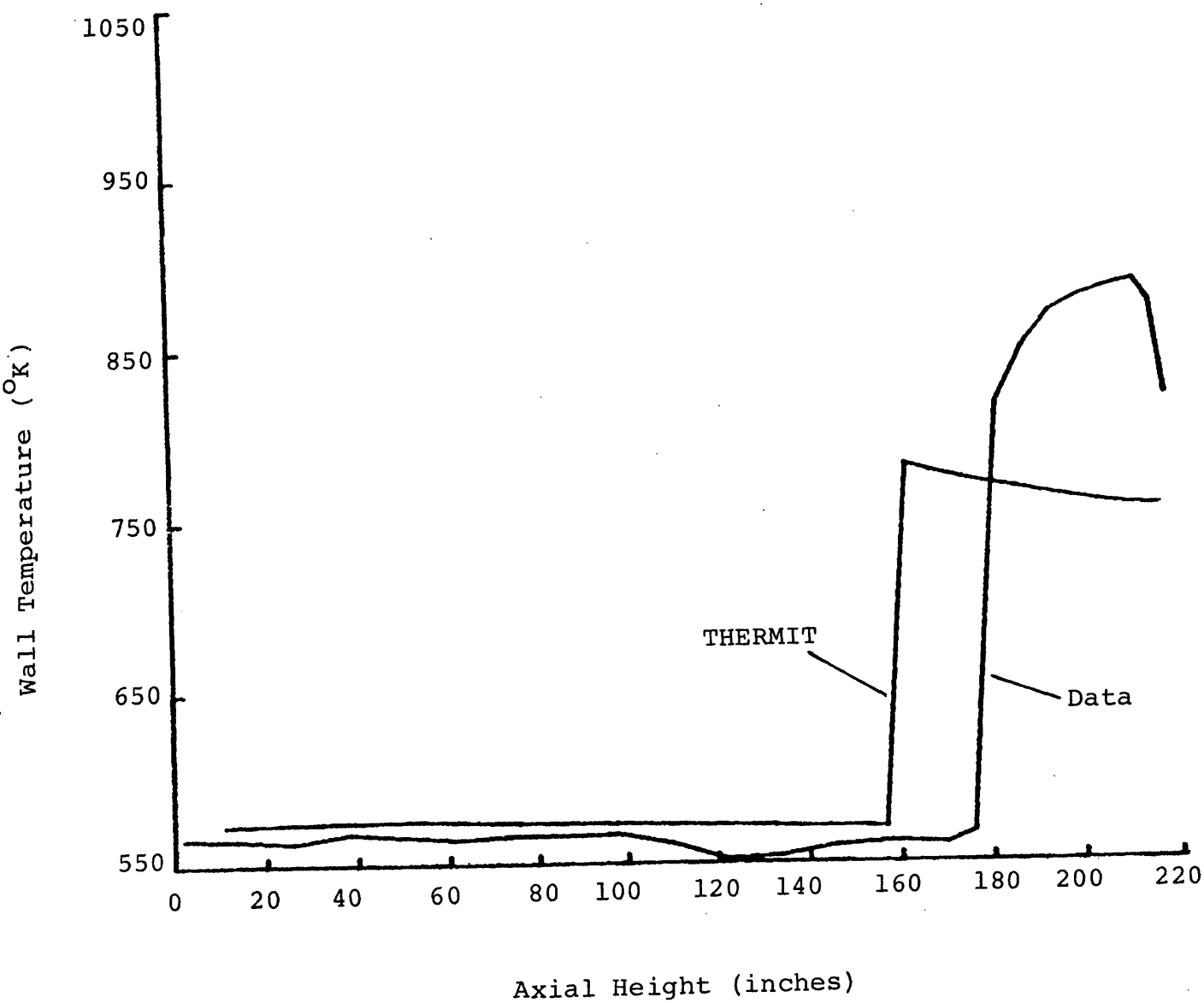

Figure D.26 Wall Temperature versus Axial Height

Bennett Case 5276

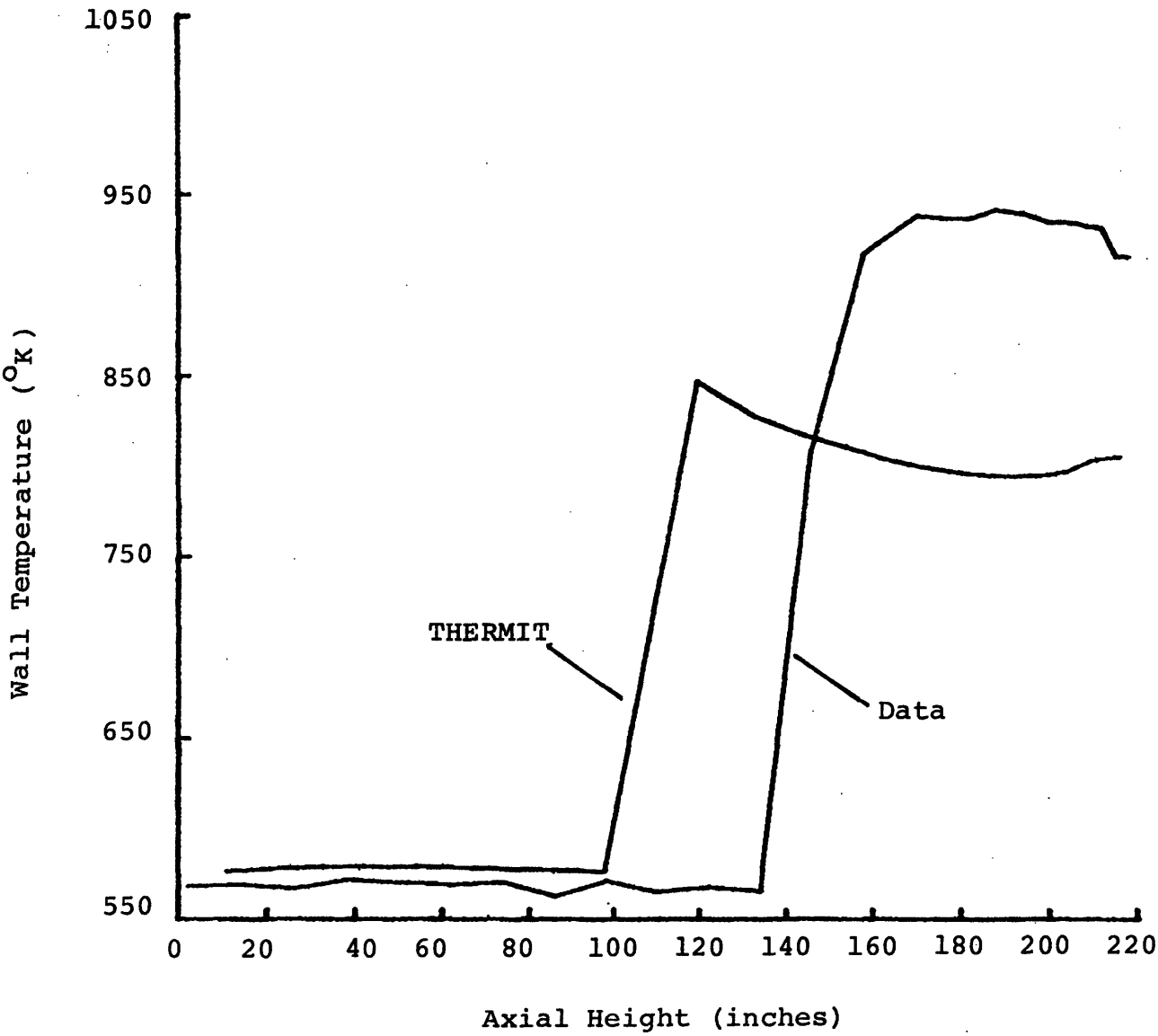

Figure D.27 Wall Temperature versus Axial Height

Bennett Case 5273

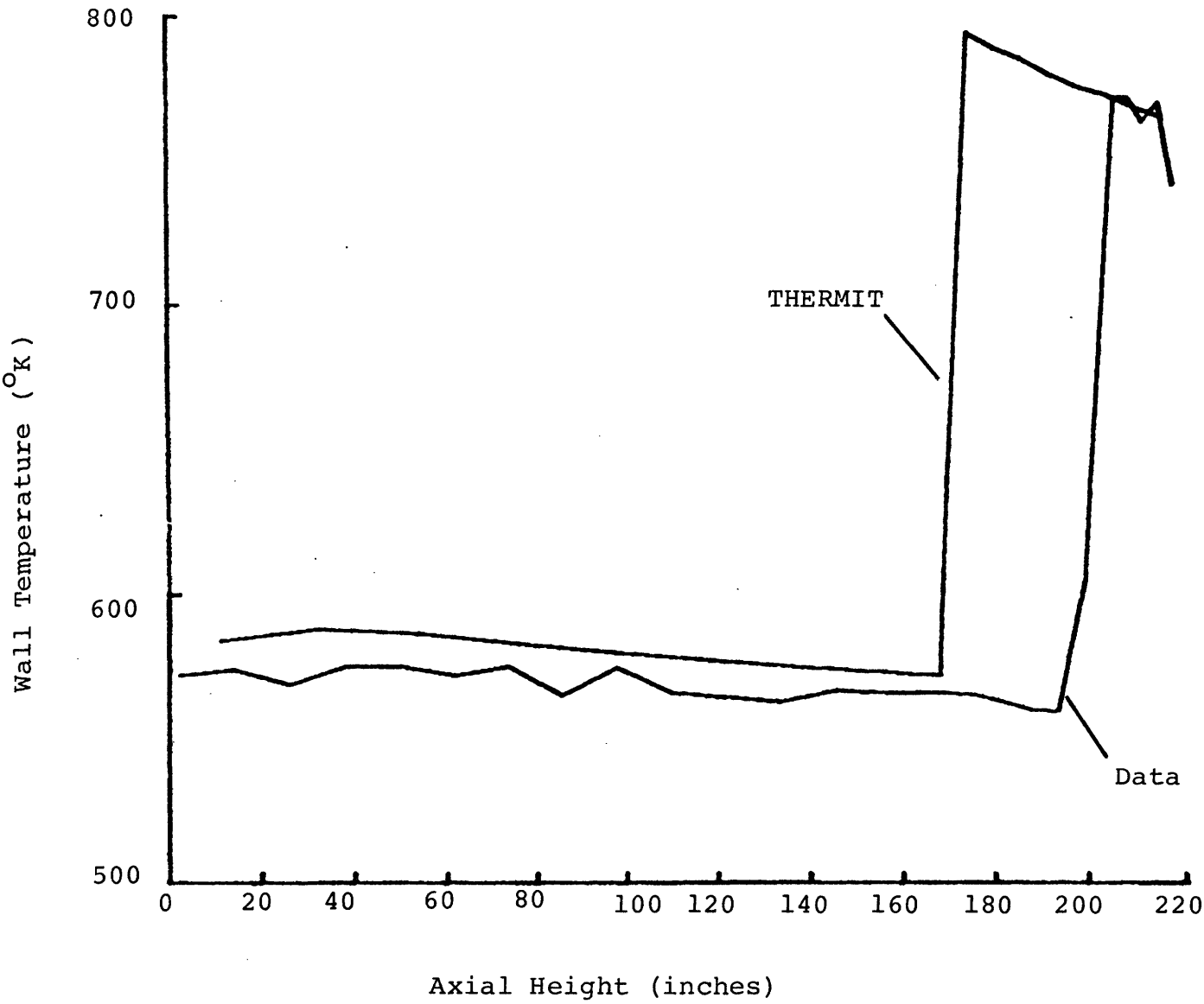

Figure D.28 Wall Temperature versus Axial Height

Bennett Case 5391

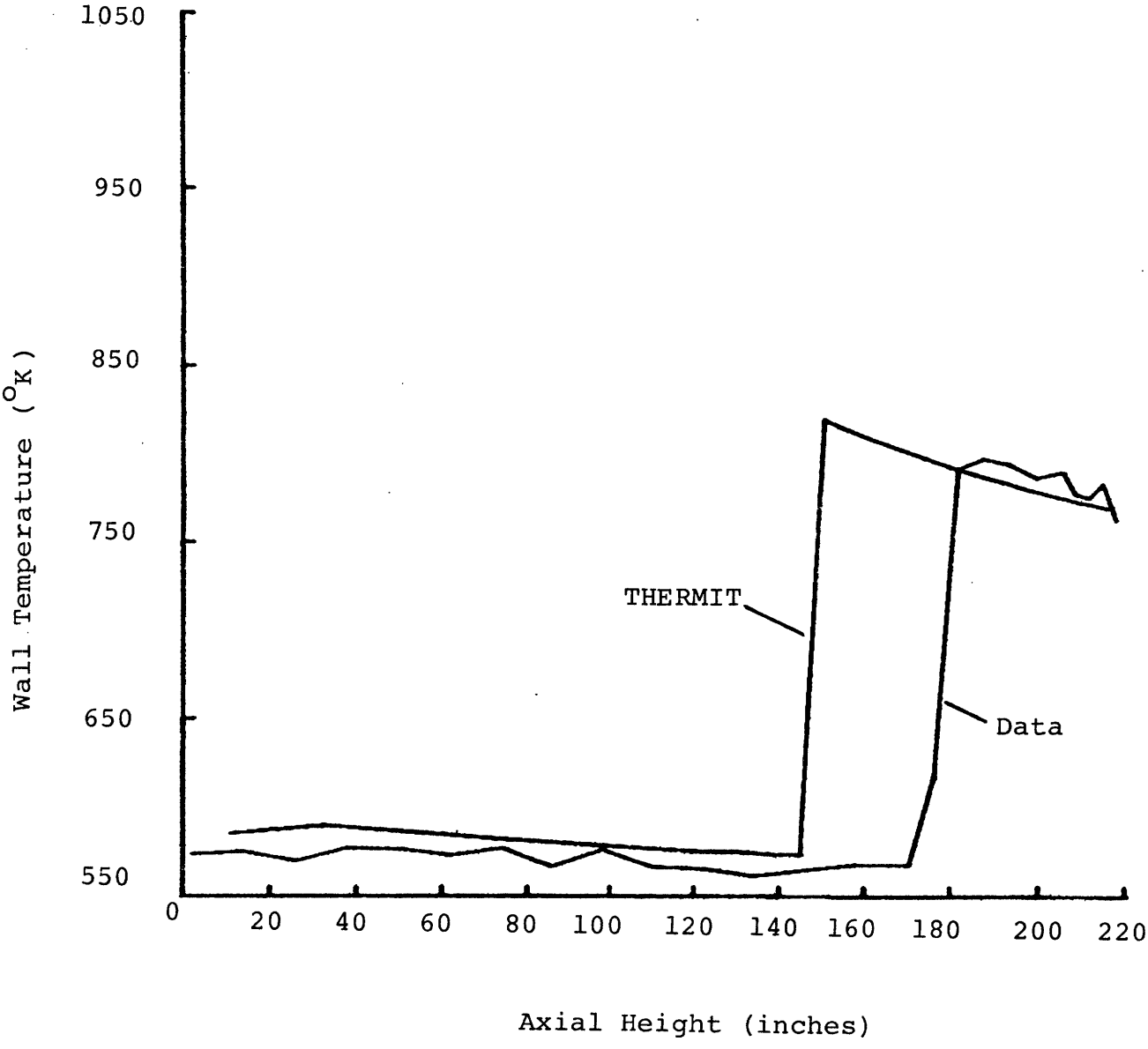

Figure D.29 Wall Temperature versus Axial Height

Bennett Case 5394

ACKNOWLEDGEMENTS

The authors would like to thank Professor Lothar Wolf, Professor John Meyer, Dr. H. Bruce Stewart and Andre Schor for their advices and they would like to express their appreciation for the efforts of Mahmoud Massoud in the testing of the code.

The financial support of their sponsors under the MIT Energy Laboratory's Electric Utility Program is also greatly appreciated.